

PROJECT REPORT

ON

“DESIGN OF KU-BAND FEEDS”

Submitted in partial fulfillment of the requirements for the award of degree of

BACHELOR OF ENGINEERING

IN

ELECTRONICS AND COMMUNICATION ENGINEERING



VISVESVARAYA TECHNOLOGICAL UNIVERSITY, BELGAUM

SUBMITTED BY:

Devaraja G P

1BM09EC030

Kishan Singh H

1BM09EC045

Kishore S

1BM09EC046

Manikanta C

1BM09EC049

Under the Guidance of:

RAMESH BALASUBRAMANYAM

ASSOCIATE PROFESSOR
DEPARTMENT OF ASTRONOMY AND ASTRO PHYSICS
RAMAN RESEARCH INSTITUTE

AMBIKA D.R

ASSISTANT PROFESSOR
DEPARTMENT OF ECE
BMSCE



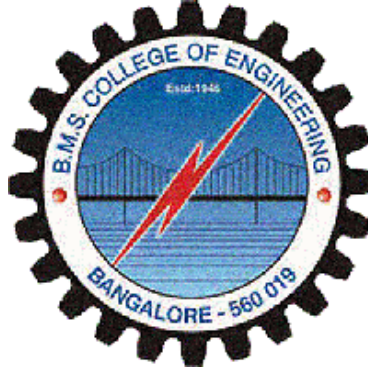
Department of Electronics and Communication Engineering

B.M.S COLLEGE OF ENGINEERING

(Autonomous College Affiliated to Visvesvaraya Technological University, Belgaum) Bull Temple

Road, Basavanagudi, Bangalore-560019

B.M.S COLLEGE OF ENGINEERING
(Autonomous College under VTU)
Department of Electronics and Communication Engineering



CERTIFICATE

This is to certify that the project entitled “**Design Of Ku-Band Feeds**” is a bonafide work carried out by

Manikanta C **1BM09EC049**
Kishore S **1BM09EC046**

Devaraja G P **1BM09EC030**
Kishan Singh H **1BM09EC045**

in partial fulfillment for the award of Bachelor of Engineering degree by VTU Belgaum, during the academic year 2012-2013.

Internal Guide :

External Guide :

Ambika D.R

Assistant Professor,
Department of ECE
BMSCE ,Bangalore.

Ramesh Balasubramanyam

Associate Professor
Department Of Astrophysics and Astronomy
Raman Research Institute

Dr.D .Seshachalam

Head Of Department
Department Of ECE
BMSCE ,Bangalore.

Dr.K.Mallikarjuna Babu

Principal, BMSCE

External Examination:

Signature with date:

- 1.
- 2.

ACKNOWLEDGEMENTS

The satisfaction and euphoria that accompanies the successful completion of any task would be incomplete without the mention of the people who made it possible and whose constant encouragement and guidance has been a source of inspiration throughout the project.

We would like to thank **Ambika D R**, Department Of ECE , BMSCE, Bangalore for being our Internal Guide and providing all the support and encouragement throughout the project. It has really been a wonderful experience for us.

We are fortunate enough to have **Ramesh Balasubramanyam** , Department of Astrophysics and Astronomy, Raman Research Institute, Bangalore as our External guide. We would take this opportunity to express our humble gratitude for his valuable guidance, whose inspiration, encouragement and immense help make this project work a success. It was a pleasure working under him , which one would feel with very few on this earth.

We are thankful to **Dr. Mallikarjuna Babu, Principal**, B.M.S.C.E, Bangalore and **Dr.Seshachalam , H.O.D**, Dept. of Electronics and Communication Engineering, B.M.S.C.E , Bangalore for their constant co-operation and support.

We feel a deep sense of gratitude for our parents for their tremendous support, constant encouragement, and great guidance.

MANIKANTA C

KISHAN SINGH H

DEVARAJA G P

KISHORE S

ABSTRACT

RRI (Raman Research Institute) is building a new radio telescope to be fitted with a 7-14 GHz 32 element array receiver. The first element of the receiver is a radiating element that impedance matches the free space wave converging at the antenna focus to the input of the LNA, set on a microstrip. Good matching needs to be achieved over a broad band for effective use of the LNA. This BE project aims to achieve this. As a part of this project, we plan to design and simulate two kinds of radiating systems: a conventional pyramidal ridge horn antenna and a modern planar stacked-patch antenna. The specific project goals are to achieve better than 2 VSWR over at least 7-14 GHz, with good E and H plane symmetry and as much as possible similar directivity over the wide band. The aim of this project is to design the feed for Active integrated antenna, which should operate in the frequency range of 7GHz to 14GHz. For the design of antenna, we have used the software tool HFSS (High Frequency Structure Simulation), which is generally used for the design and simulation of electromagnetic structures such as waveguide, horn antenna, patch antenna etc. In this project we study the different types of feeds (antennas), which could be used in the Ku band, design the antennas using the software tool HFSS and then simulate them using the same. Based on the results of the simulation we decide which antenna has to be fabricated in order to use it as the feed for the Active integrated antenna. We here study, design and simulate two particular kinds of antennas namely Double Ridged Horn Antenna (DRHA) and Microstrip Antenna, both of them have their respective advantages and disadvantages which are also the limiting factors for their applications. We will design the above mentioned antennas using the software tool HFSS and simulate them for the desired frequency range, compare their performances in the desired frequency range. The comparison is based on the typical performance parameters of electromagnetic structures such as VSWR, radiation patterns, return loss etc. The antenna which is best suited for the desired application is then fabricated.

TABLE OF CONTENTS

Approval page.....	01
Acknowledgement.....	
Abstract.....	
Table of Contents.....	
List of tables and figures.....	
List of abbreviations.....	
CHAPTER 1: INTRODUCTION.....	01
1.1 KU Band.....	01
1.1.1 Advantages.....	01
1.1.2 Disadvantages.....	02
1.2 Active Integrated Antenna.....	02
1.2.1 Active Integrated Antenna Configurations.....	03
1.2.1.1 Active Devices.....	04
1.2.1.2 Antenna Elements.....	05
1.2.2 Active Integrated Antenna Arrays.....	07
1.2.3 Applications of Active Integrated Antennas.....	08
1.3 High Frequency Structure Simulator (HFSS).....	08
1.3.1 Ansoft HFSS Features.....	09
1.3.2 Ansoft HFSS Desktop.....	10
CHAPTER 2: BACKGROUND.....	11
2.1 Radio Telescopes	11
2.2 Principles of Operation.....	13

CHAPTER 3: LITERATURE SURVEY.....	16
CHAPTER 4: INTRODUCTION TO DOUBLE RIDGED HORN ANTENNA.....	21
4.1 Design Constraints.....	22
4.1.1 Voltage Standing Wave Ratio.....	22
4.1.2 Similarity in the E plane and H plane Beam sizes.....	25
4.1.3 Symmetry of E plane and H plane Radiation Patterns.....	25
CHAPTER 5: DESIGN OF DOUBLE RIDGED HORN ANTENNA.....	26
5.1 Design of the waveguide section	27
5.2 Design of Coaxial feed line	28
5.3 Optimizing the feed position.....	29
5.4 Design of the flare section	29
5.5 Design of exponentially tapered ridges	30
5.6 Modeling the Back cavity.	31
CHAPTER 6: SIMULATION RESULTS OF DOUBLE RIDGED HORN ANTENNA USING HFSS.....	33
6.1 Double ridged horn antenna for 6-18 GHz	33
6.2 Proposing new type of tapering for the ridges	36
6.3 Novel approach to back cavity design.....	39
CHAPTER 7 : INTRODUCTION TO MICROSTRIP ANTENNA.....	44
7.1 Principle of operation	44
7.2 Transmission Line model	45

7.3 Feeding Techniques	49
7.3.1 Microstrip Line Feed	49
7.3.2 Coaxial Feed	50
7.3.3 Aperture Coupled Feed	51
7.3.4 Proximity Coupled Feed.....	51
7.4 Applications.....	53
7.5 Bandwidth enhancement techniques of patch antenna.....	53
7.5.1 Parasitically coupled (or gap-coupled) patches.....	53
7.5.2 Stacked microstrip patches.....	54
7.5.3 Slotted Microstrip patches.....	56

CHAPTER 8: DESIGN AND SIMULATION RESULTS OF MICROSTRIP PATCH

ANTENNA USING HFSS	57
8.1 Patch antenna at 11.72GHz.....	57
8.2 Stacked patch with a bandwidth of 7 to 12.5GHz.....	61

CHAPTER 9 : CONCLUSION AND FUTURE WORK.....70

BIBLIOGRAPHY.....	74
--------------------------	-----------

APPENDIX

TABLE OF FIGURES

Fig. No	Title of figure	Page No
1.1	Block diagram of conventional antenna	4
1.2	Block diagram of active integrated antenna	5
1.3	Ansoft HFSS Desktop	10
2.1	Radio Telescope	11
2.2	Practical Radio Telescope	12
5.1	Different portions of Horn Antenna	26
5.2	Waveguide portion of Horn Antenna	27
5.3	The co axial feed to the Antenna.	28
5.4	Optimising the feed position.	29
5.5	Flare section of the Horn Antenna.	30
5.6	Exponential Tapered section of the Antenna.	31
5.7	Back cavity of the Horn Antenna.	32
6.1	DRHA designed for 6-18 GHz.	33
6.2	Plot of VSWR against Frequency.	34

6.3	Radiation pattern of the DRHA at different Frequency.	35
6.4	Plot of VSWR against Frequency.	36
6.5	New type of tapering for the ridges of DRHA.	37
6.6	Modified VSWR after changing the tapering of ridges.	37
6.7	Modified radiation patterns after changing the tapering of ridges.	38
6.8	Introducing back fins to the cavity back	39
6.9	Modified VSWR after introducing the back fins	40
6.10	Radiation patterns after introducing the back fins	41
6.11	Magnitude of E-field in the plane of ridges	42
6.12	Surface current distribution	43
6.13	3D polar plot of the designed horn at $\phi=90^\circ$ and $\phi=0^\circ$	43
7.1	Transmission line model of microstrip antenna.	45
7.2	Electric field lines in transmission line model of microstrip antenna.	45
7.3	The structure of microstrip antenna.	46
7.4	Strip line fed patch antenna.	47
7.5	Fringing fields in patch antenna.	47

7.6	Microstrip feed for patch antenna.	49
7.7	Coaxial feed for patch antenna.	50
7.8	Aperture coupled feeding of patch antenna.	51
7.9	Proximity coupling for patch antenna.	51
7.10	Schematic diagram of parasitically coupled microstrip patch antennas.	54
7.11	Schematic diagram of aperture-fed arbitrarily shaped stacked microstrip patches.	55
7.12	Schematic diagram of slotted microstrip patches	56
8.1	Patch antenna for 11.72GHz	57
8.2	Isometric view of Patch antenna for 11.72GHz	58
8.3	Location of feed point: Patch antenna for 11.72GHz	58
8.4	Plot of VSWR against frequency: Patch antenna for 11.72GHz	59
8.5	Plot of S-parameter against frequency: Patch antenna for 11.72GHz	59
8.6	Plot of S-parameter against frequency: Patch antenna for 11.72GHz	60
8.7	The structure of stacked patch antenna (D=18.4mm)	61
8.8	Isometric view of the stacked patch	62
8.9	Modified feed position for the stacked patch	62

8.10	Plot of VSWR for the stacked patch (D=18.4mm)	63
8.11	Plot of S-parameter for the stacked patch (D=18.4mm)	64
8.12	Radiation patterns at different frequencies for the stacked patch (D=18.4mm)	65
8.13	The structure of stacked patch antenna (D=18.4mm)	66
8.14	Isometric view of the stacked patch (D=36.8mm)	66
8.15	Plot of VSWR for the stacked patch (D=36.8mm)	67
8.16	Plot of S-parameter for the stacked patch (D=36.8mm)	68
8.17	Radiation patterns at different frequencies for the stacked patch (D=36.8mm)	69
9.1	Side view of the designed antenna in YZ plane.	71
9.2	Side view of the designed antenna in XZ plane.	72
9.3	Top view of the designed antenna in XY plane.	72
9.4	Isometric view of the designed antenna.	73

CHAPTER 1**INTRODUCTION**

Active antennas provide a new paradigm for designing modern microwave systems. Active antennas can be explained from either the microwave or the antenna point of view. From the microwave engineer's point of view, an active antenna integrates the active RF frontend on the antenna directly. The active device and the antenna are treated as a single entity. This differs from the traditional design methodology where the antenna and RF front-ends were different components connected to standard 50-watt transmission lines or waveguides. The antenna is not only used as a radiating element, but also provides circuit functions, such as filtering, amplifying and oscillating. From the antenna designer's point of view, active antennas overcome some of the drawbacks traditionally related to conventional antennas, such as loss between the RF front-end and the antenna and they provide signal processing functions.

The aim of this project is to design the feed for Active integrated antenna, which should operate in the frequency range of 7GHz to 14GHz. For the design of antenna, we have used the software tool HFSS (High Frequency Structure Simulation), which is generally used for the design and simulation of electromagnetic structures such as waveguide, horn antenna, patch antenna etc. In this project we study the different types of feeds (antennas), which could be used in the Ku band, design the antennas using the software tool HFSS and then simulate them using the same. Based on the results of the simulation we decide which antenna has to be fabricated in order to use it as the feed for the Active integrated antenna. We here study, design and simulate two particular kinds of antennas namely Double Ridged Horn Antenna (DRHA) and Microstrip Antenna, both of them have their respective advantages and disadvantages which are also the limiting factors for their applications. We will design the above mentioned antennas using the software tool HFSS and simulate them for the desired frequency range, compare their performances in the desired frequency range. The comparison is based on the typical performance parameters of electromagnetic structures such as VSWR, radiation patterns, return loss etc. The antenna which is best suited for the desired application is then fabricated.

1.1 KU BAND:

The **K_u band** is a portion of the electromagnetic spectrum in the microwave range of frequencies. This symbol refers to (originally German: Kurz-unten)—in other words, the band directly below the K-band. In radar applications, it ranges from 12-18 GHz according to the formal definition of radar frequency band nomenclature in IEEE Standard 521-2002.

K_u band is primarily used for satellite communications, most notably for fixed and broadcast services, and for specific applications such as NASA's Tracking Data Relay Satellite used for both space shuttle and ISS communications. K_u band satellites are also used for backhauls and particularly for satellite from remote locations back to a television network's studio for editing and broadcasting. The band is split into multiple segments that vary by geographical region by the International Telecommunication Union (ITU). NBC was the first television network to uplink a majority of its affiliate feeds via K_u band in 1983.

1.1.1 ADVANTAGES:

Compared with C-band, K_u band is not similarly restricted in power to avoid interference with terrestrial microwave systems, and the power of its uplinks and downlinks can be increased. This higher power also translates into smaller receiving dishes and points out a generalization between a satellite's transmission and a dish's size. As the power increases, the dish's size can decrease. This is because the purpose of the dish element of the antenna is to collect the incident waves over an area and focus them all onto the antenna's actual receiving element, mounted in front of the dish (and pointed back towards its face); if the waves are more intense, fewer of them need to be collected to achieve the same intensity at the receiving element.

Also, as frequencies increase, parabolic reflectors become more efficient at focusing them. At 12GHz a 1-meter dish is capable of focusing on one satellite while sufficiently rejecting the signal from another satellite only 2 degrees away. This is important because satellites in FSS (Fixed Satellite Service) service (11.7-12.2GHz in the U.S.) are only 2 degrees apart. At 4GHz (C-band) a 3-meter dish is required to achieve this narrow of a focus beam. Note the inverse linear correlation between dish size and frequency. For Ku satellites in DBS (Direct Broadcast Satellite) service (12.2-12.7GHz in

the U.S.) dishes much smaller than 1-meter can be used because those satellites are spaced 9 degrees apart. As power levels on both C and Ku band satellites have increased over the years, dish beam-width has become much more critical than gain.

The K_u band also offers a user more flexibility. A smaller dish size and a K_u band system's freedom from terrestrial operations simplify finding a suitable dish site. For the end users K_u band is generally cheaper and enables smaller antennas (both because of the higher frequency and a more focused beam). K_u band is also less vulnerable to rain fade than the K_a band frequency spectrum.

The satellite operator's Earth Station antenna does require more accurate position control when operating at K_u band due to its much narrower focus beam compared to C band for a dish of a given size. Position feedback accuracies are higher and the antenna may require a closed loop control system to maintain position under wind loading of the dish surface.

1.1.2 DISADVANTAGES :

There are, however, some disadvantages of K_u band system. Especially at frequencies higher than 10 GHz in heavy rain fall areas, a noticeable degradation occurs, due to the problems caused by and proportional to the amount of rainfall (commonly known as "rain fade"). This problem can be mitigated, however, by deploying an appropriate link budget strategy when designing the satellite network, and allocating a higher power consumption to compensate rain fade loss. The K_u band is not only used for television transmission, which some sources imply, but also very much for digital data transmission via satellites, and for voice/audio transmissions.

The higher frequency spectrum of the K_u band is particularly susceptible to signal degradation, considerably more so than C-band satellite frequency spectrum. A similar phenomenon, called "snow fade" (where snow or ice accumulation significantly alters the focal point of a dish) can also occur during winter precipitation. Also, the K_u band satellites typically require considerably more power to transmit than the C-band satellites. Under both "rain fade" and "snow fade" conditions, K_a and K_u band losses can be marginally reduced using super-hydrophobic Lotus effect coatings.

1.2 ACTIVE INTEGRATED ANTENNA:

Active integrated antennas (AIAs) combine prominent features that make them usable for both military and commercial applications. The most important feature is that the antenna and the active device are treated as a single entity, allowing compactness, low cost, low profile, minimum power consumption, and multiple functionalities.

A typical AIA consists of one or more active devices such as diodes (Gunn, IMPATT, Schottky, and varactor) and/or three terminal devices (MESFET, HEMT, or HBT) integrated with planar antennas such as printed dipoles, microstrip patches, bowties, or slot antennas. To realize different functionalities, AIA's can be made frequency tunable, injection locked, or mutually coupled. Choosing the adequate configuration, multiple communication and sensor applications can be realized. This thesis presents theoretical and experimental work, which advances the state of the art in active integrated antennas for microwave and millimeter-wave applications. The block diagram showing the difference between conventional antenna and an active integrated antenna is as shown in figure 1.1 and figure 1.2.

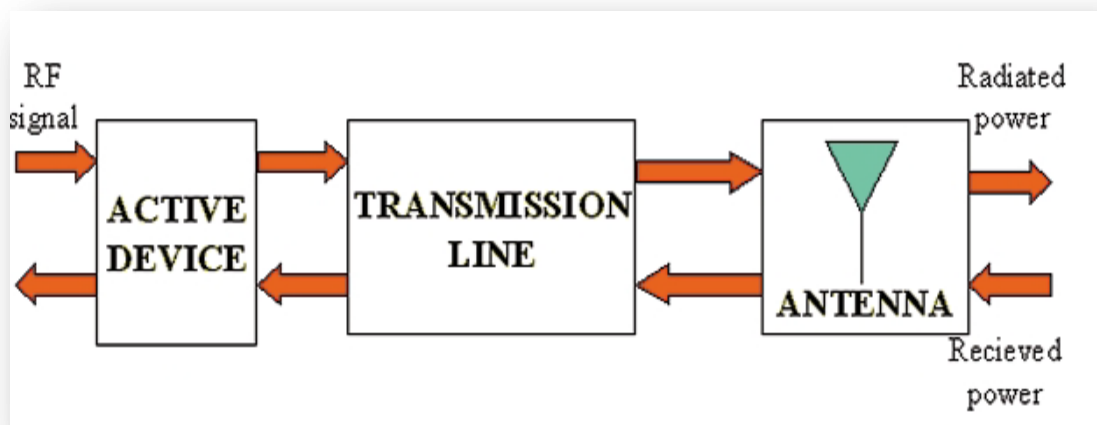


Figure 1.1: Block diagram of conventional antenna

The antenna is not only used as a radiating element, but also provides circuit functions, such as filtering, amplifying and oscillating. From the antenna designer's point of view, active antennas overcome some of the drawbacks traditionally related to conventional antennas, such as loss between the RF front-end and the antenna and they provide signal processing functions.

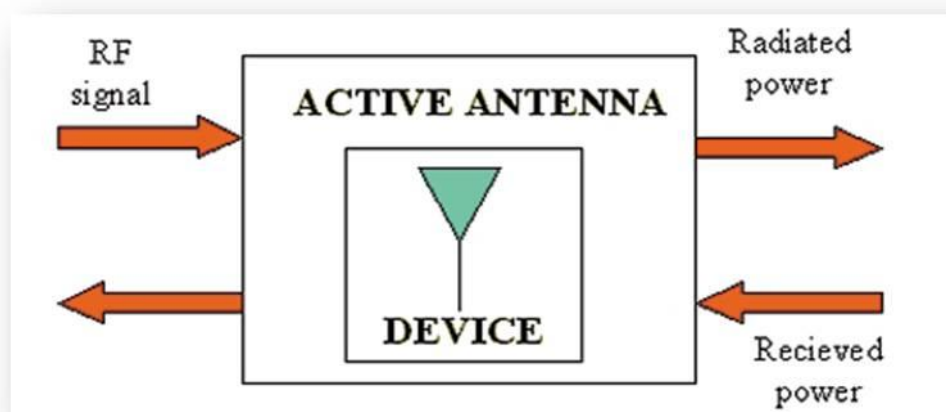


Figure 1.2: Block diagram of active integrated antenna

1.2.1 ACTIVE INTEGRATED ANTENNA CONFIGURATIONS:

1.2.1.1 ACTIVE DEVICES:

Two-terminal devices, e.g. IMPATT diodes and Gunn diodes, as well as three-terminal devices, e.g. MESFETs, HEMTs and HBTs can be used as the active sources. The early development of active integrated antennas at microwave and millimeter-wave frequencies concentrated first on two-terminal devices and then moved to three-terminal devices. Two-terminal devices are suitable for high power applications at millimeter-wave frequencies, but have the disadvantage of low DC-to-RF efficiency. Three terminal devices, on the other hand, have the advantage of high DC-to-RF efficiency but are limited by the lower cutoff frequencies. Three-terminal devices have another advantage of easy integration with planar circuit structure, in either a hybrid or monolithic approach.

1.2.1.2 ANTENNA ELEMENTS:

Recent research in active antennas has mainly concentrated on microstrip patch types, where solid-state devices (usually diodes or FETs) are integrated with microstrip patches resulting in convenient planar, low-cost radiating elements. They are not only the output loads of oscillators but serve also as resonators, determining the oscillation frequency. The input impedance of the antenna element is therefore important information for designing AIAs. Besides the oscillator type AIA, where the active device functions as the oscillator with a passive radiating element at the output port, the amplifier type AIA is also reported. In this case, the active device works as an amplifier

with passive antenna elements at the input or output port. When antenna elements are integrated at input and output ports, the circuit becomes a quasi-optical amplifier. The integration of amplifiers in passive antenna structures increases the antenna gain and bandwidth and improves the noise performance. Active microstrip patch oscillator antennas suffer from narrow bias tuning ranges and large output power variations that can be improved by using varactors connected to the radiating elements.

The majority of active microstrip antennas exhibits limited tuning ranges, high cross polarization levels, and large output power variations. At millimeter-wave frequencies, small patch antenna dimensions cause difficulties during device integration. DC bias lines also cause problems and degrade the performance. There are alternative configurations to the microstrip patch. Each has its pros and cons when applied to AIAs:

- The notch antenna is the planar equivalent to a waveguide horn, and it is capable of very broad impedance bandwidths. Since the notch antenna uses a slot line feed, it is ideal for integration with two terminal devices.
- A planar broadside radiator can also be constructed from a resonant slot line. There are several configurations such as slot line dipoles, loops, or rings. Unlike a microstrip patch, the antenna is a bi-directional radiator, which can be used with polarizer's in spatial. Amplifier applications. In 1993, Kawasaki and Itoh developed a microstrip FET oscillator using a slot antenna. Kormanyos, Katehi, and Rebeiz published in 1994 a CPW-fed active slot antenna. Active slot line antennas integrated with an IMPATT diode were investigated by Luy and Biebl in 1993.
- The inverted microstrip patch is attractive for integrated antennas because it offers two distinct advantages. First, diode or probe insertion does not require drilling through the substrate as in microstrip. This characteristic allows non-destructive device testing and position optimization in inverted microstrip. Second, the inverted substrate can serve as a built-in radome for protection.

1.2.2 ACTIVE INTEGRATED ANTENNA ARRAYS

Originally, the concept of quasi-optical power combining was proposed to combine the output power from an array of many solid-state devices in free-space to overcome the power limitations of individual devices at millimeter-wave frequencies. In fact, the development of novel quasi-optical power combiners has been one of the main

driving forces for the research on AIAs during the past ten years. There are two ways to arrange multiple active antennas. Loosely coupled AIAs are arranged in arrays with a period of at least $\lambda/2$, whereas strongly coupled AIAs, with periods on the order of $\lambda/10$, are referred to as grids. In arrays, mutual coupling is small and each element approximately behaves the same when out of the array.

Many innovative approaches have been proposed for realizing efficient quasi-optical power combining arrays. Among them were beam arrays, grid arrays, patch based arrays, slot-based arrays and monopole probed based arrays. Bi-directional amplifier arrays with both transmitting and receiving capabilities have also been demonstrated. A second harmonic patch antenna Gunn diode combiner showed 10.2% isotropic conversion efficiency at 18.6 GHz. A 5×5 array of MESFET oscillators was combined in a planar Fabry-Perot cavity at 10 GHz with an ERP of 20.7 watts and a directivity of 16.4 dB. The largest number of devices combined so far was in a planar grid oscillator in which the individual output powers were combined in free space. This grid oscillator, which operated at 5 GHz, contained 100 MESFETs and similar oscillators using 36 devices were built at C-, Ku-and Ka-bands.

For a beam steering power combining array, varactor-tuned active antennas with wide tuning ranges are used to control the phase distribution in the array and to keep minimal power variation over the collective locking range of the active elements. Several other wideband varactor tuned arrays have also been developed using varactor tunable notch antennas and tunable power combiners and quasi-optical grid VCOs consisting of two active grids. The active planar structure is versatile in that different components may be designed separately and then combined into one overall system by stacking the two-dimensional grids.

1.2.3 APPLICATIONS OF ACTIVE INTEGRATED ANTENNAS:

The potential for applications of AIAs is broad. Functions, which would normally occur in a circuit away from the antenna such as detection, modulation, mixing, and amplifying, occur within the AIA. Comparing to the conventional approach, size, weight, and costs can be reduced.

Applications for active antennas in radar and communications are listed in Table 1.1.

AUTOMOTIVE APPLICATIONS	
Doppler radar	Velocity over ground detection
Polarization sensitive radar	Road condition detection
FM-CW or pulsed radar	Distance measurements to neighboring cars
Interferometer radar	Blind area surveillance Side-crash prediction
COMMUNICATION AND SENSOR APPLICATIONS	
Doppler radar	Velocity over ground detection
Polarization sensitive radar	Road condition detection
FM-CW or pulsed radar	Distance measurements to neighboring cars
Interferometer radar	Blind area surveillance Side-crash prediction

Table 1.1 Applications for active antennas

Civil applications require designated frequency bands accessible to everyone. For this purpose, ISM (Industrial, medical, and scientific) bands are defined. Most sensor applications use the bands at 433 MHz, 2.4 GHz, 5.8 GHz, and 24 GHz. Automotive applications can be found in the 24 GHz, 60 GHz, and the 76 GHz radar bands.

1.3 High Frequency Structure Simulator (HFSS):

HFSS is a high-performance full-wave electromagnetic (EM) field simulator for arbitrary 3D volumetric passive device modeling that takes advantage of the familiar Microsoft Windows graphical user interface. It integrates simulation, visualization, solid modeling, and automation in an easy-to-learn environment where solutions to your 3D EM problems are quickly and accurately obtained. Ansoft HFSS employs the Finite Element Method (FEM), adaptive meshing, and brilliant graphics to give you unparalleled performance and insight to all of your 3D EM problems. Ansoft HFSS can be used to calculate parameters such as S Parameters, Resonant Frequency, and Fields.

The name HFSS stands for High Frequency Structure Simulator. Ansoft pioneered the use of the Finite Element Method (FEM) for EM simulation by developing/implementing technologies such as tangential vector finite elements, adaptive

meshing, and Adaptive Lanczos-Pade Sweep (ALPS). HFSS continues to lead the industry with innovations such as Modes-to-Nodes and Full-Wave Spice.

HFSS is an interactive simulation system whose basic mesh element is a tetrahedron. This allows you to solve any arbitrary 3D geometry, especially those with complex curves and shapes, in a fraction of the time it would take using other techniques.

1.3.1 Ansoft HFSS Features:

Capabilities:

- Accurate full wave simulation
- Import/export of 3D structures
- Inclusion of skin effect losses
- Direct and iterative matrix solvers
- Eigen mode and matrix solver
- Automatic adaptive mesh generation and refinement
- Adaptive Lanczos-Pade Sweep for fast frequency sweep

Solution Data (Visualization):

- S-, Y-, Z-parameter matrix (2D plot, Smith Chart)
- Port characteristic impedance
- Current, E-field, H-field (3D static and animated field plot in vector display or magnitude display)
- Far-field calculation (2D, 3D, gain, radiation pattern)
- Material losses, radiation losses

1.3.2 Ansoft HFSS Desktop:

The Ansoft HFSS Desktop provides an intuitive, easy-to-use interface for developing passive RF device models. Creating designs, involves the following:

- i. **Parametric Model Generation** – creating the geometry, boundaries and excitations.
- ii. **Analysis Setup** – defining solution setup and frequency sweeps.
- iii. **Results** – creating 2D reports and field plots.
- iv. **Solve Loop** - the solution process is fully automated.

The illustration of the general design procedure using HFSS is as shown in figure1.1.

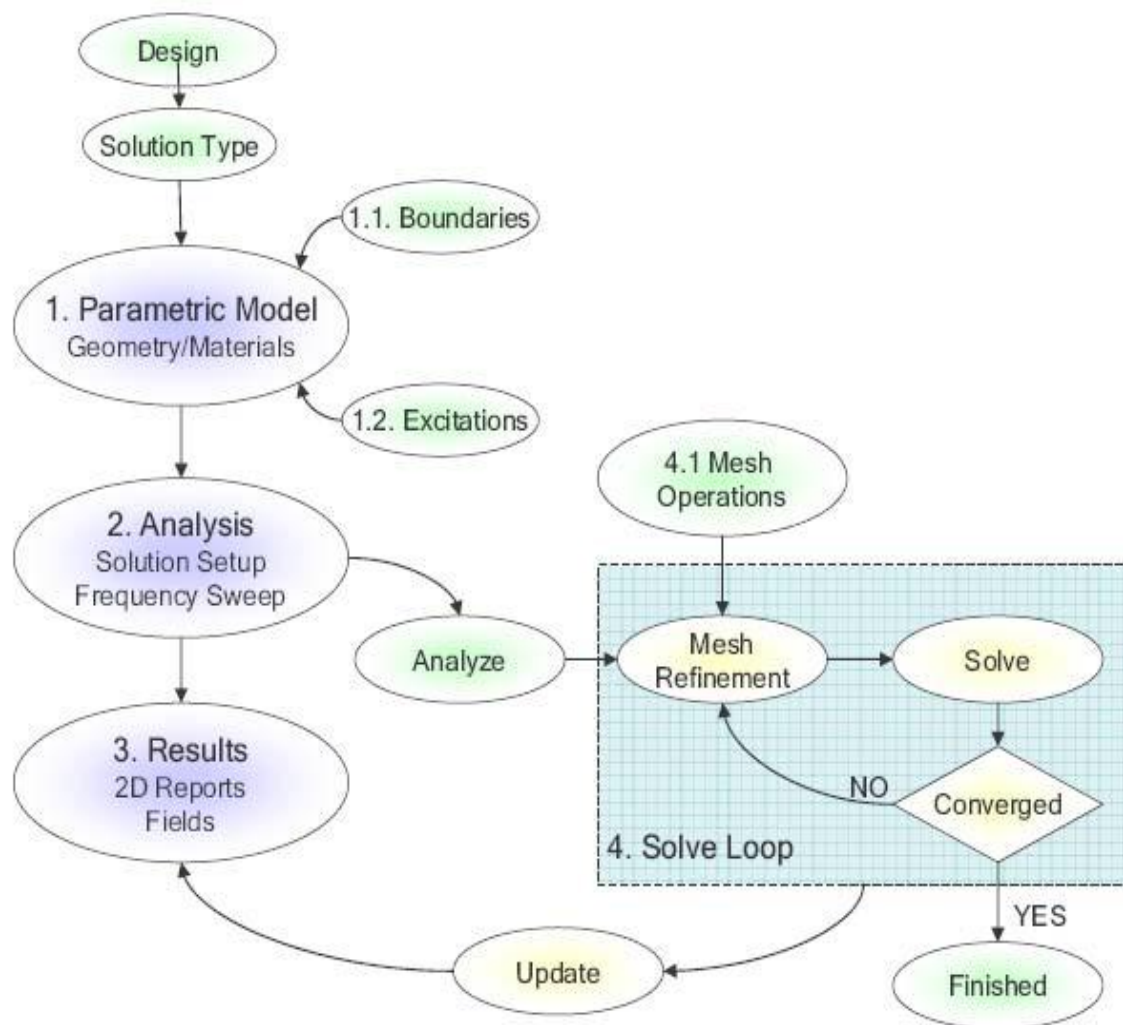


Figure 1.3: Ansoft HFSS Desktop

CHAPTER 2**BACKGROUND**

RRI (Raman Research Institute) is building a new radio telescope to be fitted with a 7-14 GHz 32 element array receiver. The first element of the receiver is a radiating element that impedance matches the free space wave converging at the antenna focus to the input of the LNA, set on a microstrip. Good matching needs to be achieved over a broad band for effective use of the LNA. This BE project aims to achieve this. As a part of this project, we plan to design and simulate two kinds of radiating systems: a conventional pyramidal ridge horn antenna and a modern planar stacked-patch antenna. The specific project goals are to achieve better than 2 VSWR over at least 7-14 GHz, with good E and H plane symmetry and as much as possible similar directivity over the wide band.

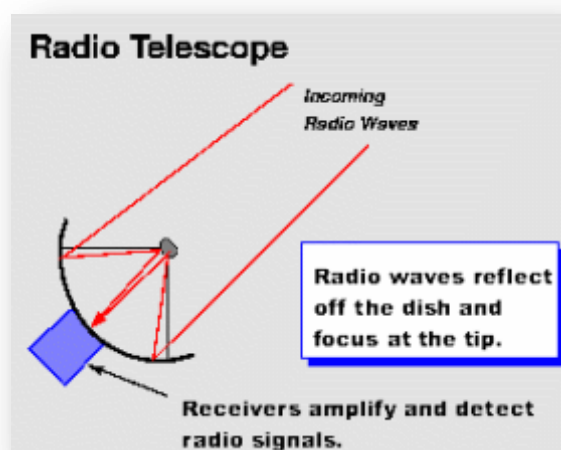
2.1 Radio Telescopes:

Figure 2.1: Radio Telescope

A radio telescope is a form of directional radio antenna used in radio astronomy. The same types of antennas are also used in tracking and collecting data from satellites and space probes. In their astronomical role they differ from optical telescopes in that they operate in the radio frequency portion of the electromagnetic spectrum where they

can detect and collect data on radio sources. Radio telescopes are typically large parabolic ("dish") antennas used singly or in an array. Radio observatories are preferentially located far from major centers of population to avoid electromagnetic interference (EMI) from radio, TV, radar, and other EMI emitting devices. This is similar to the locating of optical telescopes to avoid light pollution, with the difference being that radio observatories are often placed in valleys to further shield them from EMI as opposed to clear air mountain tops for optical observatories.

Radio telescopes are used to study naturally occurring radio emission from stars, galaxies, quasars, and other astronomical objects between wavelengths of about 10 meters (30 megahertz [MHz]) and 1 millimeter (300 gigahertz [GHz]). At wavelengths longer than about 20 centimeters (1.5 GHz), irregularities in the ionosphere distort the incoming signals. This causes a phenomenon known as scintillation, which is analogous to the twinkling of stars seen at optical wavelengths. The absorption of cosmic radio waves by the ionosphere becomes more important as wavelength increases. At wavelengths longer than about 10 meters, the ionosphere becomes opaque to incoming signals. Radio observations of the cosmic sources at these wavelengths are difficult from ground-based radio telescopes. Below wavelengths of a few centimeters, absorption in the atmosphere becomes increasingly critical. At wavelengths shorter than 1 centimeter (30 GHz), observations from the ground are possible only in a few specific wavelength bands that are relatively free of atmospheric absorption. However, between 1 and 20 cm, the atmosphere and ionosphere introduce only minor distortions in the incoming signal. Sophisticated signal processing can be used to correct for these effects, so that the effective angular resolution and image quality is limited only by the size of the instrument.

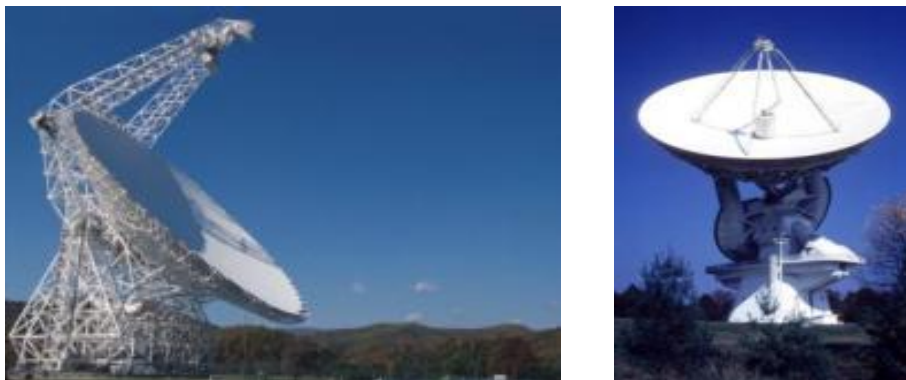


Figure 2.2: Practical Radio telescope

2.11 Principles of Operation:

Radio telescopes vary widely, but they all have two basic components: (1) a large radio antenna and (2) a sensitive radiometer or radio receiver. The sensitivity of a radio telescope--i.e., the ability to measure weak sources of radio emission--depends on the area and efficiency of the antenna and the sensitivity of the radio receiver used to amplify and detect the signals. For broadband continuum emission the sensitivity also depends on the bandwidth of the receiver. Because cosmic radio sources are extremely weak, radio telescopes are usually very large and only the most sensitive radio receivers are used. Moreover, weak cosmic signals can be easily masked by terrestrial radio interference, and great effort is taken to protect radio telescopes from man-made interference.

The most familiar type of radio telescope is the radio reflector consisting of a parabolic antenna--the so-called dish or filled-aperture telescope--which operates in the same manner as a television-satellite receiving antenna to focus the incoming radiation onto a small antenna referred to as the feed, a term that originated with antennas used for radar transmissions. In a radio telescope the feed is typically a waveguide horn and transfers the incoming signal to the sensitive radio receiver. Cryogenically cooled solid-state amplifiers with very low internal noise are used to obtain the best possible sensitivity.

In some radio telescopes the parabolic surface is equatorially mounted, with one axis parallel to the rotation axis of the Earth. Equatorial mounts are attractive because they allow the telescope to follow a position in the sky as the Earth rotates by moving the antenna about a single axis parallel to the Earth's axis of rotation. But equatorially mounted radio telescopes are difficult and expensive to build. In most modern radio telescopes a digital computer is used to drive the telescope about the azimuth and elevation axes to follow the motion of a radio source across the sky.

Observing times up to many hours are expended and sophisticated signal-processing techniques are used to detect astronomical radio signals that are as much as one million times weaker than the noise generated in the receiver. Signal-processing and analysis are usually done in a digital computer.

In the simplest form of radio telescope, the receiver is placed directly at the focal point of the parabolic reflector, and the detected signal is carried by cable along the feed

support structure to a point near the ground where it can be recorded and analyzed. However, it is difficult in this type of system to access the instrumentation for maintenance and repair, and weight restrictions limit the size and number of individual receivers that can be installed on the telescope. More often, a secondary reflector is placed in front (Cassegrain focus) or behind (Gregorian focus) of the focal point of the paraboloid to focus the radiation to a point near the vertex of the main reflector. Multiple feeds and receivers may be located at the vertex where there is more room, less stringent weight restrictions and where access for maintenance and repair is more straightforward. Secondary focus systems also have the advantage that both the primary and secondary reflecting surfaces may be carefully shaped so as to improve the gain over that of a simple parabolic antenna.

While earlier radio telescopes used a symmetric tripod or quadrupoid structure to hold the feed or secondary reflector, such an arrangement blocks some of the incoming radiation, and the reflection of signals from the support legs back into the receiver distorted the response. In newer designs, the feed or secondary reflector is placed off axis and does not block the incoming signal. Off axis radio telescopes are thus more sensitive and less affected by terrestrial interference reflected off of the support structure into the feed.

The performance of a radio telescope is limited by various factors: the accuracy of a reflecting surface that may depart from the ideal shape because of manufacturing irregularities; the effect of wind load; thermal deformations that cause differential expansion and contraction; and deflections due to changes in gravitational forces as the antenna is pointed to different parts of the sky. Departures from a perfect parabolic surface become important when they are a few percent or more of the wavelength of operation. Since small structures can be built with greater precision than larger ones, radio telescopes designed for operation at millimeter wavelength are typically only a few tens of meters across, whereas those designed for operation at centimeter wavelengths range up to 100 meters in diameter.

Traditionally, the effect of gravity has been minimized by designing the movable structure to be as stiff as possible in order to reduce the deflections resulting from gravity. A more effective technique, based on the principle of homology, allows the structure to

deform under the force of gravity, but the cross section and weight of each member of the movable structure are chosen to cause the gravitational forces to deform the reflecting structure into a new paraboloid with a slightly different focal point. It is then necessary only to move the feed or secondary reflector to maintain optimum performance. Homologous designs have become possible only since the development of computer-aided structural analysis known as finite element analysis.

Radio telescopes are used to measure broad-bandwidth continuum radiation as well as spectroscopic features due to atomic and molecular lines found in the radio spectrum of astronomical objects. In early radio telescopes, spectroscopic observations were made by tuning a receiver across a sufficiently large frequency range to cover the various frequencies of interest. This procedure, however, was extremely time-consuming and greatly restricted observations. Modern radio telescopes observe simultaneously at a large number of frequencies by dividing the signals up into as many as several thousand separate frequency channels that may range over a total bandwidth of tens to hundreds of megahertz.

The most straightforward type of radio spectrometer employs a large number of filters, each tuned to a separate frequency and followed by a separate detector to produce a multichannel, or multifrequency, receiver. Alternatively, a single broad-bandwidth signal may be converted into digital form and analyzed by the mathematical process of autocorrelation and Fourier transformation (see below). In order to detect faint signals, the receiver output is often averaged over periods of up to several hours to reduce the effect of noise generated in the receiver.

CHAPTER 3**LITERATURE SURVEY**

It is a well known fact that the traditional 1-18 GHz Double Ridge Guide Horn (DRGH) antenna suffers from pattern deterioration above 12 GHz. At these frequencies, instead of maintaining a single main lobe radiation pattern, the pattern splits up into four lobes. It was shown in the literature that higher order modes are causing the pattern breakup. A benchmark study is performed to establish the performance of typical current and historic 1-18 GHz DRGH antennas. The performance of the antennas are evaluated in terms of gain, VSWR and radiation patterns. An improved 1-18 GHz DRGH antenna is presented. It also consists of significantly fewer parts, reducing the possibility of performance deterioration due to gaps between parts.

The traditional 1-18 GHz DRGH antenna was adapted from designs by Kerr for a 1-12 GHz horn [1]. The 1-18 GHz antenna is used extensively in antenna and Electromagnetic Compatibility (EMC) measurements and in feeds for reflector systems. In these applications, a well behaved antenna pattern is an absolute necessity. Standards such as MIL-STD-461F, ANSI-C 63.2-1987 and CISPR 16-1-4 specifies wideband 1- 18 GHz DRGH antennas suitable for radiated emissions and susceptibility testing [2]-[4].

It is well known that the pattern of this antenna deteriorates in the upper frequency band above 12 GHz, [5]-[7]. The main beam splits into four large side lobes and the bore sight gain reduces by approximately 6 dB. This makes the use of these antennas for EMC and measurement applications less desirable. A number of tolerance and sensitivity studies using commercial numerical solvers viz. FEKO, CST and HFSS followed to investigate the causes of the pattern deterioration [8]-[11]. Subsequently, a new open boundary type of horn design that produces a single main beam across the band was developed [10]-[12]. The new design included a number of changes:

- The dielectric sidewalls were removed to improve the radiation characteristics of the DRGH antenna above 12 GHz. It was found in [10] that the dielectric rather than the metallic strips of the sidewalls causes an on axis gain drop at 18 GHz.

The removal of the sidewalls was at the expense of the low frequency (1-4 GHz) performance – the beam widths increased and the gain decreased.

- The ridges and the conducting flares (top and bottom) were redesigned to reduce edge diffraction and improve the aperture match. The ridge's curvature was modified to a linear section near the feed point, an intermediate exponential section and a circular section near the aperture [11]. The flare outlines were changed to eliminate sharp corners due to the removal of the sidewalls.
- The coax to ridge waveguide transition was redesigned and mode suppression fins were included to prevent the excitation of higher order modes. A cavity was included (just behind the mode suppression fins) to reduce the VSWR [12].
- The antenna was finally scaled down to further improve the high frequency behavior.

These changes significantly improved the antenna performance at the higher frequencies, but by discarding the dielectric sidewalls and scaling the antenna to improve the high frequency behaviour of the antenna, the performance in the low frequency band deteriorated. The alternative open boundary horn design therefore suffers from an increase in VSWR and a decrease in gain between 1 and 3 GHz.

In addition to the pattern and gain performance issues, the traditional DRGH antenna also suffers from performance deterioration when incorrect assembly or manufacturing tolerances causes gaps between individual parts. Recently in [13] it was shown that gaps in the order of 0.5-0.05 mm between various subsections in the waveguide launcher assembly leads to severe resonance effects in bore sight gain and VSWR, and it was found that the coaxial feeding section is especially sensitive.

Finally, a benchmark study compares the performances of the different variations of 1-18 GHz DRGH antennas and illustrated the improved gain, VSWR, and pattern performance of the proposed antenna compared to the other DRGH antennas in literature. Here the design, simulation, of a double-ridged antenna is presented. The designed double-ridged antenna is most suitable as a feed element in reflectors of the radar systems and EMC applications. The designed antenna has a voltage standing wave ratio (VSWR) less than 2 for the frequency range of 8–18 GHz. Moreover, the proposed antenna exhibits satisfactory far-field radiation characteristics in the entire operating bandwidth. A coaxial line to rectangular double-ridged waveguide transition is introduced for coaxial

feeding of the designed antenna. The proposed antenna is simulated with commercially available packages such as CST microwave studio and Ansoft HFSS in the operating frequency range. Simulation results for the VSWR, radiation patterns, and gain of the designed antenna over the frequency band 8–18 GHz are presented and discussed. Broadband, ultra wide band and high gain antennas are one of the most important devices for microwave and millimeter wave applications, electromagnetic compatibility testing, and standard measurements [17–25]. The proposed antenna is similar to horn antennas.

The conventional horn antennas have a limited bandwidth. To extend the maximum practical bandwidth of these antennas, ridges are introduced in the flare section of the antenna. The idea of using ridges in waveguides was adopted in horn by Walton and Sundberg [26], and completed by Kerr in early 1970 when they suggested the use of a feed horn launcher whose dimensions were found experimentally [27]. This is commonly done in waveguides to increase the cutoff frequency of the second propagating mode (TE₁₁) and thus expands the single-mode range before higher order modes occur [28–30]. In [31,32], an E-plane sectoral horn for broadband application using a double-ridged antenna is provided.

A detailed investigation on 1–18 GHz broadband pyramidal double-ridge horn (DRH) antenna was reported in [33]. As indicated in that paper there is some deterioration in the radiation pattern at higher frequencies. In [34], a broadband electromagnetic compatibility pyramidal DRH antenna for 1 to 14 GHz was reported by Botello, Aguilar and Ruiz. An improved design of the double-ridged pyramidal horn antenna was presented in [35]. Another design of the double ridged pyramidal horn antenna in the 1–18 GHz frequency range with redesigned feeding section was presented in [36] where several modifications were made in the structure of a conventional double ridged guide horn antenna.

In this paper, based on the double-ridged rectangular waveguide, a double-ridged antenna including a 50Ω coaxial feed input is proposed. Accordingly, a waveguide transition structure for the single-mode, the TE₁₀ mode, with low return loss performance and a new technique for synthesizing the exponential taper is presented. The proposed antenna is simulated with commercially available packages such as Ansoft HFSS which is based on the finite

element method and CST microwave studio which is based on the finite integral technique. Simulation results for the VSWR, gain, and radiation patterns of the designed antenna at various frequencies are presented.

A rectangular microstrip patch antenna has been investigated and its performance has been analyzed with the aid of HFSS. An additional rectangular conductive plate of comparable dimensions was placed above the patch in order to enhance the bandwidth. The package was used to analyze the effect of the top patch, in particular the variation of VSWR with two parameters, namely the distance between the two patches and the size of the upper patch. A bandwidth of 11% for $VSWR < 2$ has been achieved for stacked rectangular patch designed to operate in the S-band when a dielectric of thickness one centimeter and relative permittivity $\epsilon_r = 2.6$ has been taken into consideration.

A microstrip antenna possesses many advantages such as low profile, light weight, small volume, conformal and mass production in addition to low cost [37,38]. It has attracted increasing attention of many researchers to investigate this type of antenna or arrays of various configurations to meet various practical applications. The analysis and design of various -shapes of microstrip antenna mounted on different structures has been extensively reviewed [39]. However, one of the restrictions of these antennas that limit their wide applications is the intrinsic narrow bandwidth [40].

A microstrip antenna consists of a sandwich of two parallel conducting layers separated by a single thin dielectric substrate. The lower conductor functions as a ground plane and the upper conductor represent the antenna radiating part. This is a simple configuration that is rugged and relatively easy to fabricate, but it is limited in its bandwidth. The bandwidth limit is 0.5%-2%. Nowadays several methods have been attempted to increase the bandwidth. One effective method to overcome this problem is to add a second patch in front of the basic one resulting in the so called dual patch microstrip antenna. The concept of stacking patches is realized through electromagnetic coupling form which gives bandwidth enhancement [41]. It has been shown that the obtainable bandwidth of a microstrip antenna is approximately proportional to its volume [42]. However, it is possible to increase the bandwidth of microstrip antenna by simply using thicker substrates. This technique introduces several problems. A thicker substrate will support surface waves, which will deteriorate the radiation pattern as well as reduce

the radiation efficiency. Also problems with the feeding technique of the antenna arise. In addition, depending upon the z-direction, higher order modes may arise, introducing further distortions in the pattern and impedance characteristics. In view of the above problems, electromagnetic coupling (instead of direct coupling) has been studied as a possible feed technique for electrically thick microstrip antennas [43]. The basic geometry of the stacked dual-patch electromagnetic coupled microstrip antenna is shown in Fig. 2. The top and bottom patches are referred to as the radiating patch and the feeding patch, respectively. Electromagnetic coupling technique applied for microstrip patches was first proposed by Saban, who has reported experimental results in the frequency range of 2-4 GHz. on electromagnetic coupled patches [44].

HFSS has been used to analyze various types of microstrip antennas. Here, it is used to analyze single and stacked rectangular microstrip patch antennas. The impedance locus and the radiation pattern are the dominant characteristics analyzed by the package. In order to demonstrate the performance of the package in analyzing these types of antennas, a comparison has been carried out between previously published results that have been obtained by different approaches. For a single patch microstrip antenna the well-known work published by Lo [45, 46] was studied where the experimental data of impedance locus and the radiation pattern were in good agreement with the theory. The impedance loci of this antenna with three different feed locations were computed by the MW-package. There is good agreement between the computed and the published results shown in figures 3a and 3b respectively. The radiation pattern for both E_ϕ and E_θ in the same operating (0,1) mode has been computed for each of the two cuts, $\phi=0$ (Fig.3c) and $\phi=90$ (Fig.3e). It is seen that there is excellent agreement between the published radiation pattern of the two cuts one as shown in Fig.3d and f respectively.

CHAPTER 4**INTRODUCTION TO
DOUBLE RIDGED HORN ANTENNA**

A horn antenna or microwave horn is an antenna that consists of a flaring metal waveguide shaped like a horn to direct radio waves in a beam. An advantage of horn antennas is that since they have no resonant elements, they can operate over a wide range of frequencies, a wide bandwidth. The usable bandwidth of horn antennas is typically of the order of 10:1. The ridges are introduced to the waveguide section in order to increase the bandwidth of the waveguide. The ridges in the flare section of the horn antenna as well as the waveguide section are introduced in order to enhance the fundamental mode of excitation (in case of double ridged horn which is TE₁₀ or TE₀₁). The incorporation of the ridges also suppresses the other higher order modes of excitation. The double ridged horn antenna (DRHA) does have the single polarization.

Horn antennas are widely used since they have special features of relative simple construction, easy excitation, high directivity performance, and high peak power handling capability. They are commonly employed as feed elements in satellite tracking systems or communication dishes and serve as standard antenna for calibration and gain measurements. Since regular horn antenna exhibits limited bandwidth, due to the inherent modal properties of waveguides, the most common method to broaden the maximum usable bandwidth is to ridge-load the flare part of the antenna, similar to ridges in a waveguide mode (TE₁₀) and thus expands the single mode range before higher order modes occur. The idea of using ridges in waveguides was adopted in horn by Walton and Sundberg, and completed by Kerr in early 1970. Double ridged horn (DRH) antenna has been the most common broadband horn in the fields of EMC, probing and standard measurement over half a century. In the late 2003, it was reported that the conventional DRH antennas suffer from a major problem in their radiation pattern and broadside gain especially at higher frequencies. This deficiency has become the motivation of research to design a practical DRH antenna in high frequency.

4.1 Design Constraints:

Antennas are often big, ugly, and usually need to be high and on top of the product or around the edges where the other internal components, end user and environment are less likely to interfere with antenna performance. When antennas are built its performance has to be compromised with lot of antenna quality measuring parameters. Antenna measurement techniques refer to the testing of antennas to ensure that the antenna meets specifications or simply to characterize it. Typical parameters of antennas are gain, radiation pattern, beam width, polarization, impedance, VSWR, E plane and H plane Beam sizes, and symmetry in e plane and H plane radiation Pattern.

The important design constraints that are considered for designing an electromagnetic radiating structure are as follows

- VSWR.
- Similarity of E plane Beam sizes.
- Similarity of H plane Beam sizes.
- E and H plane radiation symmetry

Antenna delivers best performance if it achieves the above said parameters. HFSS deals with varying the antenna dimensions and simulating the results so that better performance is achieved. The significance of the antenna parameters are described below.

4.1.1 Voltage Standing Wave Ratio (VSWR):

The SWR is usually defined as a voltage ratio called the VSWR, (voltage standing wave ratio). For example, the VSWR value 1.2:1 denotes maximum standing wave amplitude that is 1.2 times greater than the minimum standing wave value. It is also possible to define the SWR in terms of current, resulting in the ISWR, which has the same numerical value. The power standing wave ratio (PSWR) is defined as the square of the VSWR.

SWR is used as an efficiency measure for transmission lines, electrical cables that conduct radio frequency signals, used for purposes such as connecting radio transmitters and receivers with their antennas, and distributing cable television signals. A problem with transmission lines is that impedance mismatches in the cable tend to reflect

the radio waves back toward the source end of the cable, preventing all the power from reaching the destination end. SWR measures the relative size of these reflections. An ideal transmission line would have an SWR of 1:1, with all the power reaching the destination and no reflected power. An infinite SWR represents complete reflection, with all the power reflected back down the cable. The SWR of a transmission line can be measured with an instrument called an SWR meter, and checking the SWR is a standard part of installing and maintaining transmission lines. The voltage component of a standing wave in a uniform transmission line consists of the forward wave (with amplitude V_f) superimposed on the reflected wave (with amplitude V_r). Reflections occur as a result of discontinuities, such as an imperfection in an otherwise uniform transmission line, or when a transmission line is terminated with other than its characteristic impedance. The reflection coefficient Γ is defined thus:

$$\Gamma = \frac{V_r}{V_f}.$$

Γ is a complex number that describes both the magnitude and the phase shift of the reflection. The simplest cases, when the imaginary part of Γ is zero, are:

- $\Gamma = -1$: maximum negative reflection, when the line is short-circuited,
- $\Gamma = 0$: no reflection, when the line is perfectly matched,
- $\Gamma = +1$: maximum positive reflection, when the line is open-circuited.

For the calculation of VSWR, only the magnitude of Γ , denoted by ρ , is of interest. Therefore, we define

$$\rho = |\Gamma|.$$

At some points along the line the two waves interfere constructively, and the resulting amplitude V_{\max} is the sum of their amplitudes:

$$V_{\max} = V_f + V_r = V_f + \rho V_f = V_f(1 + \rho).$$

At other points, the waves interfere destructively, and the resulting amplitude V_{\min} is the difference between their amplitudes:

$$V_{\min} = V_f - V_r = V_f - \rho V_f = V_f(1 - \rho).$$

The voltage standing wave ratio is then equal to:

$$VSWR = \frac{V_{\max}}{V_{\min}} = \frac{1 + \rho}{1 - \rho}.$$

As ρ , the magnitude of Γ , always falls in the range [0,1], the VSWR is always $\geq +1$.

The SWR can also be defined as the ratio of the maximum amplitude of the electric field strength to its minimum amplitude, E_{\max}/E_{\min} .

The most common case for measuring and examining SWR is when installing and tuning transmitting antennas. When a transmitter is connected to an antenna by a feed line, the impedance of the antenna and feed line must match exactly for maximum energy transfer from the feed line to the antenna to be possible. The impedance of the antenna varies based on many factors including: the antenna's natural resonance at the frequency being transmitted, the antenna's height above the ground, and the size of the conductors used to construct the antenna.

When an antenna and feed line do not have matching impedances, some of the electrical energy cannot be transferred from the feed line to the antenna. Energy not transferred to the antenna is reflected back towards the transmitter. It is the interaction of these reflected waves with forward waves which causes standing wave patterns. Reflected power has three main implications in radio transmitters: Radio Frequency (RF) energy losses increase, distortion on transmitter due to reflected power from load and damage to the transmitter can occur.

4.1.2 Similarity of E-Plane and H-Plane Beam sizes:

For a linearly-polarized antenna, this is the plane containing the electric field vector and the direction of maximum radiation. The electric field or "E" plane determines the polarization or orientation of the radio wave. For a vertically-polarized antenna, the E-plane usually coincides with the vertical/elevation plane. For a horizontally-polarized antenna, the E-Plane usually coincides with the horizontal/azimuth plane. E-plane and H-plane should be 90 deg apart.

In the case of the same linearly polarized antenna, this is the plane containing the magnetic field vector and the direction of maximum radiation. The magnetizing field or "H" plane lies at a right angle to the "E" plane. For a vertically polarized antenna, the H-plane usually coincides with the horizontal/azimuth plane.

4.1.3 Symmetry of E-plane and H-plane radiation Patterns:

The symmetry of the E-plane and H-plane radiation patterns is another design constraint, which is automatically fulfilled if there is acceptable similarity of the E-plane and H-plane beam sizes. However the symmetry of the E-plane and H-plane radiation patterns depend upon the dimensions of the aperture section that is if the aperture is symmetric we expect the E-plane and H-plane radiation patterns to be also symmetric. The symmetry of E-plane and H-plane as explained earlier is determined by observing the radiation patterns of the design at various frequencies. The comparison is based on the beam widths at different levels for example 3dB beam width, 10 dB beam width , 15 dB beam width etc. We are intended to observe the far field radiation patterns of the design, and a spherical far field setup is inserted in HFSS.

CHAPTER 5**DESIGN OF DOUBLE RIDGED HORN ANTENNA**

A horn antenna constitutes the following sections in its design as shown in the above picture. Its complete design includes design of waveguide section, flare section, tapered section, feed point, the back cavity. Designing any section primarily consists of deciding the dimensions of each section mentioned. Each dimension decision is going to affect the performance of the antenna. The dimensions are mainly decided on the basis of the frequency range in which the antenna is being operated. The design part of each section is explained below:

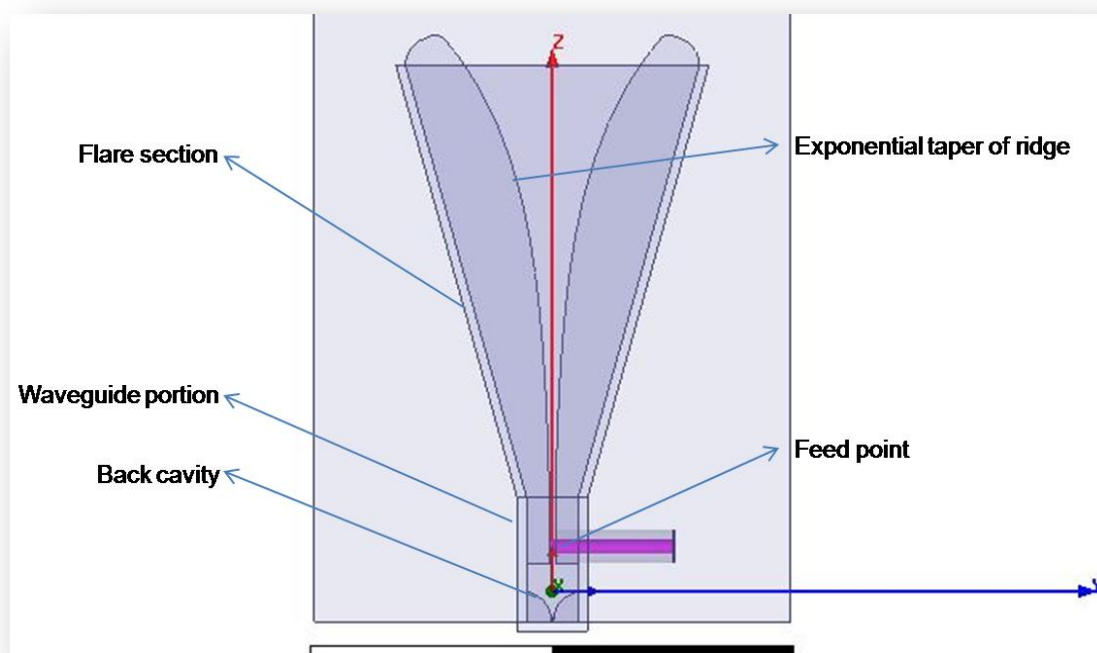


Figure 5.1: Different portions of the horn antenna

Each section of the horn antenna is designed as per the requirements, based on the relevant theoretical equations as explained in the further sections.

5.1 Design of the waveguide section:

Rectangular waveguide is chosen to wave propagation in case of horn antenna. Its length breadth and height are decided accordingly to the desired cutoff frequency and the mode of operation. The waveguide for our design operates in its dominant TE₁₀ mode with cut off frequency 6 GHz.

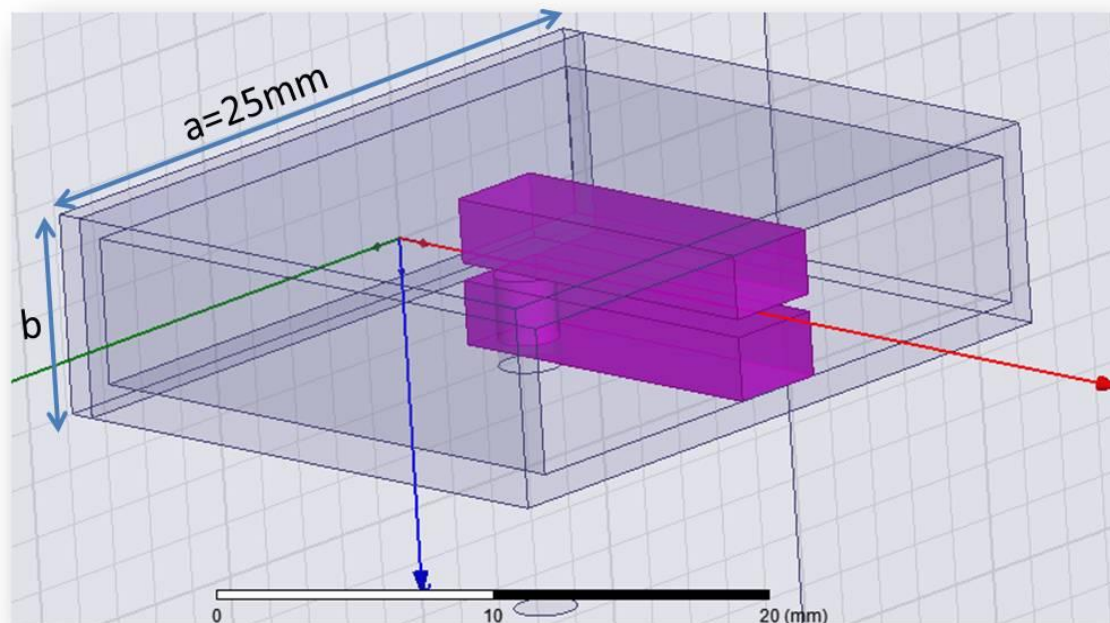


Figure 5.2: The waveguide portion of the horn antenna

The larger dimensions of the waveguide is to be decided on the relation

$$a = \lambda/2$$

Where λ corresponds to the lower frequency of desired bandwidth.

λ for our desired operation is

$$\frac{c}{f} = \frac{3 \cdot 10^8}{6 \cdot 10^9} = 50 \text{mm.}$$

Which gives $a = \lambda/2 = 25 \text{mm.}$

5.2 Design of Coaxial feed line:

Feeding the waveguide for the input power is through coaxial feed. Coaxial feed has coaxial cable with inner and outer conductor with dielectric substance between the conductors.

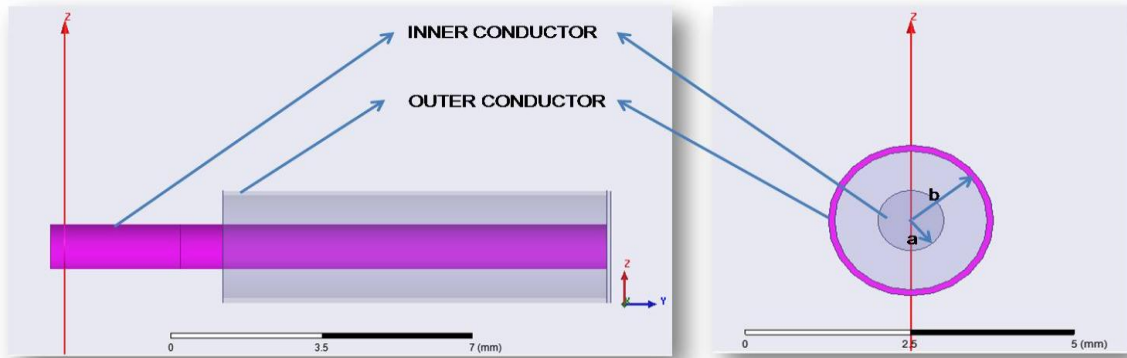


Figure 5.3: The Coaxial feed line to the antenna.

The characteristic impedance of such a feed satisfies the following relation.

$$Z_o = \frac{138}{\sqrt{\mu_r}} \log \frac{b}{a} \text{ ohm}$$

Where b is the radius of the outer conductor and the a is the radius of the inner conductor.

The dielectric substance used is Teflon in most of the cases ($\mu_r = 2.3$). Normally available coaxial cable has 50 or 75 as characteristic impedance. We have chosen 50 ohm coaxial cable as feed to the rectangular waveguide. Here the inner conductor of the coaxial connector extends through the dielectric and is soldered to the opposite ridge, while the outer conductor is connected to the base ridge. The main advantage of this type of feeding scheme is that the feed can be placed at any desired location inside the patch in order to match with its input impedance. This method of feeding is easy to fabricate and has low spurious radiation. However, the major disadvantage is that it is difficult to model since a hole has to be drilled in the substrate and the connector protrudes outside the ground plane, thus not making it completely planar for thick substrate. In thicker substrates, the increased probe length makes the input impedance more inductive which leads to matching problems. The non contacting feed techniques solve these problems.

5.3 Optimizing the feed position:

The point at which the coaxial feed is to be connected to the ridges of the DRHA is an important aspect of the horn antenna design.

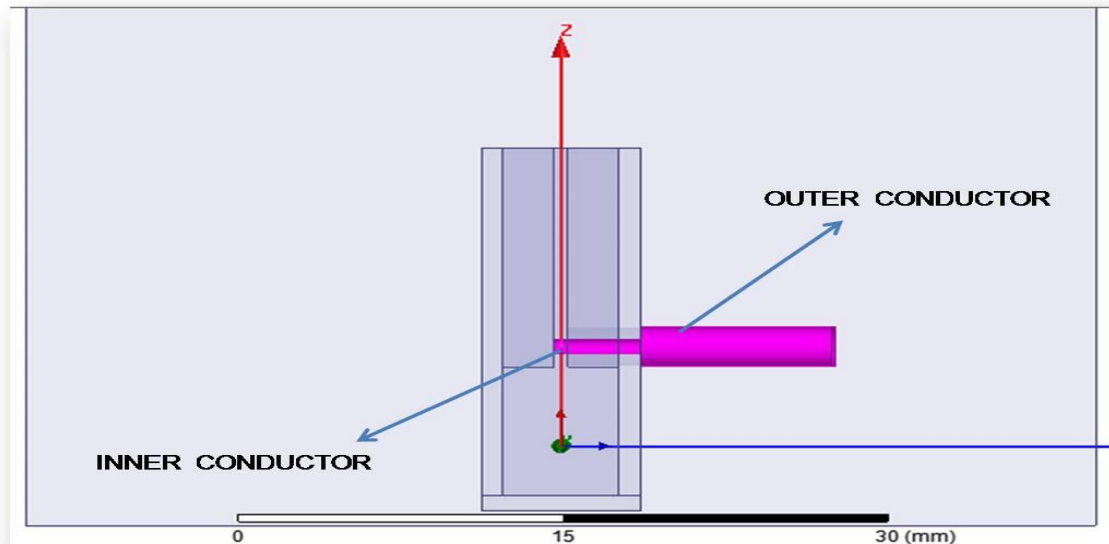


Figure 5.4: Optimizing the feed position.

The inner conductor of the coaxial cable should touch the opposite ridge as soon as the ridges in the waveguide start.

5.4 Design of the flare section:

The main part of the whole antenna is the flare design. It is the flare section of the antenna which transfers the electrical wave as a spherical wave front to the space. It happens through impedance transition from 50ohm to 377ohm which is free space wavelength.

The flare section also includes the aperture of the antenna. Aperture of the antenna decides how much wave energy is radiated outside the space and how the wave energy is received from the space. Flare angle and the size of the aperture are the dimensions to decide.

For optimum horn design the flare angle should be less than 30° and the aperture should be a square with side = $\lambda/2$.

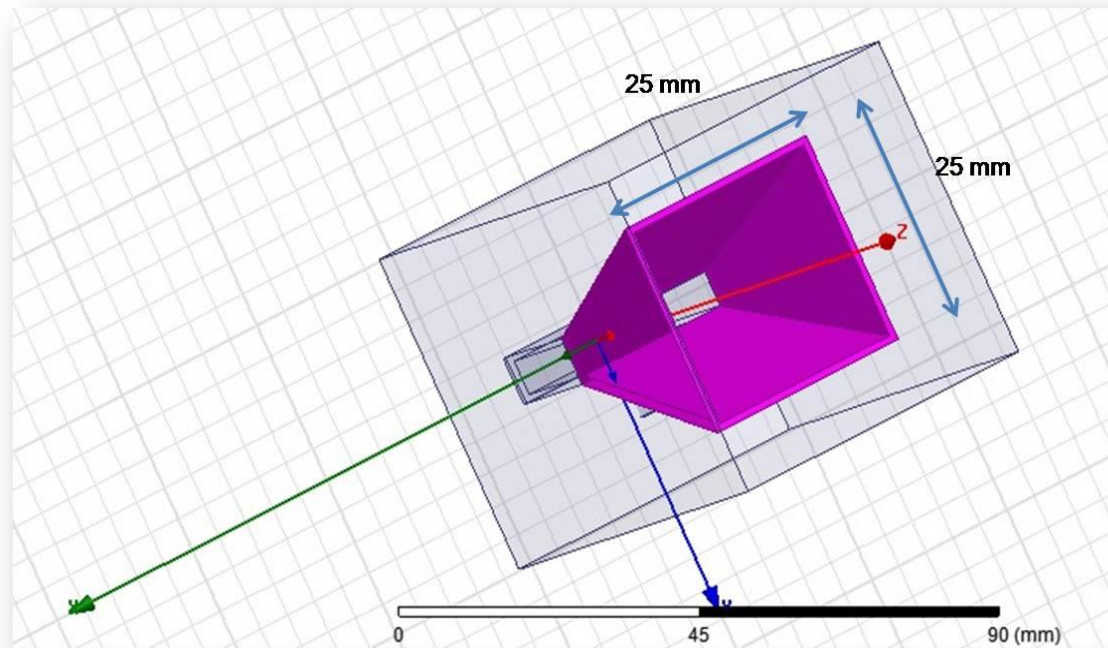


Figure 5.5: Flare section of the horn antenna.

Where λ is the lower cut of wavelength of the antenna's operating frequency range. By such a design the E-plane and the H-plane radiation are expected to be in symmetry. And the antenna is directional with high gain.

5.5 Design of exponentially tapered ridges:

The wave flow in horn antenna is similar to stream line flow of a liquid. If the wave guide is not flared into a wide aperture then due to sudden termination of the waveguide wall the reflections do happen resulting in a large VSWR. So the transition of the wall should be such that step by step impedance transmission should be smooth and not abrupt. Impedance is the ratio of electric field and the magnetic field ratio. The ratio is maintained with smooth transition through an exponential tapered section. The ridges in the waveguide are extended in the flare section of the wall as an exponential taper. The exponential equation which guides the design of the tapered section is mainly depends on the frequency range of operation.

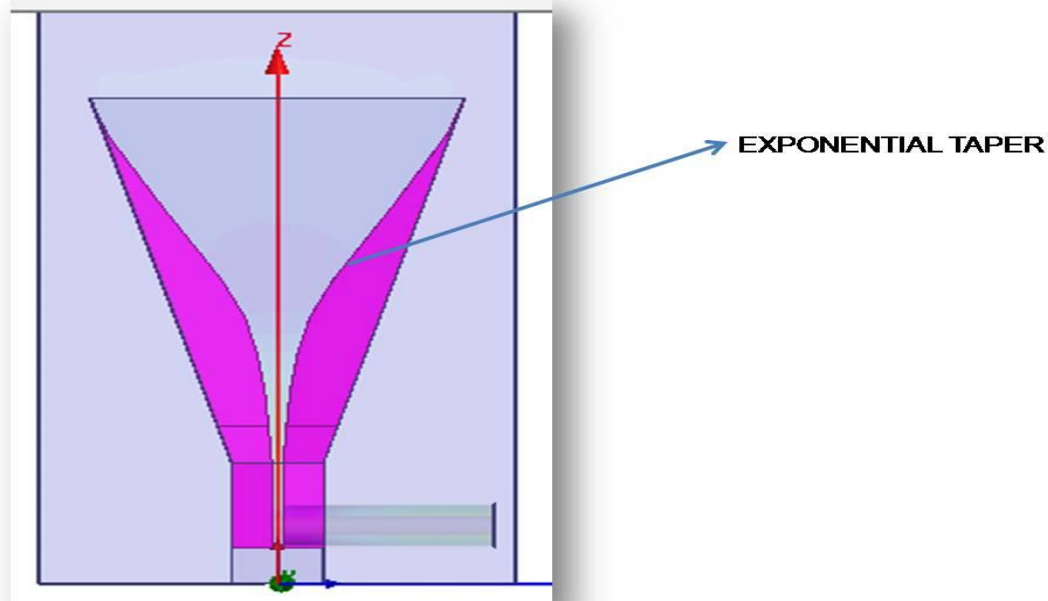


Figure 5.6: Exponentially tapered ridge of the horn antenna

The tapered part is extended from the ridges which is a perfect electric conductor. Surface currents do flow on the ridges and the tapered section to initiate the wave propagation inside the horn antenna and to the free space.

5.6 Modeling the Back cavity:

The coaxial feed so given to the waveguide also produces back radiation which may be contribute in constructive or destructive interference. Destructive interference deteriorates the directional radiation of the antenna and the constructive interference improves the radiation pattern. So in order to avoid the destructive and to enhance the radiation by supporting the constructive interference back cavity is to be designed. The main dimension decided is length of the back cavity and it should obey the following relation

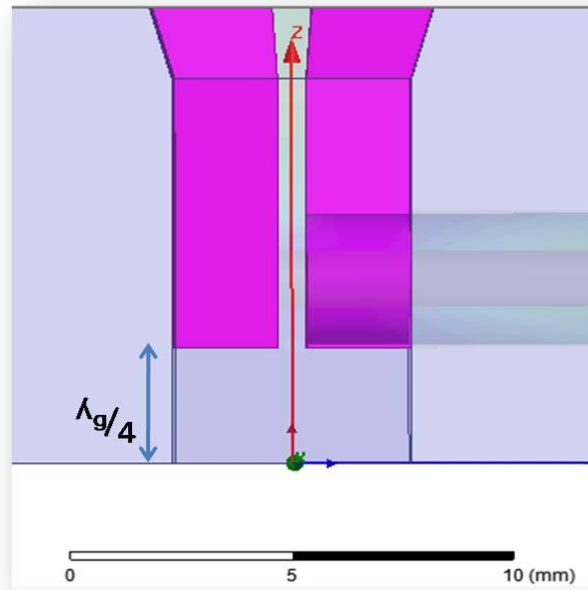


Figure 5.7: Back cavity of the horn antenna

$$\lambda_{g,mn} = \frac{\lambda}{\sqrt{1 - \left(\frac{\lambda}{\lambda_c}\right)^2}}$$

Where λ_g is the guide wave length which is decided from the above relation and the length of the back cavity should be $\lambda_g / 4$.

CHAPTER 6**SIMULATION RESULTS OF
DOUBLE RIDGED HORN ANTENNA USING HFSS**

In the process of designing the double ridged horn antenna which is then used as the feed for the radio telescope, we adopted several modifications for the betterment of the characteristics of the horn antenna, such as VSWR, radiation patterns etc. In this chapter we provide the details of the modifications done and the modified results.

The results that we are going to show include the VSWR plots against the frequency, over the operating range of the antenna and the far field radiation patterns at different frequencies.

6.1 Double ridged horn antenna for 6-18 GHz :

The basic design was done following the general design steps of the double ridged horn antenna as explained in the previous chapter. The basic design is as shown in the figure given below.

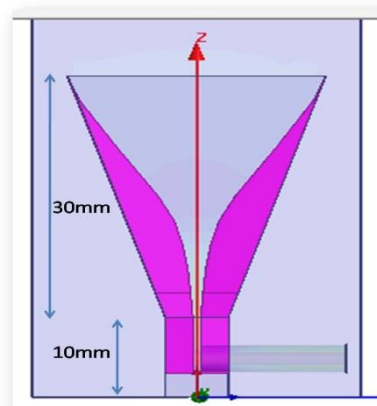


Figure 6.1 : DRHA designed for 6-18GHz

It is clearly indicated in the figure that the height of the flare section for this design is 30mm and the height of the waveguide section including the back cavity is 10mm.

The simulation results for the design are obtained using HFSS and are as shown in the figures given below. They include the plots of VSWR against the frequency and radiation patterns at different frequencies.

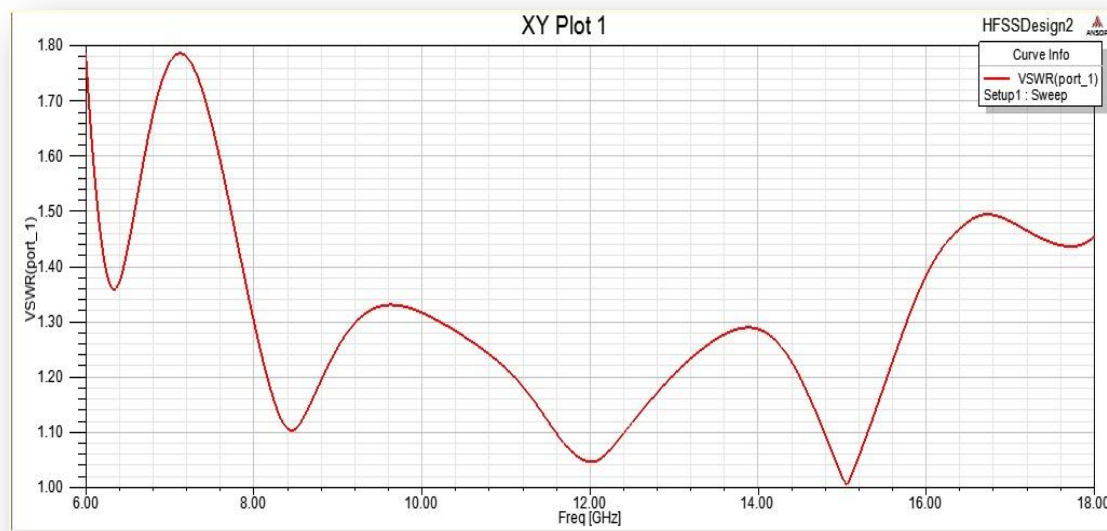


Figure 6.2: Plot of VSWR against Frequency.

The above graph shows the plot of the Voltage Standing Wave Ratio (VSWR) against the frequency. In general a horn antenna is said to have the good VSWR characteristics if the VSWR value is less than 1.6 over the whole bandwidth of the designed antenna.

Next the far field radiation patterns of the designed Double ridged horn antenna for different frequencies in its bandwidth are plotted. The analysis of which gives us a clear picture about the similarity of beam sizes of the E-plane and H-plane. It also throws light on the symmetry of the E-plane and H-plane radiation patterns. Though the proposed radio telescope uses a feed of the bandwidth 7-14GHz, we are testing the behaviour of the DRHA in the frequency range of 6-18GHz. The radiation patterns of the designed DRHA at different frequencies of its bandwidth are as shown in the figure 6.3. We can see the E-plane and H-plane patterns at two different planes that is $\phi=0^{\circ}$ and $\phi=90^{\circ}$.

The figure 6.3 given below shows the radiation patterns of the designed DRHA at frequencies 6GHz, 9GHz, 12GHz and 18GHz.

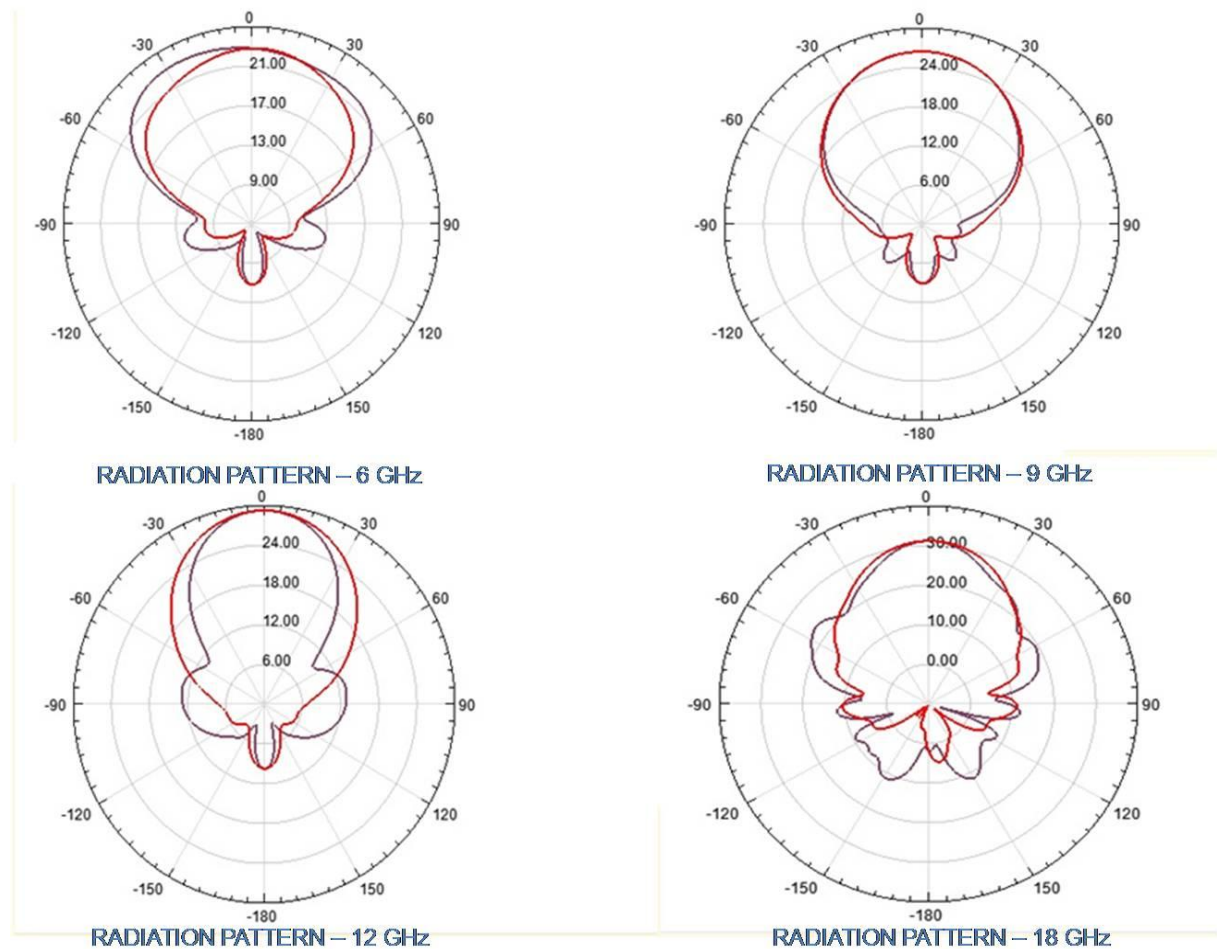


Figure 6.3: Radiation patterns of the DRHA at different frequencies.

By the analysis of the radiation patterns so obtained we can notice that the side lobes of the radiation pattern increase with the frequency, which is the clear sign of existence of multimode excitation at the higher frequencies which has to be minimized in order to avoid the wastage of incident power on the antenna in the form of side lobes which do not contribute to the betterment of directivity of the antenna.

6.2 Proposing new type of tapering for the ridges:

Along with the problem of multimode excitation at the higher frequencies, we also notice the problem at the lower frequencies which is high VSWR (>1.6), as shown in the figure 6.4, which is also not desirable.

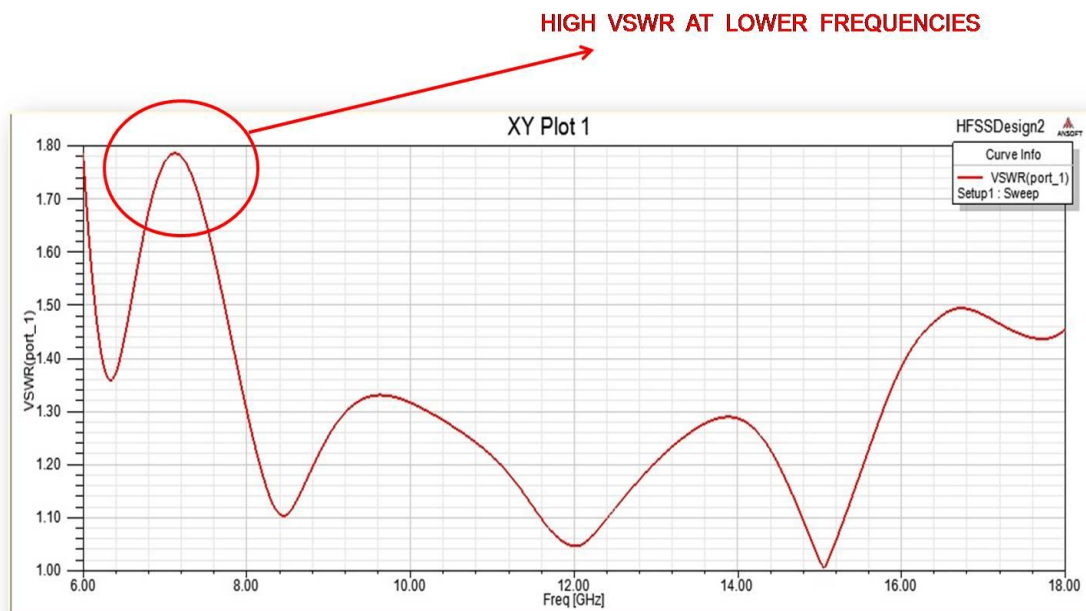


Figure 6.4: Plot of VSWR against Frequency.

In the first design of the DRHA, the shape we proposed for the ridges is the exponential tapering, which will start at the neck region where waveguide flares out and end with the flare itself and we have observed high VSWR at lower frequencies. In general the larger dimensions of the horn antenna correspond to the lower frequencies and the smaller dimensions correspond to the higher frequencies. If we have to reduce the VSWR at the lower frequencies, we have to incorporate the modifications in the portions of the horn antenna where the lower frequency waves are radiated out. This region is nothing but the end region of the flares on which the ridges are located.

We propose a new kind of tapering for the ridges, which is a hybrid of exponential and circular tapering. This means that, the ridges initially taper exponentially and at the end the tapering will be the combination of exponential curve and quarter-circle as shown in the figure 6.5. The modified results are also shown.

The figure given below clearly shows that the ridges extend out of the flare section of the DRHA, unlike in previous design.

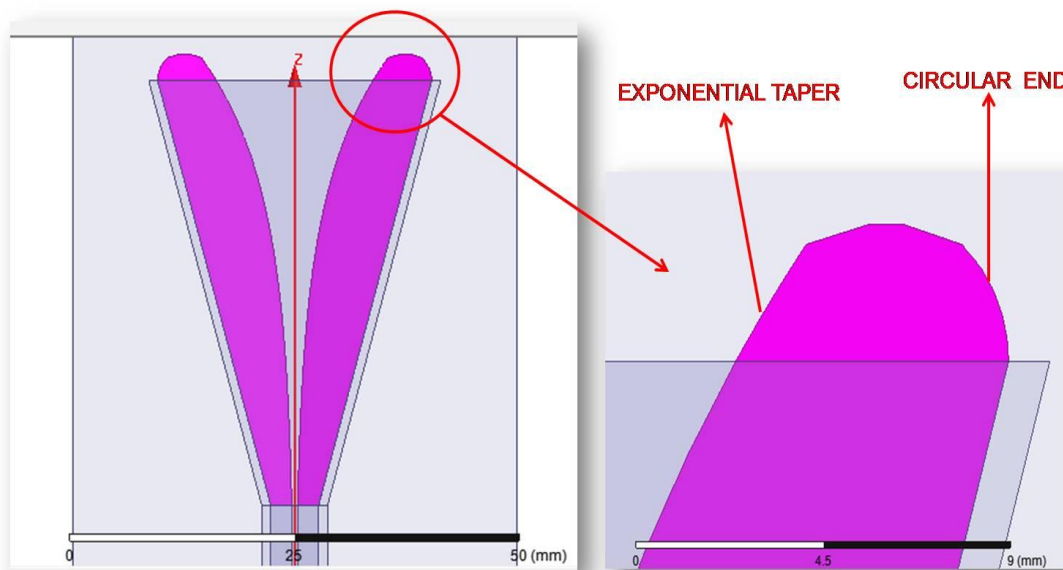


Figure 6.5: New type of tapering for the ridges of DRHA.

The incorporation of the new type of tapering for the ridges resulted in lowering of the high VSWR at the lower frequencies, which is desirable for any antenna design.

The plot of modified VSWR against frequency is as shown in the figure 6.6.

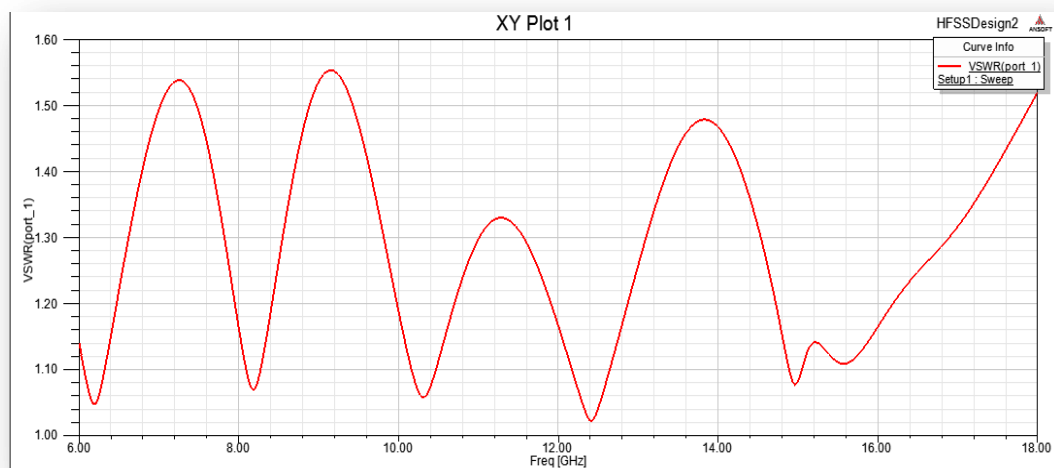


Figure 6.6: Modified VSWR after changing the tapering of ridges.

The radiation patterns for the different frequencies after changing the tapering of the ridges are as shown in the figure 6.7.

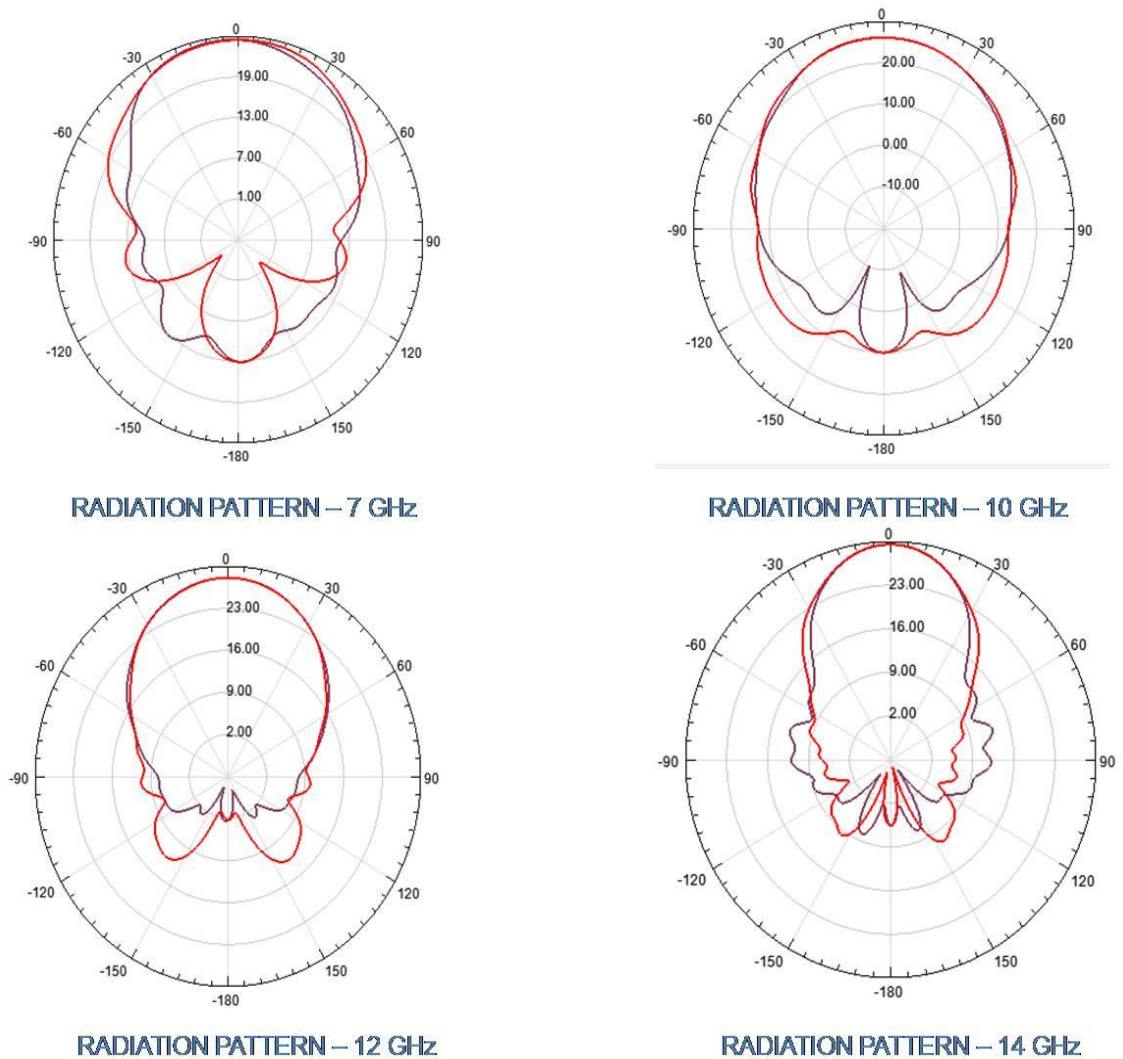


Figure 6.7: Modified radiation patterns after changing the tapering of ridges.

The figure 6.7 shows the radiation patterns of the modified DRHA at various frequencies namely 7GHz, 10GHz, 12GHz and 14GHz, but the problem of numerous side lobes at higher frequencies still remain.

6.3 Novel approach to back cavity design:

We have seen that the solution for the problem of high VSWR at the lower frequencies is the introduction of new kind of tapering for the ridges. The cavity back also plays an important role in the performance of the horn antenna. As explained earlier the length of the cavity back should be one fourth of the Guide wavelength for the middle frequency of bandwidth of the pyramidal horn antenna. However this calculated length of the back cavity would not correspond to each and every frequency of the bandwidth of antenna. To overcome this disadvantage many techniques were proposed earlier including conical cavity back, semispherical cavity back, irregular ending for the ridges at the waveguide section of the horn etc.

Out of the above mentioned techniques it was proposed [35] that conical cavity back would give better performance when compare to the semi spherical cavity back. However it was also mentioned that the fabrication of such cavity backs contributes to the existing complexity of the horn antennas in general.

In our project we are incorporating new concept of back fins, which are literally the ridges in the back cavity to improve the performance of the Double Ridged Horn Antenna (DRHA). The new kind of the back cavity design is as shown in the figure 6.8 given below.

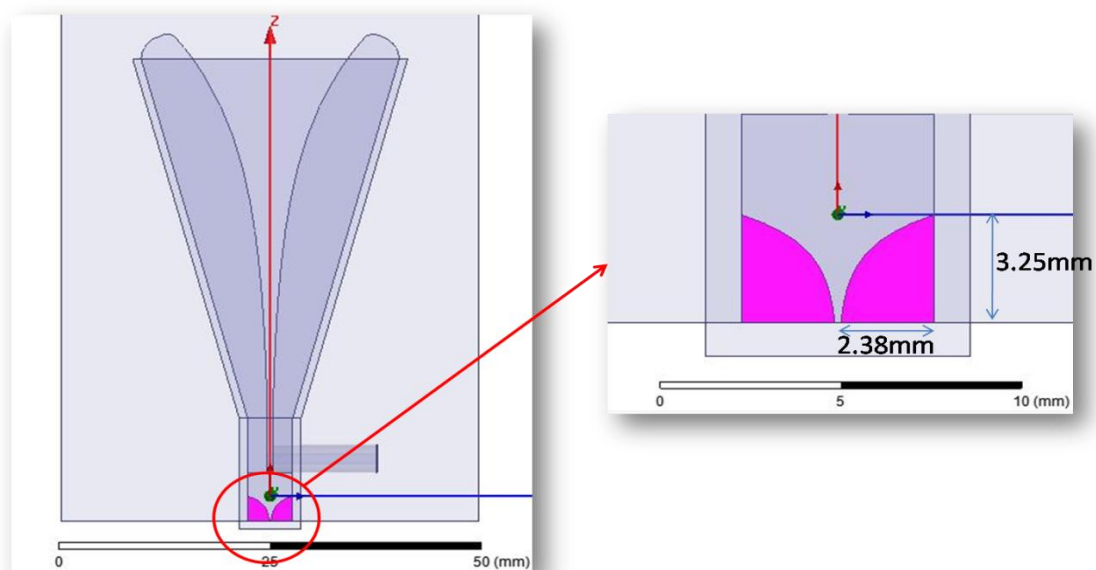


Figure 6.8: Introducing back fins to the cavity back

The problem with the flat cavity back is that there will be more reflected waves towards the coaxial feed than the absorbed waves. The incorporation of the back fins would solve that problem there will be more absorption of the waves and hence less will be the reflected which will contribute to the impedance matching of the whole structure. The radiation patterns were better when back fins are introduced.

The design was simulated after introducing the back fins and the antenna parameters VSWR and radiation patterns at different frequencies were plotted. It was observed that the radiation patterns were satisfactory over the desired frequency range of 7GHz to 14GHz. The VSWR of <1.7 was achieved over the entire desired frequency range.

The graph given below shows the plot of Voltage Standing Wave Ratio (VSWR) plotted against the frequency. It can be seen that the VSWR is <1.7 over the desired frequency range, which is good enough for the desired application.

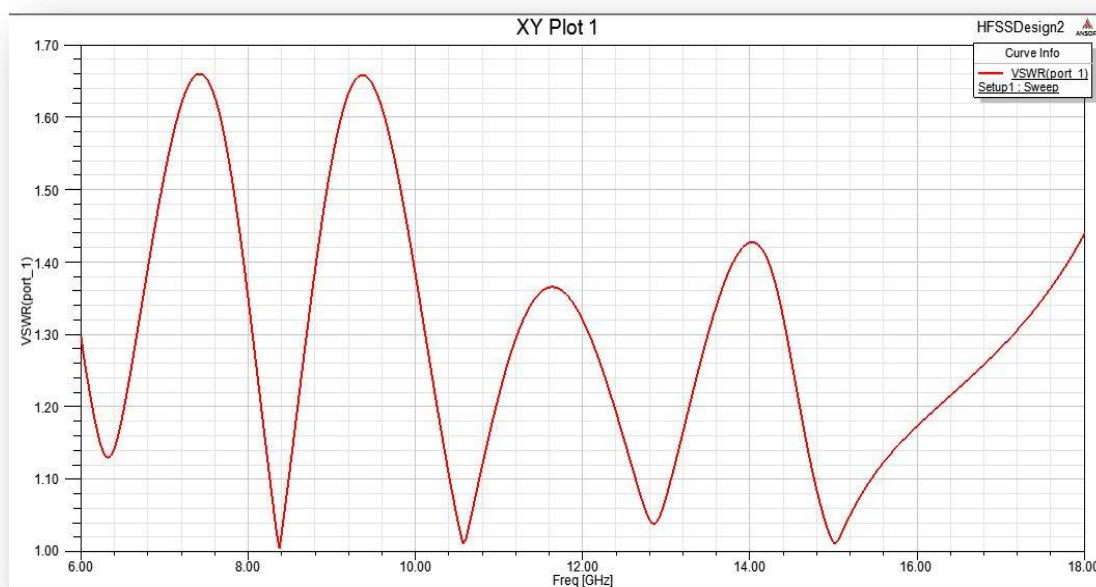
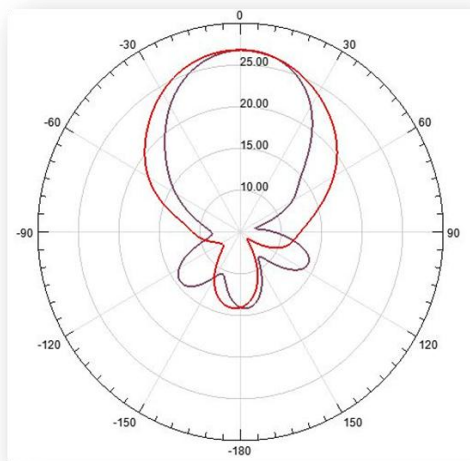
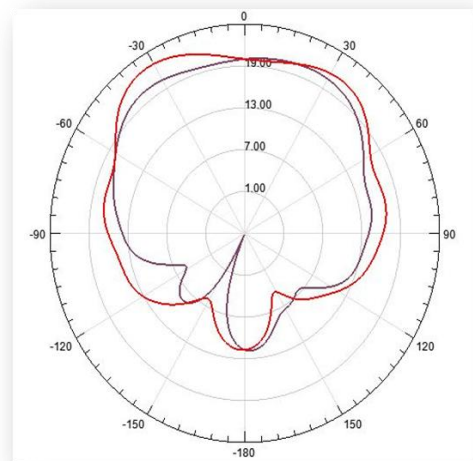


Figure 6.9: Modified VSWR after introducing the back fins.

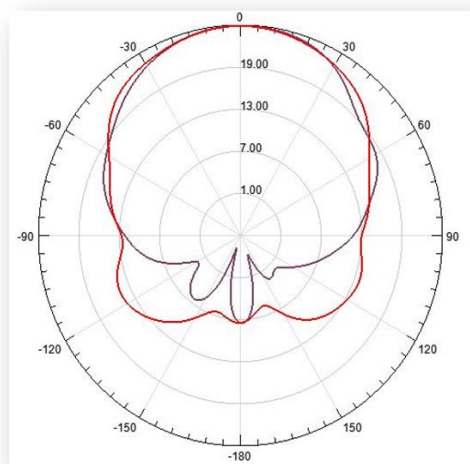
The radiation patterns were also plotted for this modified design (after introducing the back fins). The radiation patterns were plotted for the frequencies 6GHz, 8GHz, 10 GHz, 11GHz, 12GHz and 14GHz. The figure 6.10 shows the radiation patterns for the different frequencies over the bandwidth of the designed antenna.



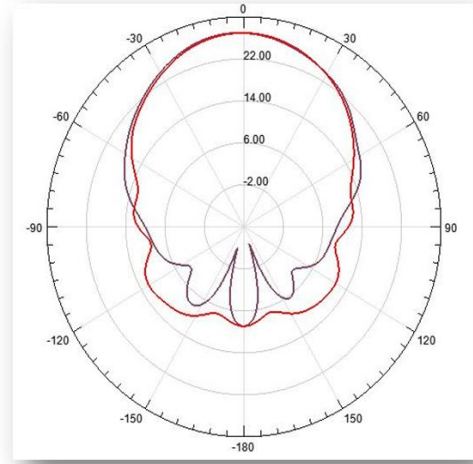
RADIATION PATTERN – 6GHz



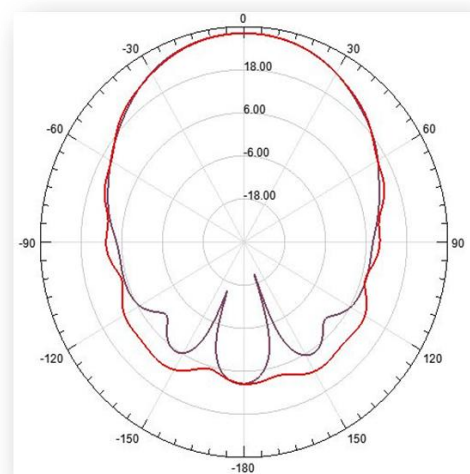
RADIATION PATTERN – 8GHz



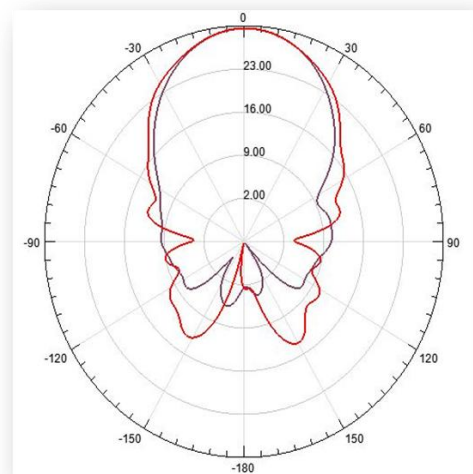
RADIATION PATTERN – 10GHz



RADIATION PATTERN – 11GHz



RADIATION PATTERN – 12GHz



RADIATION PATTERN – 14GHz

Figure 6.10: Radiation patterns after introducing the back fins.

The radiation patterns as shown in the previous graph are satisfactory over the desired bandwidth. We can also plot the magnitude of the electric field in the plane of ridges, which is as shown in the figure 6.11.

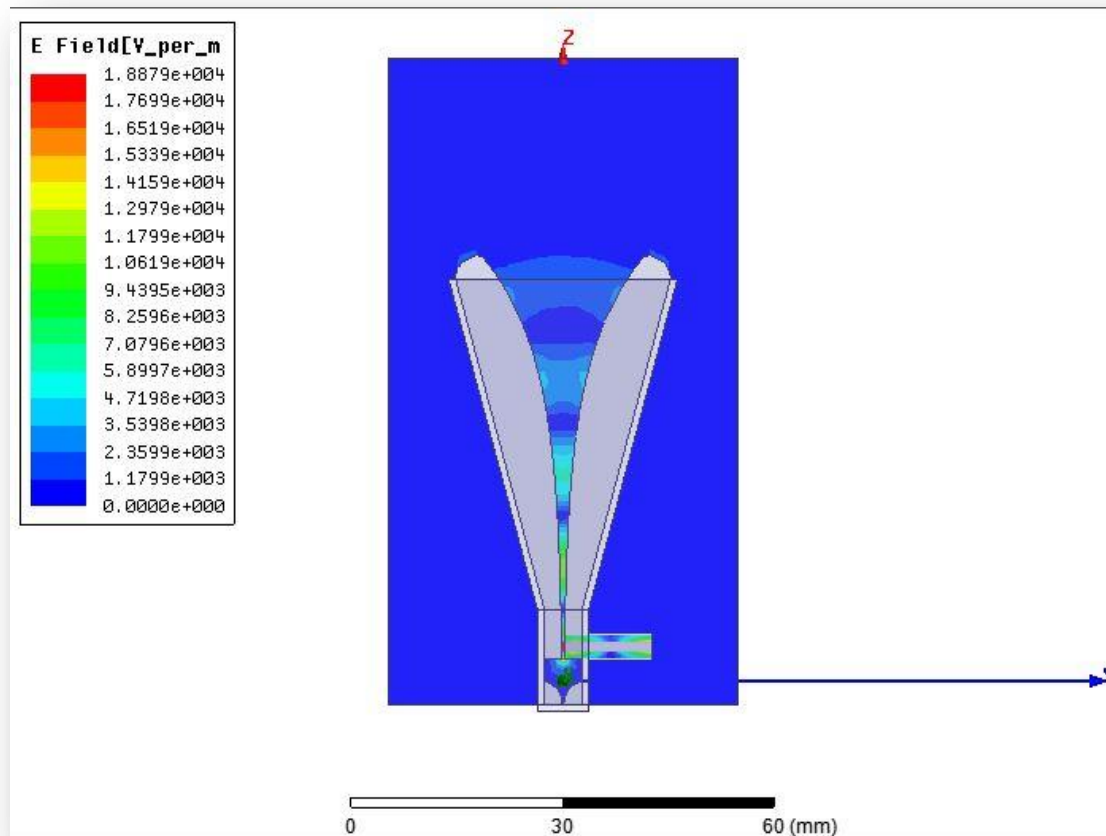


Figure 6.11: Magnitude of E-field in the plane of ridges.

The surface currents are confined to the ridges. We know that the Double Ridged Horn Antenna (DRHA) is excited in the TE_{10} mode, which means that electric field lines will be in the plane of ridges. On applying the boundary conditions to the material used for the design of horn antenna, which is aluminium we can notice that the electric field lines will be normal to it, as it is a conductor. It also indicates that the currents that flow will be the surface currents which are perpendicular to the electric field lines. The distribution of the surface currents over the ridges of the horn antenna can be noticed. The magnitude of the surface currents over the design is as shown in the figure 6.12

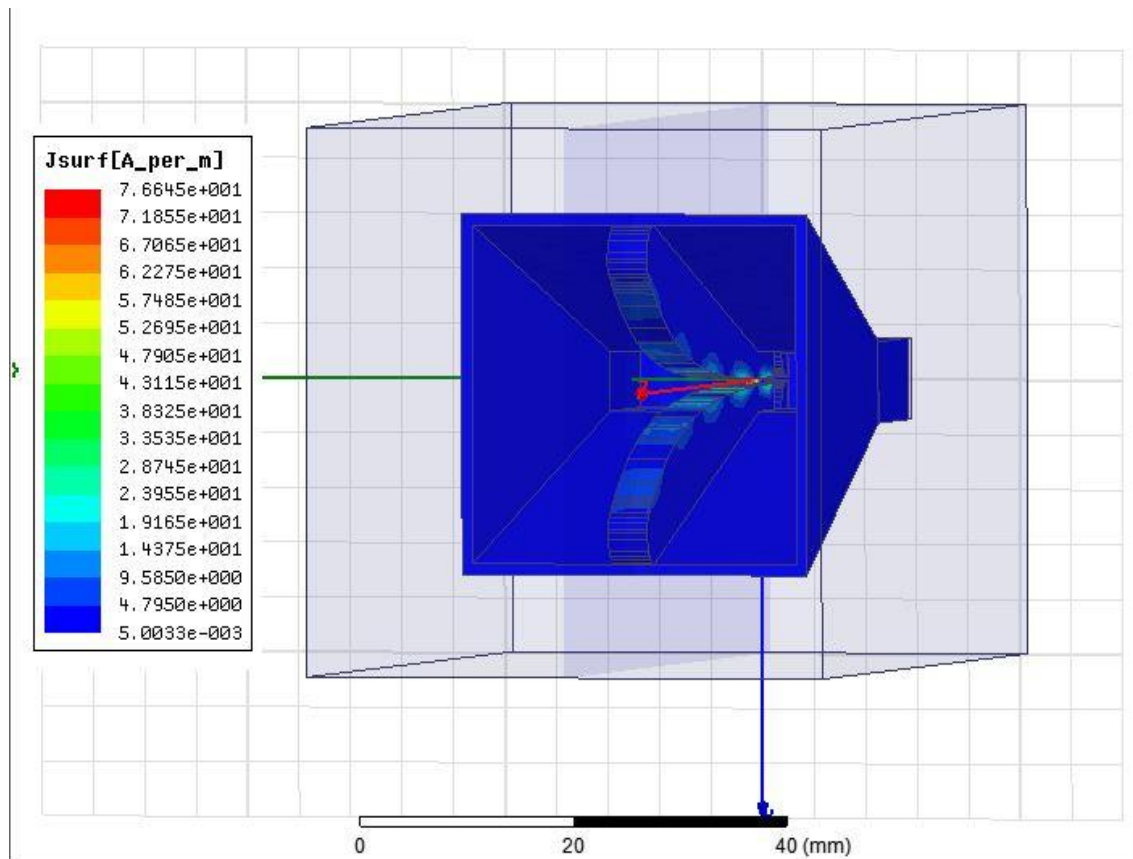


Figure 6.12: Surface current distribution.

The 3D polar plot for the designed Double Ridged Horn Antenna (DRHA) at 11GHz is as shown in the figure given below.

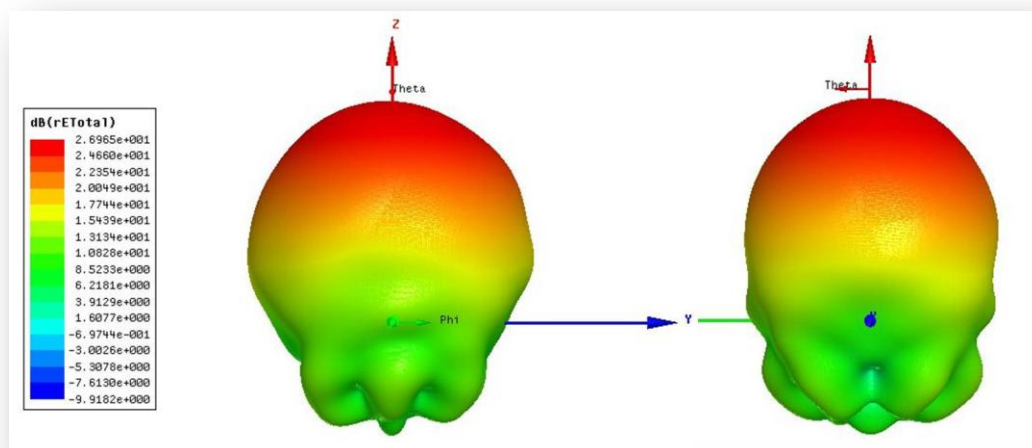


Figure 6.13: 3D polar plot of the designed horn at $\phi=90^\circ$ and $\phi=0^\circ$.

CHAPTER 7**INTRODUCTION TO MICROSTRIP ANTENNA**

Patch antenna has a low profile with a number of advantages over other types of antennas as lightweight, less expensive, easy to fabricate. They are called planar antennas because their elements are usually flat. The use of this type of antennas started as early 70s when conformal antennas were needed for missile applications. Rectangular and circular patch antennas have been used in a variety of array configurations. Large scale integration developments in electronic circuit miniaturization have led to a major contributing factor for advances in antenna fabrication. Micro strip antennas based on photolithographic technology are a breakthrough as conventional antennas are often bulky and costly part of an electronic system.

7.1 Principle of operation:

The basic form of patch antenna consists of a radiating patch on one side of a dielectric substance with a ground plane on other side as shown below. Generally the patch is made of conducting material such as gold or copper and can take any possible shape. The feed lines and the patch are photo etched on the substrate.

Microstrip antenna radiates because of the fringing fields around the antenna. The current at the end of the patch is zero (open circuit end), the current is maximum at the center of the half-wave patch and (theoretically) zero at the beginning of the patch. This low current value at the feed is the reason why the impedance is high when fed at the end.

The patch acts approximately as a resonant cavity (short circuit walls on top and bottom, open-circuit walls on the sides). In a cavity, only certain modes are allowed to exist, at different resonant frequencies. If the antenna is excited at a resonant frequency, a strong field is set up inside the cavity, and a strong current on the (bottom) surface of the patch. This produces significant radiation. This project is centered on the transmission line model and uses all of the empirical equation this model is based on. The cavity model is not the center of the project and hence not explained.

7.2 Transmission Line model:

The patch in this model is represented by two slots of width W and height h , separated by a transmission line of length L . Essentially micro strip antenna is a non homogeneous line of two dielectrics, usually the substrate and air. The figure below shows the illustration.

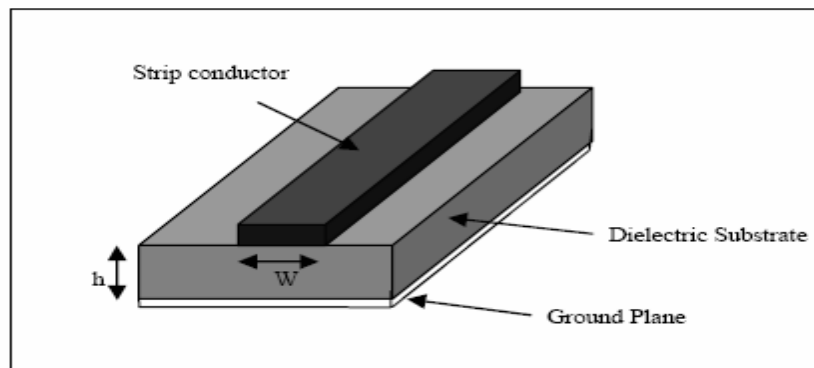


Figure 7.1: Transmission line model of microstrip antenna.

The figure below shows that major portion of the electric field lines stay in the substrate and some parts emerge in air. Due to this the transmission line cannot support pure TEM mode of transmission, as the phase velocities would be different in air and substrate. Instead, the dominant mode of propagation would be quasi- TEM mode. Hence, an effective dielectric constant (ϵ_{reff}) must be considered so that fringing and wave propagation can be accounted for.

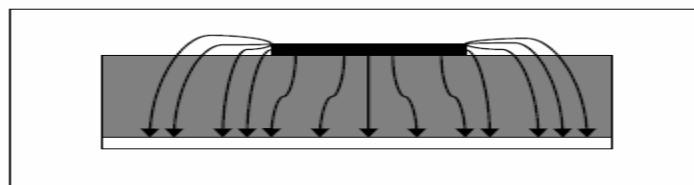


Figure 7.2: Electric field lines in transmission line model of microstrip antenna.

The value of ϵ_{reff} is slightly less than ϵ_r as the fringing fields around the periphery of the patch are not confined within the dielectric substrate but are also spread in the air as shown in figure above. The expression for ϵ_{reff} is given as -

$$\epsilon_{\text{reff}} = (\epsilon_r + 1)/2 + (\epsilon_r - 1)/2[1 + 12h/W]^{-1/2}$$

where ϵ_{reff} = Effective dielectric constant

ϵ_r = Dielectric constant of substrate

h = height of dielectric substrate

W = Width of the patch

The figure shows a rectangular micro strip patch antenna of dimensions L along length and W along width resting on a substrate height of h . The figure coordinate selection makes the length to orient along x direction and width along y direction and height along z direction. In order to operate in fundamental TM mode, the length of the patch must be slightly less than $\lambda/2$ where λ is the wavelength in the dielectric medium and is equal to $\lambda_0/\sqrt{\epsilon_{\text{reff}}}$ where λ_0 is the wavelength in free space.

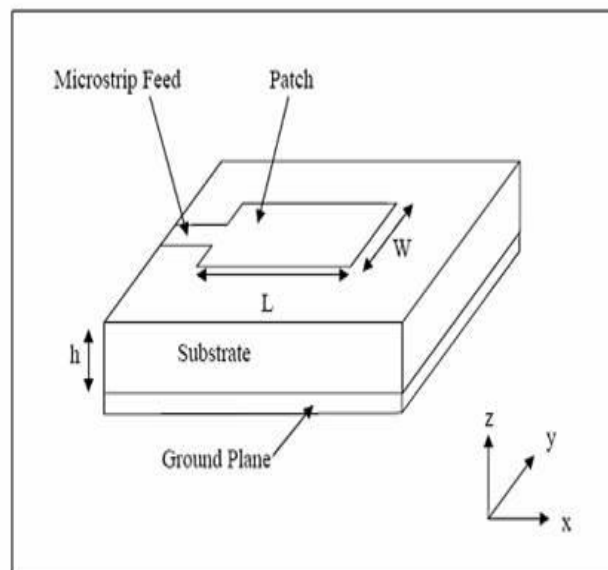


Figure 7.3: The structure of microstrip antenna.

The TM mode implies that the field varies half wavelengths along length, and there is no variation along the width of the patch. The figure below shows the patch represented by two slots, separated by a transmission line of length L and open circuited at both the ends. Along the width of the patch, the voltage is maximum and current is minimum due to the open ends. The fields at the edges can be resolved into normal and tangential component with respect to the ground plane.

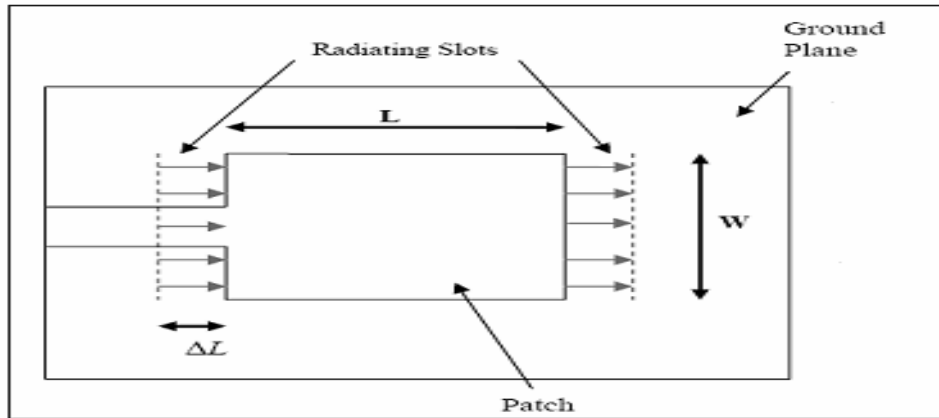


Figure 7.4: Strip line fed patch antenna.

The fringing fields along the width can be modeled as radiating slots and electrically the patch of the micro strip antenna looks greater than its physical dimensions.

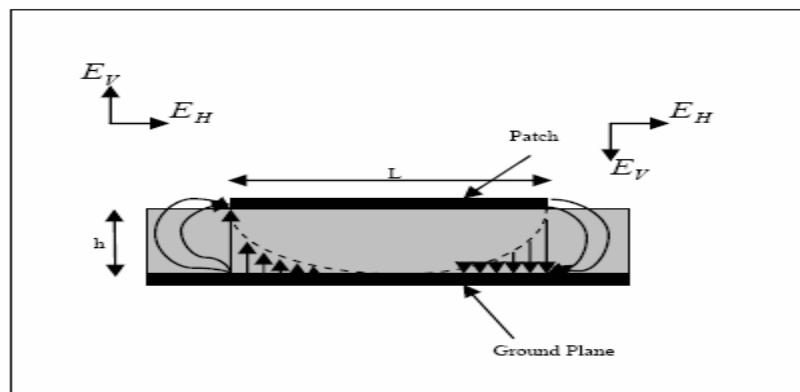


Figure 7.5: Fringing fields in patch antenna.

The fringing fields along the width can be modeled as radiating slots and electrically the patch of the micro strip antenna looks greater than its physical dimensions. The dimensions of the patch along its length is extended on each end by a distance ΔL , which is given empirically by as –

$$\Delta L = .412h (\epsilon_{\text{reff}} + 0.3) (W/h + 0.264) / ((\epsilon_{\text{reff}} - 0.258) (W/h + 0.8)) \text{ -----(7.1)}$$

The effective length of the patch L_{eff} now becomes:

$$L_{\text{eff}} = L + 2 \Delta L \text{ -----(7.2)}$$

For a given resonance frequency f_0 , the effective length is given as –

$$L_{\text{eff}} = c / (2f_0 \sqrt{\epsilon_{\text{reff}}}) \quad \text{-----}(7.3)$$

For a rectangular patch antenna, the resonance frequency for any TM mode is given as –

$$f_0 = c / (2f_0 \sqrt{\epsilon_{\text{reff}}}) [(m/L)^2 + (n/W)^2]^{1/2} \quad \text{-----}(7.4)$$

where m and n are modes along L and W respectively. For efficient radiation, the width W is given as-

$$W = c / (2f_0 \sqrt{((\epsilon_r + 1)/2)}) \quad \text{-----}(7.5)$$

The region between the two conductors acts as a $\lambda/2$ transmission line cavity that is open circuited at its ends. The electric field lines are perpendicular to the conductors satisfying the boundary conditions. The fringing fields which are responsible for the radiation, are exposed to upper half space ($z > 0$). The standing wave mode with a half-wavelength separation between the two ends leads to electric fields that are of opposite phase on the left and right halves. Therefore, the total fringing fields at the edges are 180° out of phase and equal in magnitude. From the figure we see that the x components of the fringing fields are in phase, which leads to a broadside radiation pattern. The fields along the edges associated with slots 1 and 2 are constant, whereas those along the other edges have odd symmetry and their radiation cancels in the broadside direction. The patch radiation is linearly polarized in xz plane, which is parallel to the electric fields in the slots.

The electric and magnetic fields in the far field region are given as –

$$F_E(\theta) = \cos(\beta L/2 * \sin\theta) \quad \text{E- plane } \phi = 0^\circ$$

$$F_H(\theta) = \cos\theta * \sin(\beta W/2 * \sin\theta) / (\beta W/2 * \sin\theta) \quad \text{H- plane } \phi = 90^\circ$$

7.3 Feeding Techniques:

There is variety of ways to feed a patch antenna. These can be categorized into two types as contacting and non- contacting. In the contacting method, the RF power is fed directly to the radiating patch using connecting element such as a microstrip line. In the non-contacting scheme, electromagnetic field coupling is done to transfer the power between the microstrip line and radiating patch. The following are most popular feed techniques used in feeding a patch antenna.

7.3.1 Microstrip Line Feed:

This is a contacting feeding technique in which a conducting strip is connected to the edge of the patch as shown. This strip is smaller in width as compared to the patch and this kind of feed arrangement has the advantage that the feed can be etched on the same substrate to provide a planar structure.

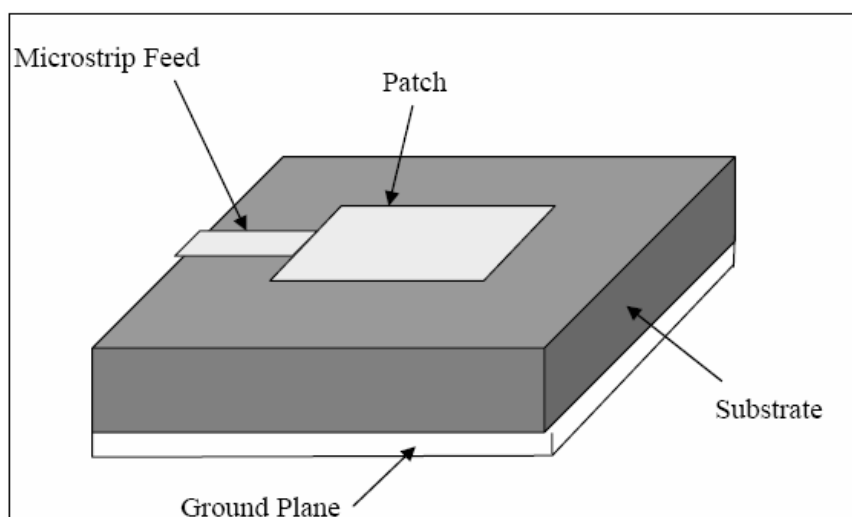


Figure 7.6: Microstrip feed for patch antenna.

The cut is made in the patch to meet impedance match of the feed line with the patch without using an additional matching element. The impedance matching is controlled by varying the inset position. This is an easy feeding scheme as it provides ease of fabrication and simplicity in modeling as well as impedance matching. The disadvantage of this technique is as thickness of dielectric substrate increases, surface waves and spurious feed radiation also increases, which hampers the bandwidth of the antenna. The feed radiation also leads to undesired cross polarized radiation.

7.3.2 Coaxial Feed:

The Coaxial feed or probe feed is also a common contacting feed technique. Here the inner conductor of the coaxial connector extends through the dielectric and is soldered to the radiating patch, while the outer conductor is connected to the ground plane. The main advantage of this type of feeding scheme is that the feed can be placed at any desired location inside the patch in order to match with its input impedance. This method of feeding is easy to fabricate and has low spurious radiation. However, the major disadvantage is that it provides narrow bandwidth and is difficult to model since a hole

has to be drilled in the substrate and the connector protrudes outside the ground plane, thus not making it completely planar for thick substrate. In thicker substrates, the increased probe length makes the input impedance more inductive which leads to matching problems. It is seen above that for a thick dielectric substrate, which provides broad bandwidth, the microstrip line feed and the coaxial feed suffer from numerous disadvantages. The non contacting feed techniques solve these problems.

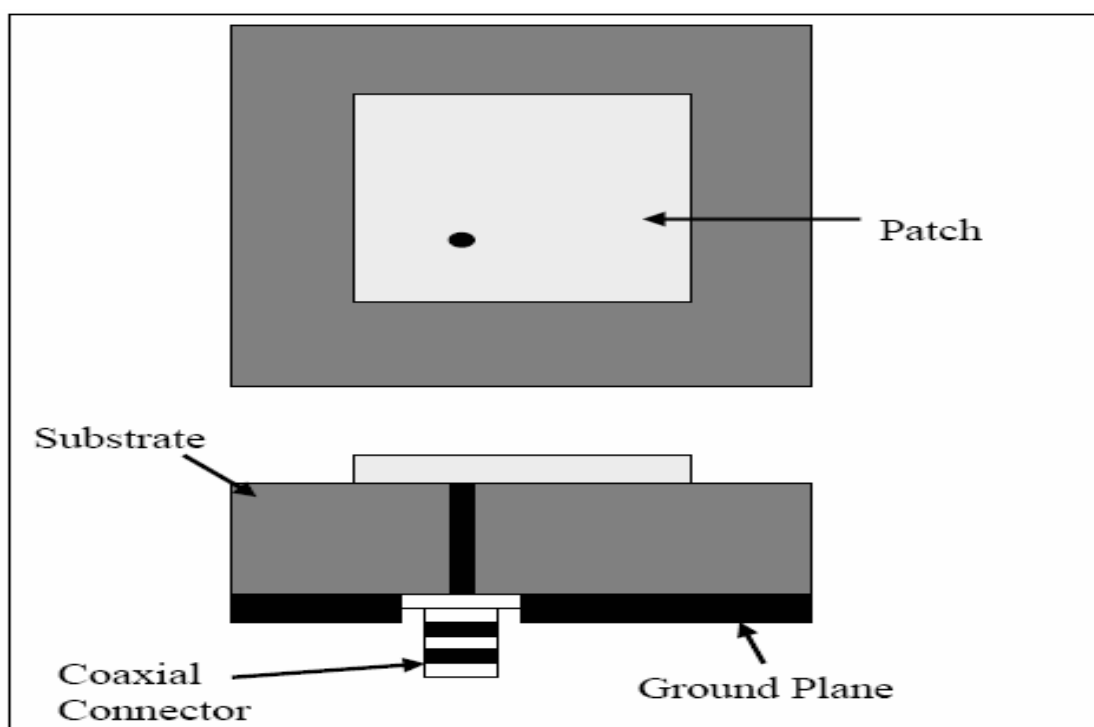


Figure 7.7: Coaxial feed for patch antenna.

7.3.3 Aperture Coupled Feed:

This is a type of non-contacting feed technique, in which the radiating patch and the microstrip feed line are separated by the ground plane as shown in the figure. Coupling between the patch and the feed line is made through a slot or an aperture in the ground plane. Under the patch the coupling aperture is at the center which leads to lower cross polarization as the configuration is symmetric. The size, shape and location of the aperture decide the amount of coupling from the feed line to the patch. The ground plane separates the patch and the feed line, which minimizes the spurious radiation. Usually, a thick, low dielectric material is used for top substrate and a high dielectric material is used for the bottom substrate to optimize radiation from the patch. The difficulty in fabrication due to multiple layers, which also increases the antenna thickness, is a major disadvantage of this technique. Also this feeding scheme provides narrow bandwidth.

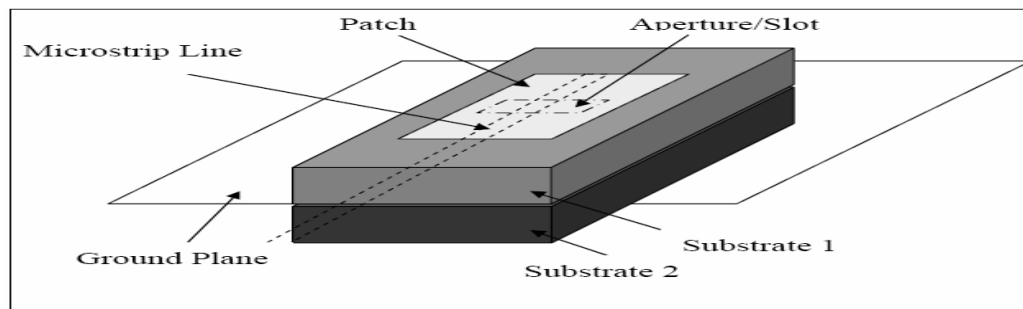


Figure 7.8: Aperture coupled feeding of patch antenna.

7.3.4 Proximity Coupled Feed:

This is also a non contacting feed technique which is also known as the electromagnetic coupling scheme. As shown in the figure two dielectric substrates are used such that the feed line is between the two substrates and the radiating patch is on top of the upper substrate. The major advantage of this technique is the elimination of spurious radiation and high bandwidth (13%), due to overall increase in the thickness of the patch antenna. Matching is achieved by controlling the length of the feed line and width to line ratio of the patch. Difficulty in fabricating two dielectric layers with proper alignment is a major disadvantage.

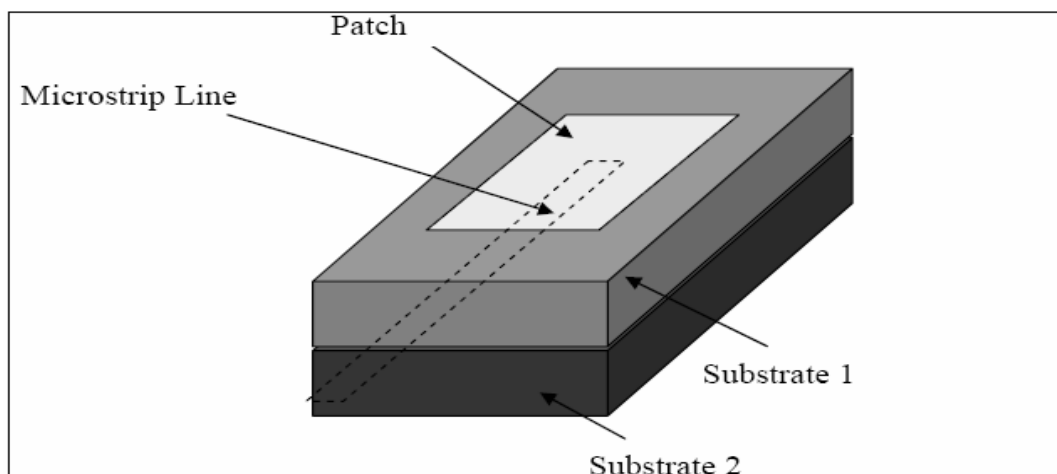


Figure 7.9: Proximity coupling for patch antenna.

Characteristics	Microstrip Line Feed	Coaxial Feed	Aperture coupled Feed	Proximity coupled Feed
Spurious feed radiation	More	More	Less	Minimum
Reliability	Better	Poor due to soldering	Good	Good
Ease of fabrication	Easy	Soldering and drilling needed	Alignment required	Alignment required
Impedance Matching	Easy	Easy	Easy	Easy
Impedance Bandwidth	2-5%	2-5%	2-5%	13%

Table 7.1: Comparison of different feed techniques

7.4 Applications:

There are numerous applications of planar antennas. [Reference number] lists some of the application as below -

- Aircraft and ship antennas – Communication and navigation, altimeter, blind landing systems.
- Missiles – Radar, proximity fuses and telemetry.
- Satellite communications – Domestic direct broadcast TV, vehicle-based antennas, communication.
- Mobile radio – Pagers and hand telephones, man pack systems, mobile vehicles.
- Remote sensing – Large lightweight apertures.
- Biomedical – Applications in microwave hyperthermia.
- Others – Intruder alarms, personal communication and so forth.

7.5 Bandwidth enhancement techniques of patch antenna:

The microstrip patch in its pure form cannot satisfy the bandwidth requirements for most wireless communication systems. Typically, a modification to the structure of the printed antenna must be undertaken to meet the impedance bandwidth specifications. Over the years there have been numerous bandwidth enhancements investigated, all with varying degrees of success and complexity. The general philosophy of most of these techniques is to add one or more resonant antennas to the microstrip patch configuration. These additional elements may be in the form of slots or other patches. Once the additional radiator or radiators have been chosen, the objective of the antenna designer is to ensure there is the right degree of interaction between these elements so that the performance of the printed antenna is enhanced.

7.5.1 Parasitically coupled (or gap-coupled) patches:

Parasitically coupling patches in a horizontal manner to the driven patch were proposed and investigated. The philosophy behind this technique is that if the resonant frequency of the coupled element or elements is slightly different to that of the driven patch, then the bandwidth of the entire antenna may be increased. Figure 7.10 shows an example of a driven probe-fed rectangular patch with two parasitic patches positioned on either side of the excited patch in the y-axis direction. The critical parameters are the lengths and widths of each patch for the control of resonant frequency and bandwidth, as well as the gap between the elements. The gaps tend to control the coupling between the patches and therefore the tightness of the resonant loop (or loops) in the impedance locus of the antenna.

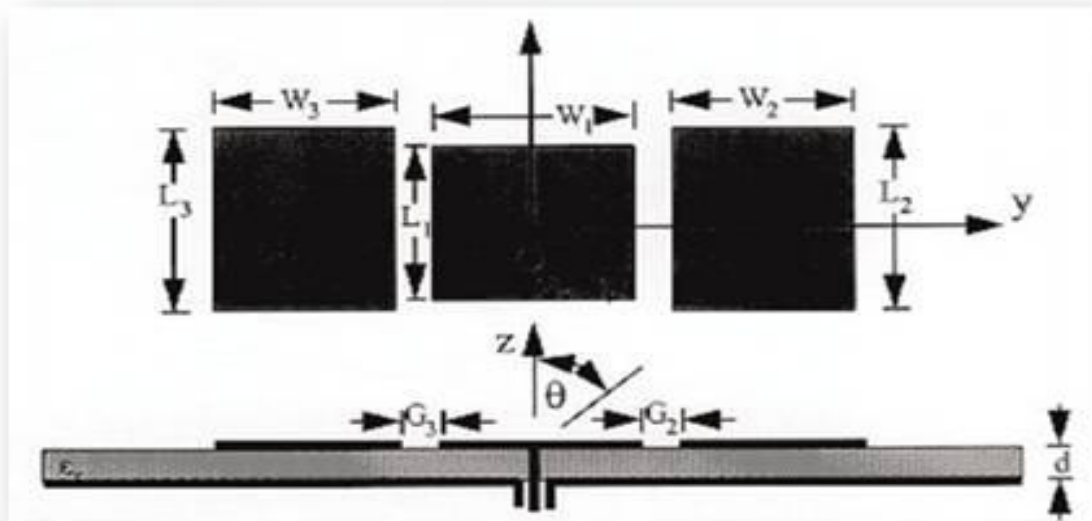


Figure 7.10: Schematic diagram of parasitically coupled microstrip patch antennas

Bandwidths on the order of 20% have been achieved using this enhancement technique, although there are several shortcomings of using parasitically coupled patches. First, to achieve these reasonable bandwidths, wide parasitic elements are required to make the overall size of the printed antenna configuration electrically large and, therefore, it is difficult to develop an array without incurring grating lobe problems.⁷ Second, the radiation patterns of parasitically coupled patches tend to be somewhat distorted across the useful impedance bandwidth, because of the lack of symmetry of the generated currents with respect to the center of the printed antenna.

7.5.2 Stacked microstrip patches:

Stacking patches on top of each other is probably the most common procedure utilized to enhance the bandwidth of a microstrip antenna. Figure 7.11 shows a schematic diagram of an aperture-fed stacked patch configuration, where an arbitrarily shaped patch is etched on a grounded substrate and is fed by a microstrip transmission line. Another patch antenna is mounted on a second laminate (with no ground plane) and is placed directly above the driven patch. Bandwidths approaching 30% have been achieved.

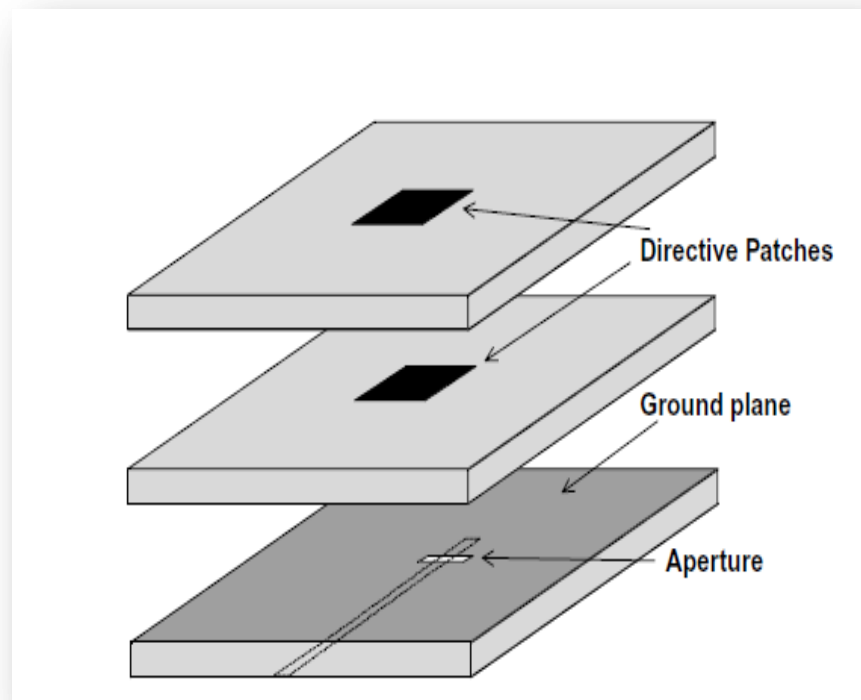


Figure 7.11: Schematic diagram of aperture-fed arbitrarily shaped stacked microstrip patches.

Stacked patch geometry over other bandwidth enhancement techniques has several advantages:

- They are relatively easy to design once the design trends have been established.
- Their radiation pattern remains reasonably constant over the 10-dB return loss bandwidth.
- They can be easily accommodated into an array environment.

It is possible to stack more patches on top of the driven element, such as a triple-stacked patch. The success of such a configuration is very susceptible to the dielectric layers used and in fact has been shown to give minimum improvement over a conventional stacked patch when low dielectric constant laminates are utilized.

7.5.3 Slotted Microstrip patches:

One more method to increase the bandwidth of patch is by cutting slots in the patch as shown in figure 7.12. The slot resonates at a particular frequency and the patch resonates at another frequency. These resonating frequencies can be combined to obtain

increased bandwidth. Variations in the bandwidth can be achieved by increasing or decreasing the size of the slot.

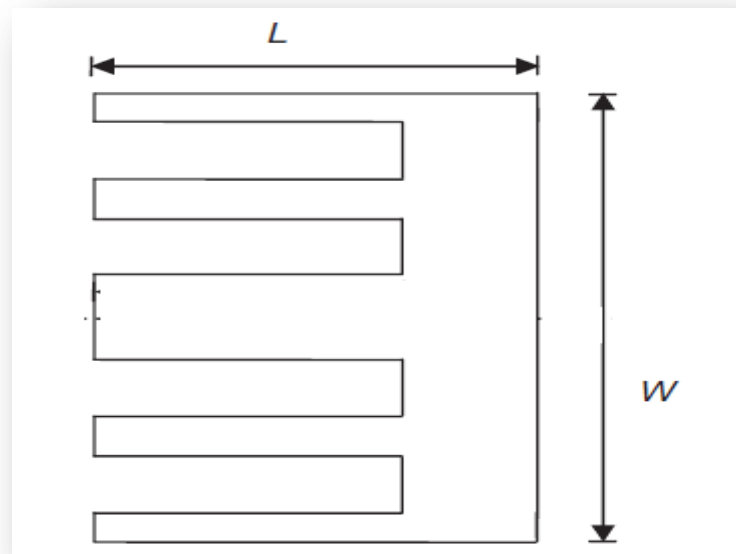


Figure 7.12: Schematic diagram of slotted microstrip patches

Shorting pins or shorting walls on U-shaped patch, U-slot patch, or L-probe feed patch antennas can be used in wideband and dual band antenna. Other techniques involves employing multilayer structures with parasitic patches of various geometries such as E, V and H shapes, which excites multiple resonant modes. These antennas are generally fabricated on thicker substrates. Using this method impedance bandwidth of 20% has been achieved.

CHAPTER 8**DESIGN AND SIMULATION RESULTS OF
MICROSTRIP PATCH ANTENNA USING HFSS**

Narrow bandwidth of patch antenna is to be made wideband using several broadband techniques as mentioned earlier. This process involves lots of modifications during the design for achieving good results of VSWR; return loss and radiation pattern symmetry. In this chapter we present the various modifications done and the modified results.

The results that we are going to show include the VSWR and S-parameter plots against the frequency, over the operating range of the antenna and the far field radiation patterns at different frequencies.

8.1 PATCH ANTENNA AT 11.72GHz:

Initially a single Patch was designed at an operating frequency of 11.72GHz following the basic design steps. The basic design is as shown below in figure 8.1.

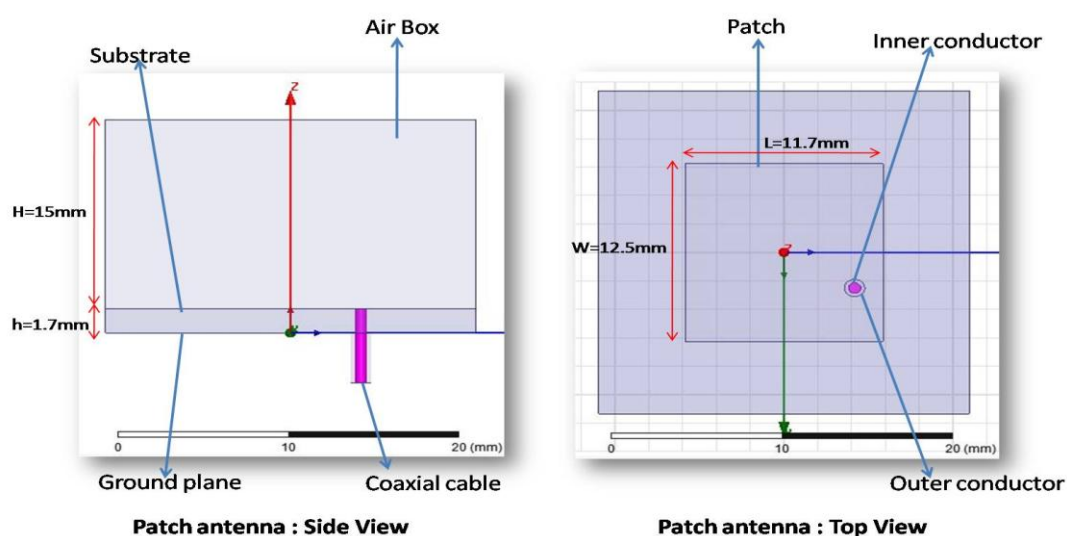


Figure 8.1: Patch antenna for 11.72GHz

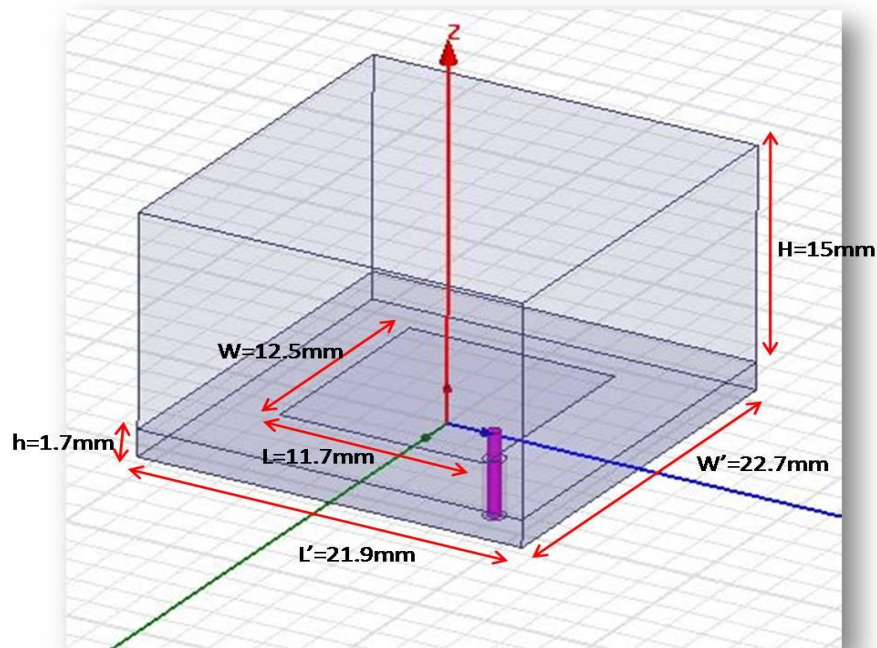


Figure 8.2: Isometric view of Patch antenna for 11.72GHz

It is clearly indicated that the width of the patch is 12.5mm and length is 11.7mm. The height of the substrate is 1.7mm with a width and length of 22.7mm and 21.9mm respectively.

The location of the feed is very important aspect in the design of patch. By using theoretical formulas and observing the plots at different frequencies optimal point was selected at (2.5mm, 4.17mm).

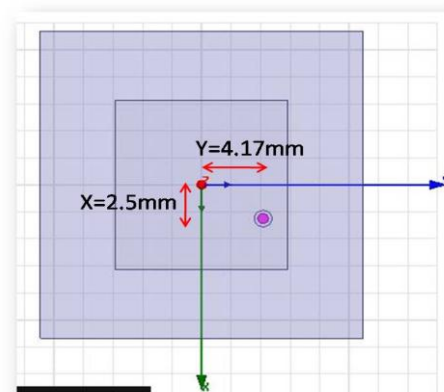


Figure 8.3: Location of feed point: Patch antenna for 11.72GHz

The simulation results for the design are obtained using HFSS and are as shown in the figures given below. They include the plots of VSWR and S-parameter against the frequency and radiation patterns at different frequencies.

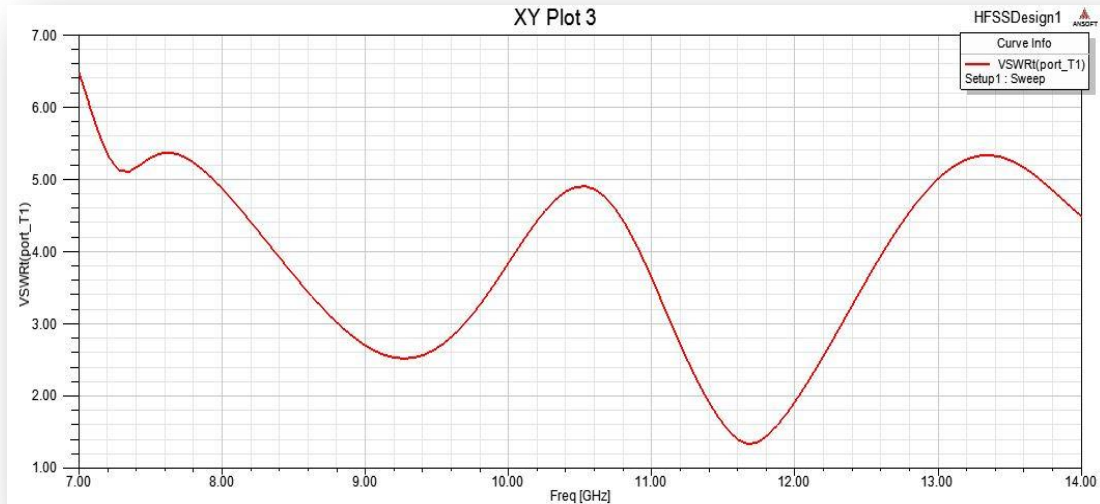


Figure 8.4: Plot of VSWR against frequency: Patch antenna for 11.72GHz

The above graph shows the plot of the Voltage Standing Wave Ratio (VSWR) against the frequency. In general a patch antenna is said to have the good VSWR characteristics if the VSWR value is less than 1.5 over the whole bandwidth of the designed antenna.

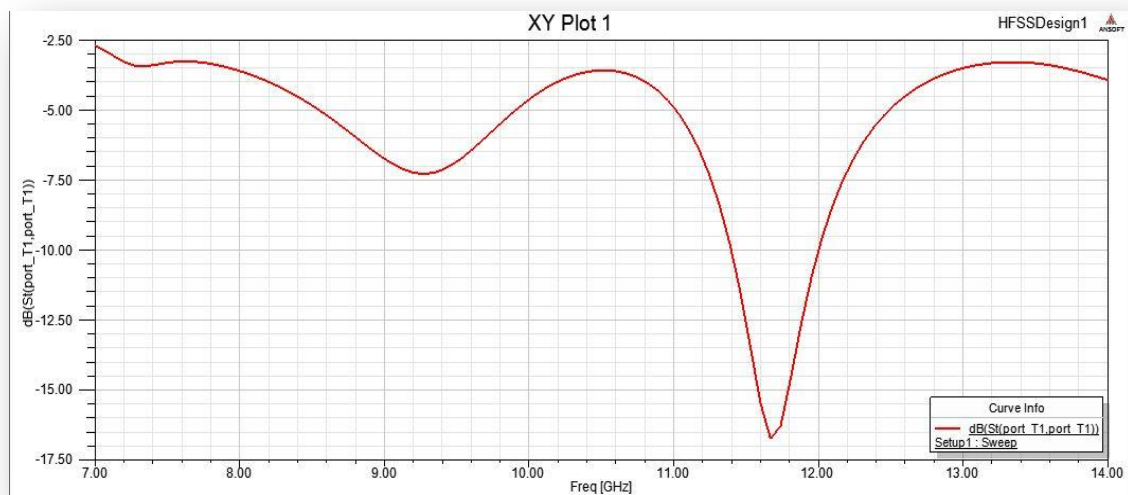


Figure 8.5: Plot of S-parameter against frequency: Patch antenna for 11.72GHz

The above graph shows the plot of the S-parameter (Return Loss) against the frequency. In general a patch antenna is said to have the good return loss characteristics if the return loss value is less than -15db over the whole bandwidth of the designed antenna.

Next the far field radiation patterns of the designed patch antenna for different frequencies in its bandwidth are plotted. The analysis of which gives us a clear picture about the similarity of beam sizes of the E-plane and H-plane. It also throws light on the symmetry of the E-plane and H-plane radiation patterns. We are testing the behaviour of the patch antenna in the frequency range of 11.5 to 11.8 GHz. The radiation patterns of the designed patch at different frequencies of its bandwidth are as shown in the figure 8.6. We can see the E-plane and H-plane patterns at two different planes that is $\phi=0^\circ$ and $\phi=90^\circ$.

The figure 8.6 given below shows the radiation patterns of the designed patch antenna at frequencies 11.5GHz, 11.72GHz and 11.8GHz.

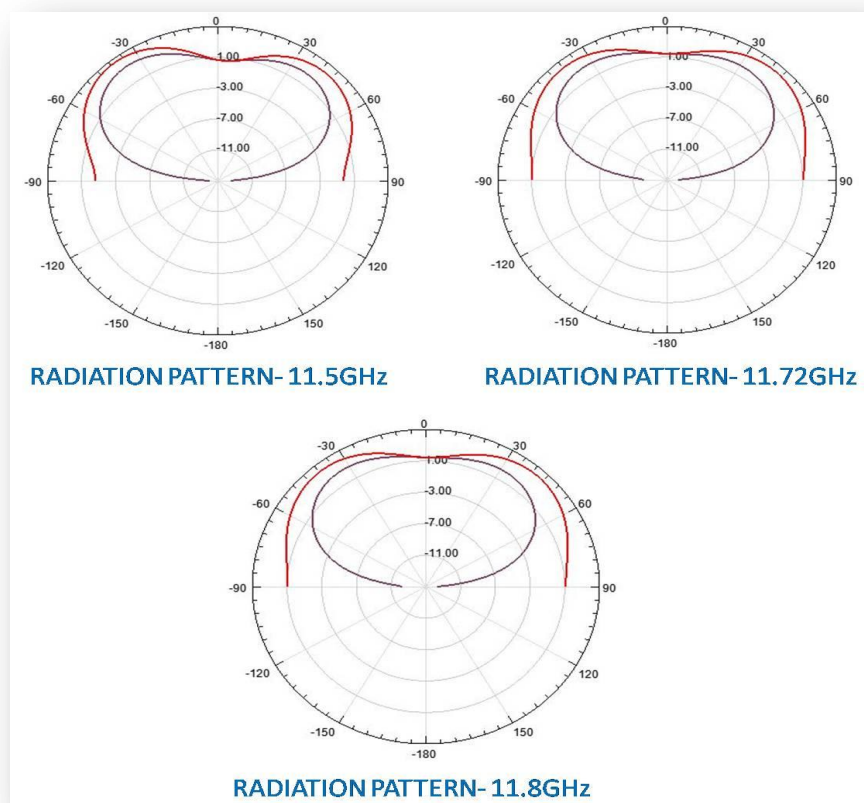


Figure 8.6: Plot of S-parameter against frequency: Patch antenna for 11.72GHz

Note that the E-plane pattern is broader than the H-plane pattern. The directivity is approximately 6 dB. The radiation efficiency of the patch antenna is affected not only by conductor and dielectric losses, but also by surface-wave excitation -- since the dominant TM_{10} mode of the grounded substrate will be excited by the patch. As the substrate thickness decreases, the effect of the conductor and dielectric losses becomes more severe, limiting the efficiency. On the other hand, as the substrate thickness increases, the surface-wave power increases, thus limiting the efficiency. Surface-wave excitation is undesirable for other reasons as well, since surface waves contribute to mutual coupling between elements in an array, and also cause undesirable edge diffraction at the edges of the ground plane or substrate, which often contributes to distortions in the pattern and to back radiation.

. Once the design of patch at a particular frequency is complete the next step is broad banding the patch using any of the techniques mentioned previously.

8.2 Stacked patch with a bandwidth of 7-12.5GHz:

The single patch designed had a narrow bandwidth hence to increase its bandwidth stacked patch method was followed. The stacked coupled patch structures have been favored in most applications because of the ease with which the coupling coefficient can be controlled by adjusting their separation height. Their other parameters such as the size of the patches and substrate parameters can also be modified independently to facilitate the designs.

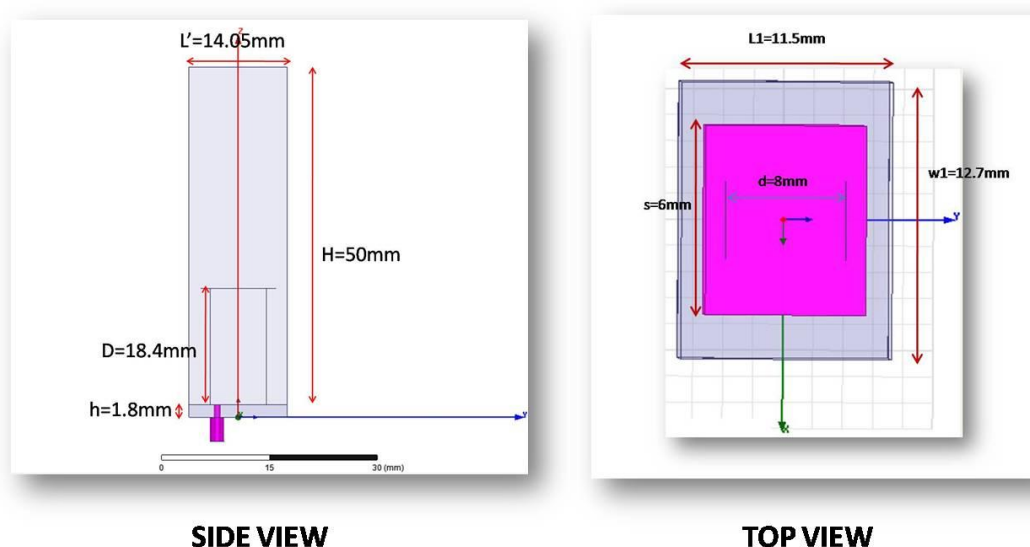


Figure 8.7: The structure of stacked patch antenna ($D=18.4\text{mm}$).

This method involves placing another radiating patch at a certain distance from the patch which we are feeding. We perform stacking using shorting plates which can hold the patch on it. The complete design of stacked patch is as shown below in figure 8.7.

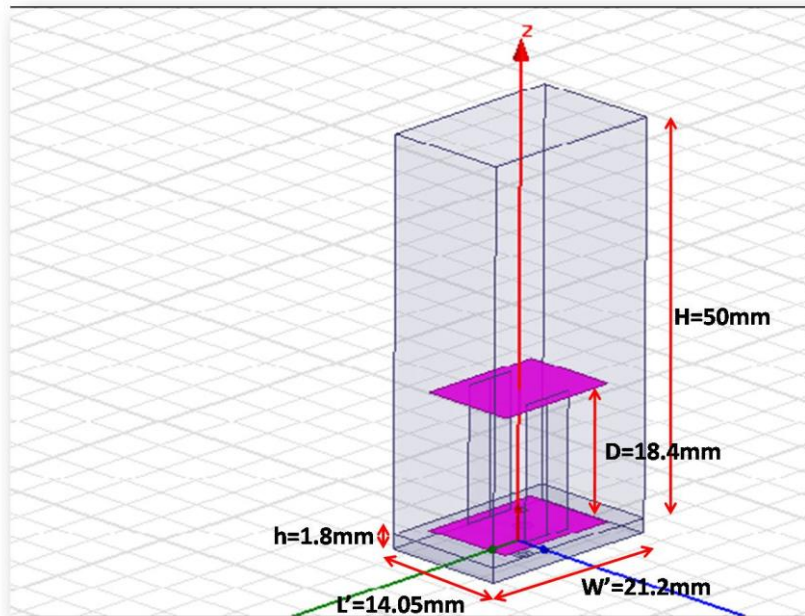


Figure 8.8: Isometric view of the stacked patch.

In this design the characteristics of the patch depend mostly on the distance and the dimensions of the second patch. We considered the second patch to be as same size as the first one and the distance was chosen such that it is at a distance of multiples of $\lambda/2$ the ground plane.

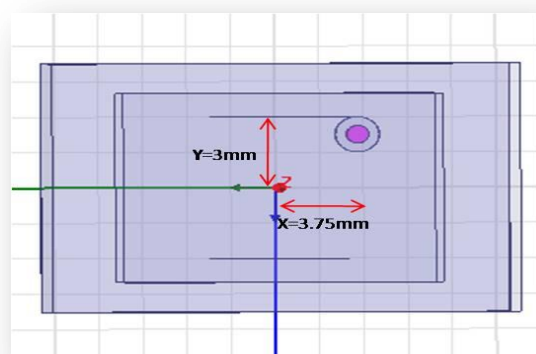


Figure 8.9: Modified feed position for the stacked patch.

Once the design was complete we observed the plots of VSWR and return loss and the variations in the dimensions of patches were made to obtain the required values of VSWR and return loss over the required operating bandwidth of the patch antenna.

The figures given below shows the stacked patch design, VSWR, return loss and radiation patterns over the frequency range for a height of **18.4mm** from the ground plane.

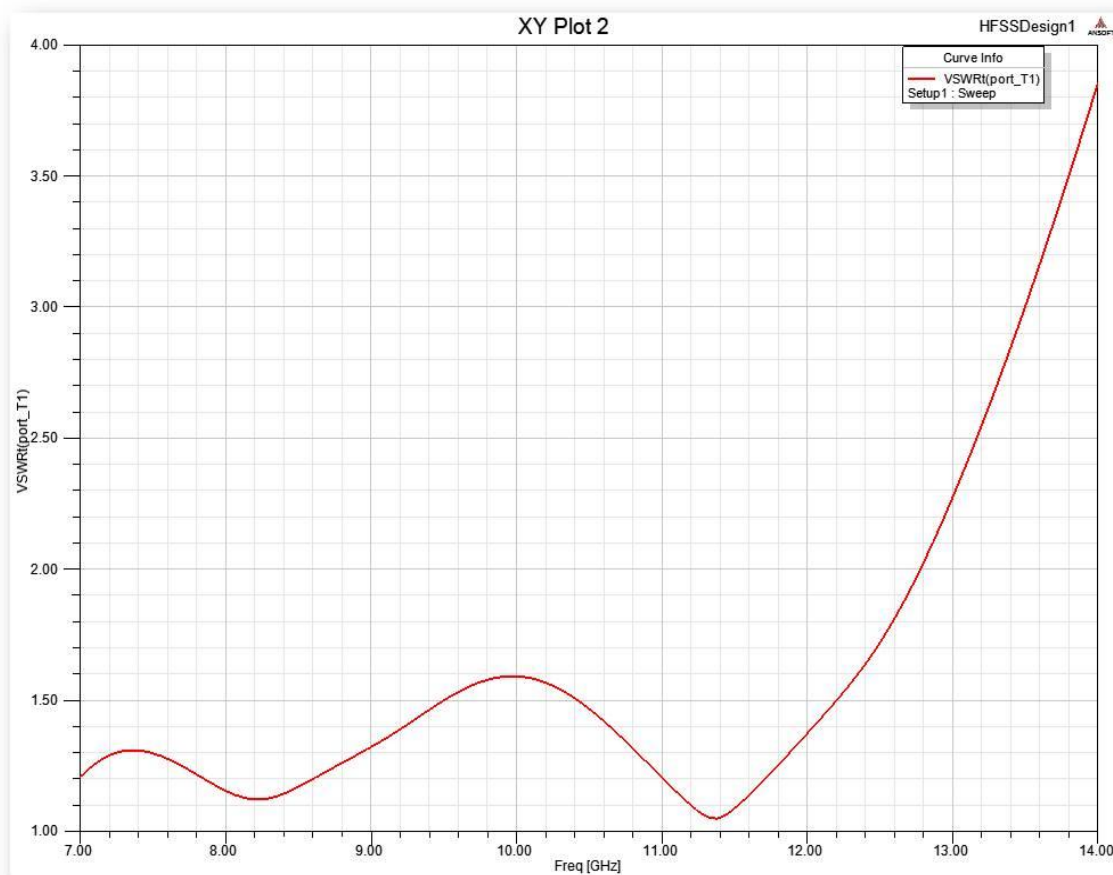


Figure 8.10: Plot of VSWR for the stacked patch ($D=18.4\text{mm}$).

As seen in the plot VSWR is below 1.6 for the frequencies in the range 7 to 12 GHz which is an acceptable level. There is a steep rise in the VSWR for the frequencies above 12 GHz which is not desirable since there is multimode excitation at higher frequencies resulting in standing wave formation. Hence we restrict the operating bandwidth of our antenna to 7 to 12 GHz.

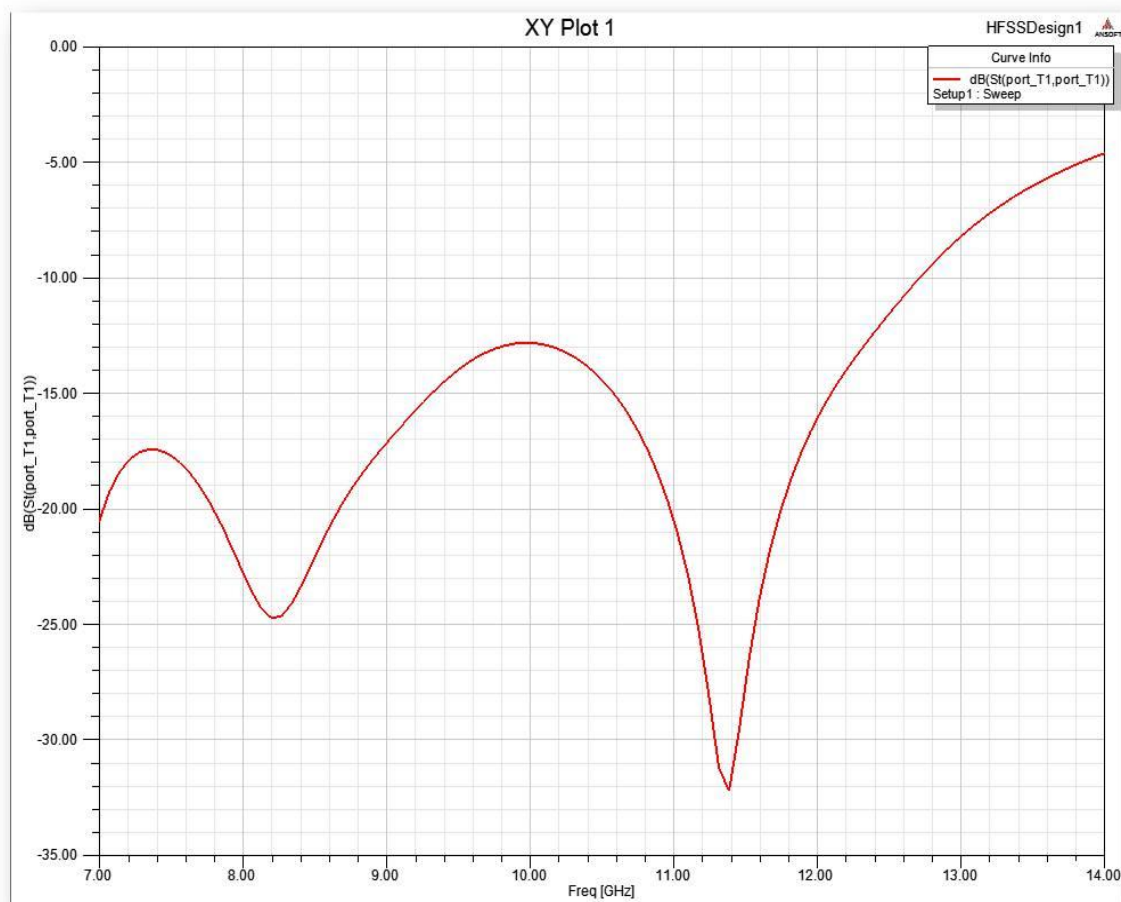
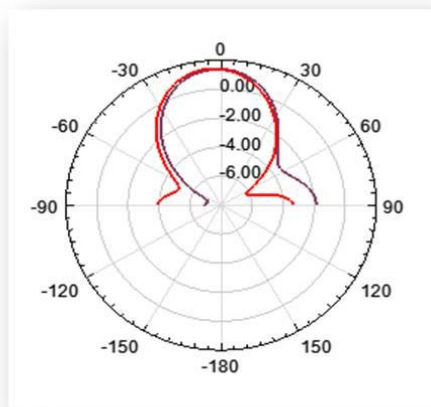
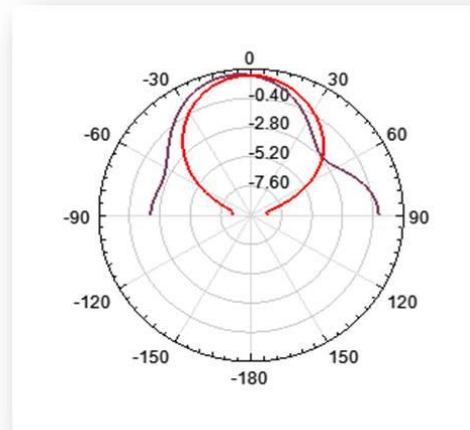


Figure 8.11: Plot of S-parameter for the stacked patch ($D=18.4\text{mm}$).

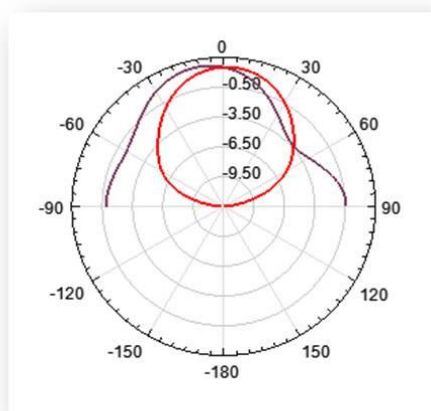
As seen in the S-parameter plot or return loss plot the loss is below -10dB for the frequencies in the range 7 to 12 GHz which is an acceptable level. There is a steep rise in the return loss for the frequencies above 12 GHz which is not desirable and indicates that there is mismatch at these frequencies. The antenna impedance and the feed impedance are well matched in the frequency range 7 to 12 GHz.



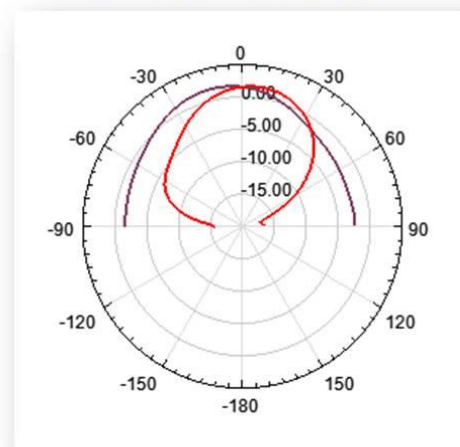
RADIATION PATTERN – 7GHz



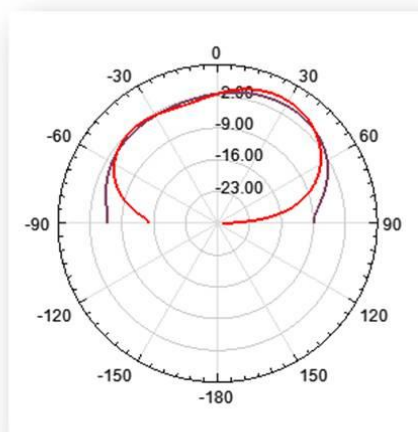
RADIATION PATTERN – 7.8GHz



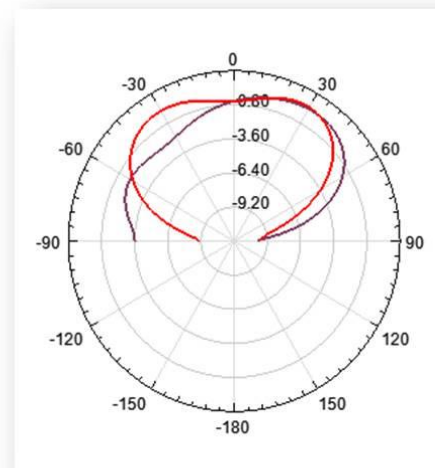
RADIATION PATTERN – 8.6GHz



RADIATION PATTERN – 9.4GHz



RADIATION PATTERN – 11GHz



RADIATION PATTERN – 12GHz

Figure 8.12: Radiation patterns at different frequencies for the stacked patch (D=18.4mm).

As seen the VSWR and return loss changes abruptly over the frequency range although it is around the acceptable level in certain frequencies. Hence the distance is modified to 36.8mm.

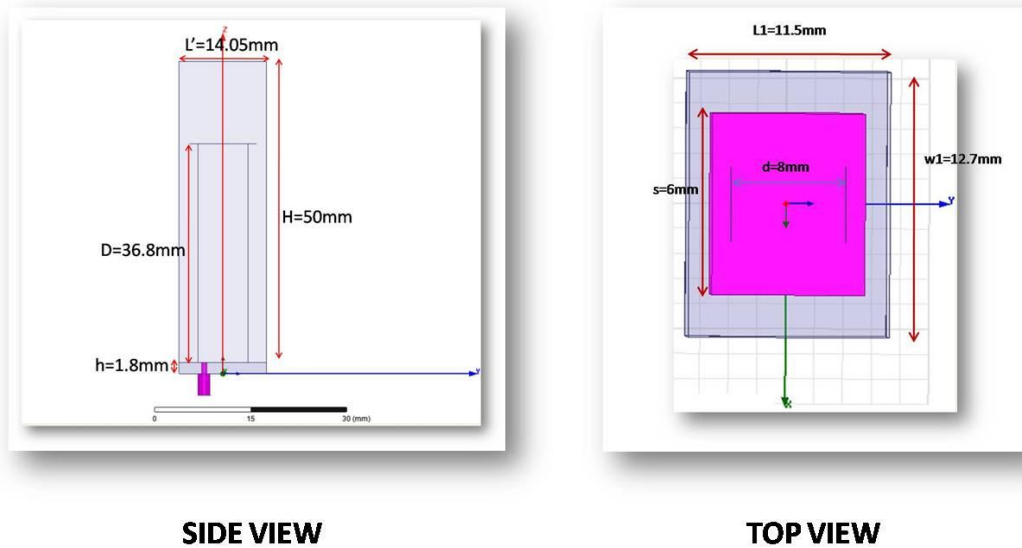


Figure 8.13: The structure of stacked patch antenna ($D=36.8\text{mm}$).

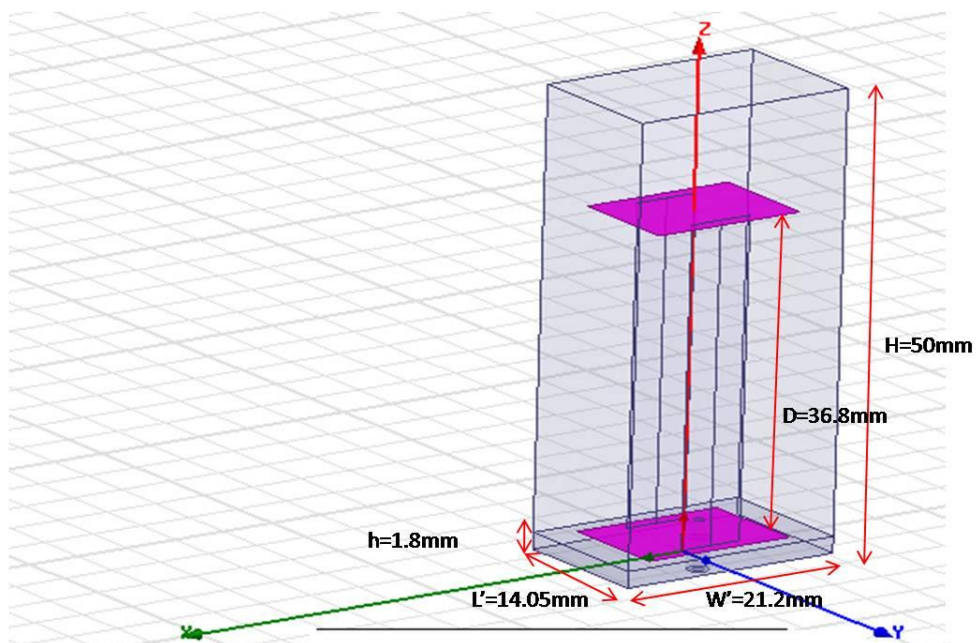


Figure 8.14: Isometric view of the stacked patch ($D=36.8\text{mm}$).

The figures given below shows the basic design, VSWR, return loss and radiation patterns over the frequency range for a height of **36.8mm** from the ground plane.

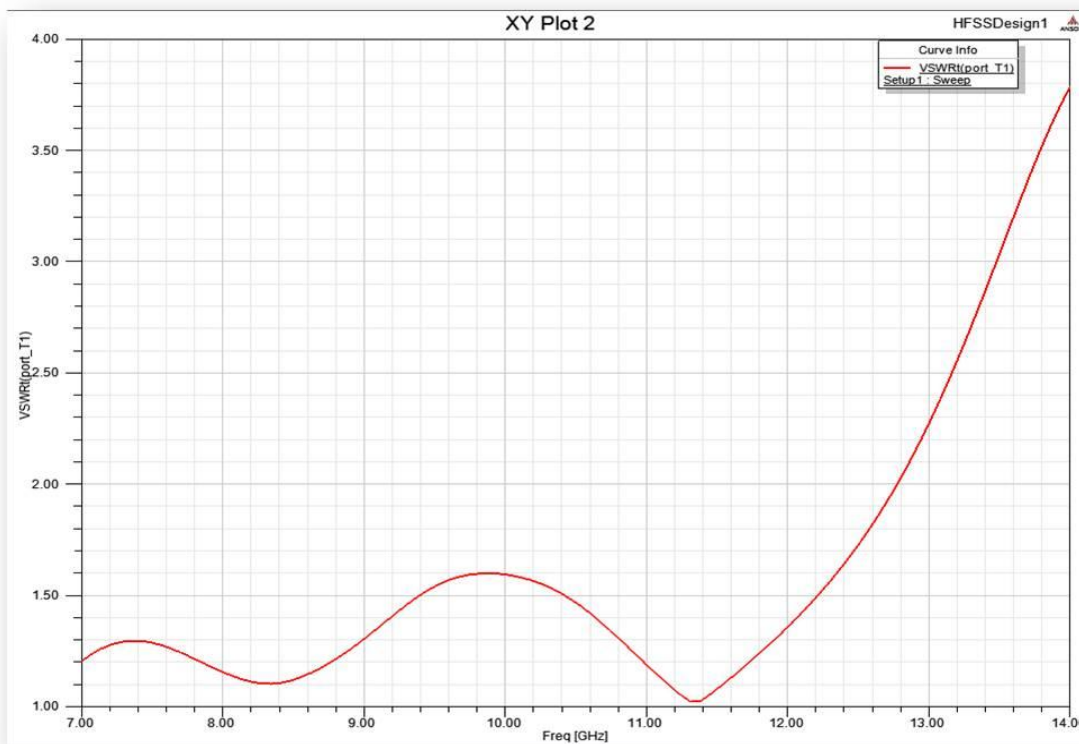


Figure 8.15: Plot of VSWR for the stacked patch ($D=36.8\text{mm}$).

As compared to VSWR results for the height of $d=18.4\text{mm}$ the VSWR has lowered slightly in the frequency range 7 to 12 GHz for $d=36.8\text{mm}$. This is because of the decrease in coupling between the patches when the distance between them is increased. Capacitance between them decreases as distance increases. The operating frequency range increases which is as shown in the plot where the $\text{VSWR} < 1.5$ in the frequency range 7 to 12.5GHz. Hence the operating bandwidth of our antenna is increased to 7 to 12.5 GHz.

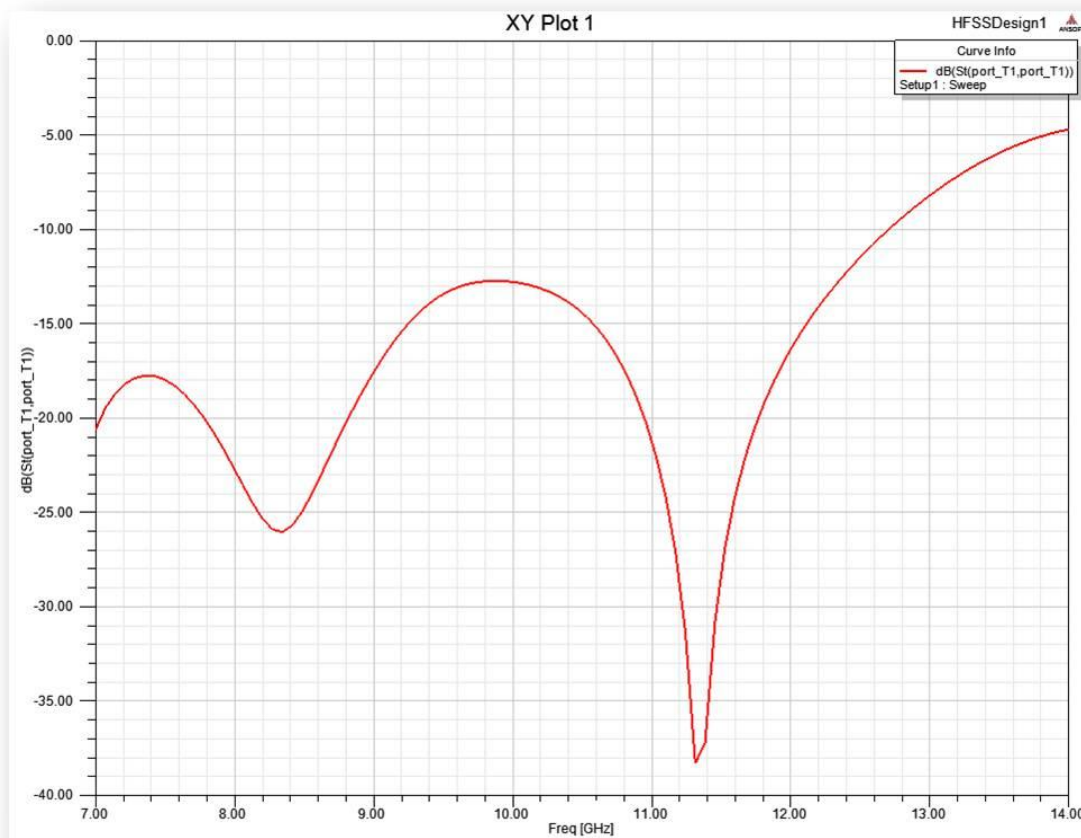
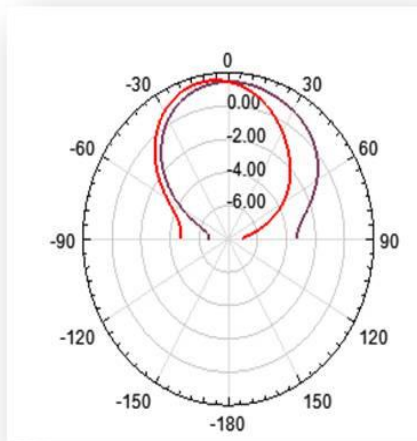
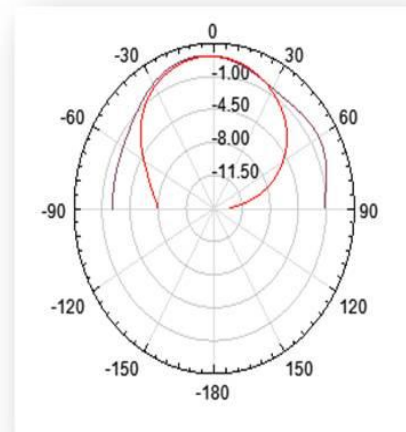


Figure 8.16: Plot of S-parameter for the stacked patch ($D=36.8\text{mm}$).

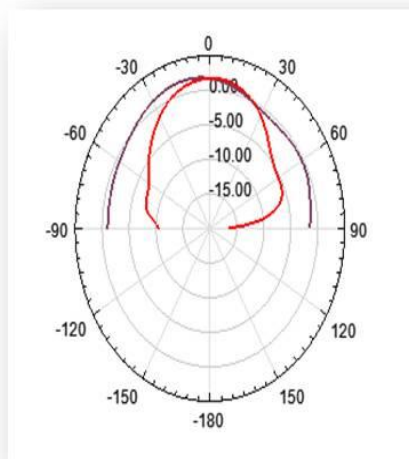
As compared to the S-parameter plot for $d=18.4\text{ mm}$ the return loss is increased for the frequencies in the range 7 to 12 GHz and is much better matched than the previous result. Although the increase in distance has improved the VSWR and return loss but the radiation patterns obtained for $d=36.8\text{mm}$ when compared with those for $d=18.4\text{mm}$ are less symmetrical. The decrease in coupling between the patches is the reason for the deterioration of the radiation pattern. Hence a compromise in the design has to be reached according to the operation for which we are going to use the antenna.



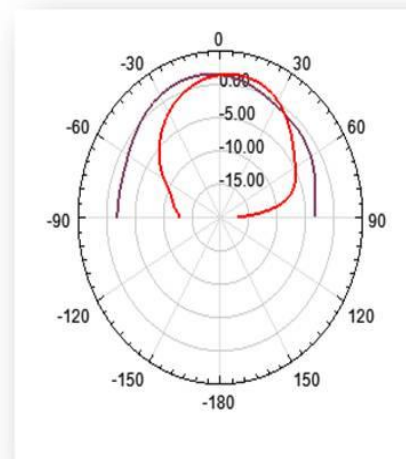
RADIATION PATTERN – 7GHz



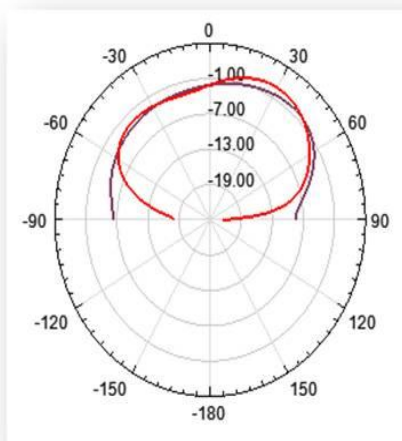
RADIATION PATTERN – 7.8GHz



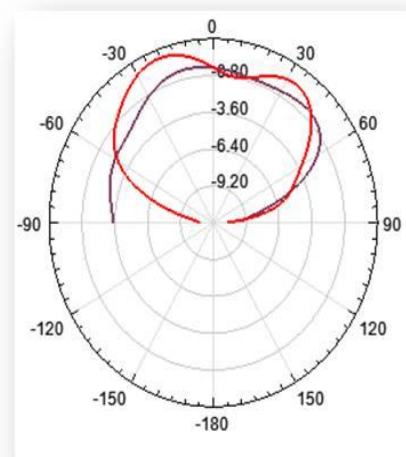
RADIATION PATTERN – 8.6GHz



RADIATION PATTERN – 9.4GHz



RADIATION PATTERN – 11GHz



RADIATION PATTERN – 12GHz

Figure 8.17: Radiation patterns at different frequencies for the stacked patch
($D=36.8\text{mm}$)

CHAPTER 9**CONCLUSION AND FUTURE WORK**

In this project we have used the software tool HFSS for the design of the Double Ridged Horn Antenna (DRHA) and Patch antenna and simulation of the designs. The results were obtained for the various antenna parameters like VSWR, radiation patterns and the two designs were compared. Several novel modifications were also incorporated for both the designs to enhance their performances.

In case of the Double Ridged Horn Antenna (DRHA) the modifications incorporated were new type of the tapering for the ridges and the introduction of the back fins for the cavity back. The incorporation of these two modifications improved the VSWR and the radiation patterns over the frequency band.

In case of the micro strip antenna, the technique used for the bandwidth enhancement was stacking of patches. The stacking was also done for different distances between the two patches, out of which two variations are shown in this report.

Horn antennas are most common at microwave frequencies. Horn antennas are very practical for space applications. Horn antennas are used when the power gain needed is moderate. The horn is widely used as the feed element for large radio astronomy, satellite tracking and communication dishes, found installed throughout the world. In addition to its utility as a feed for reflectors and lenses it is a common element of phased arrays, and serves as universal standard for the calibration and gain measurements of the other high gain antennas. Its widespread applicability stems from its simplicity in construction, ease of excitation, versatility, large gain and preferred overall performance.

On the other hand the patch antennas, there are certain disadvantages. Major operational disadvantages of the patch antennas are their low efficiency, low power, high Q, poor polarization purity, poor scan performance, spurious feed radiation and very narrow frequency bandwidth, which is typically only fraction of the percent or at most a few percent. However we have used the bandwidth enhancement technique of stacking of the patches to increase the bandwidth of the patch antenna the results obtained were not satisfactory when compared to the horn antenna. The criteria for the selection were the similarity of the E-plane and the H-plane in the radiation patterns, power handling capability and poor polarization purity.

The major limitation of the micro strip antenna is its limited bandwidth. We have seen that even after using the bandwidth enhancement technique such as stacking of the patches, the bandwidth achieved was 5.5GHz. This is because the patch antenna is a resonant antenna, it has a particular resonant frequency. On the other hand the Horn antenna does not have any resonant elements in it. Hence the bandwidth of operation of the horn antenna is not limited.

Based on the aforesaid reasons the Double Ridged Horn Antenna (DRHA) was selected for the fabrication. The figures given below shows the design specifications of the Double Ridged Horn Antenna.

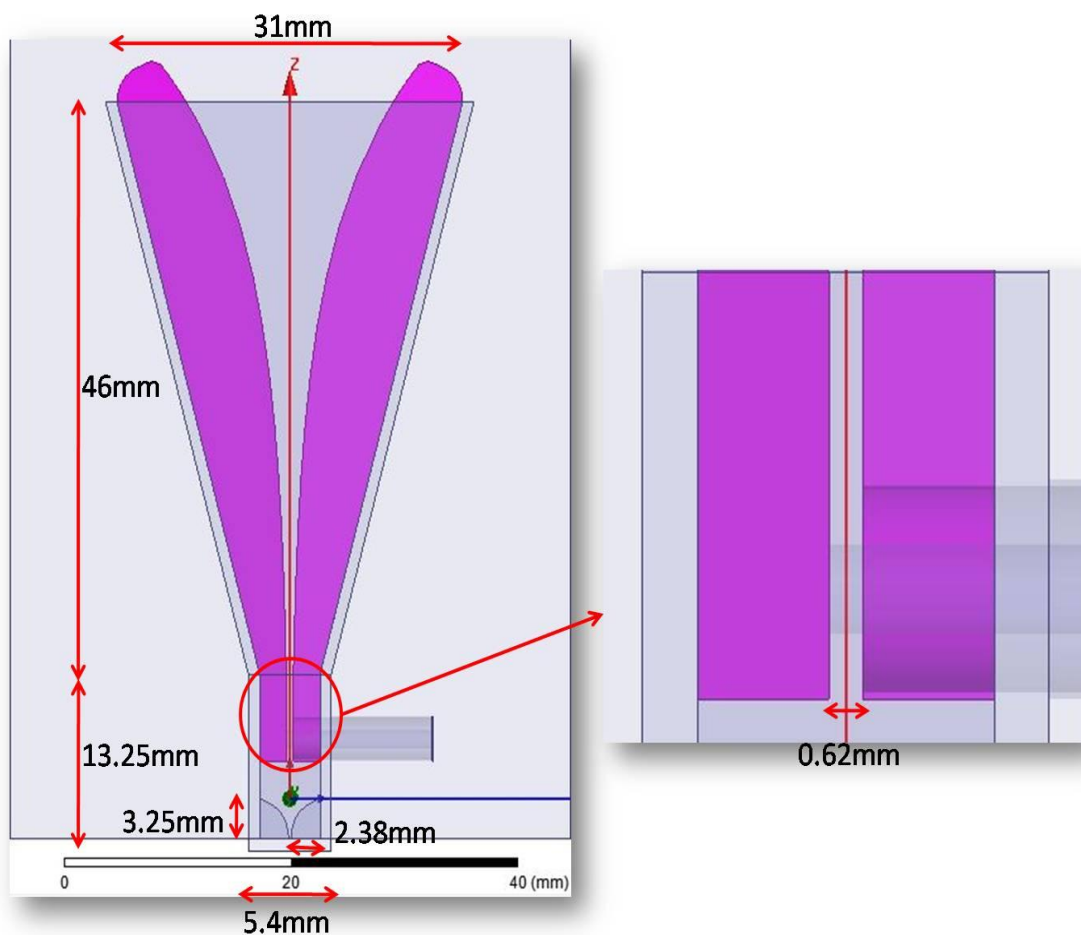


Figure 9.1: Side view of the designed Antenna in YZ plane

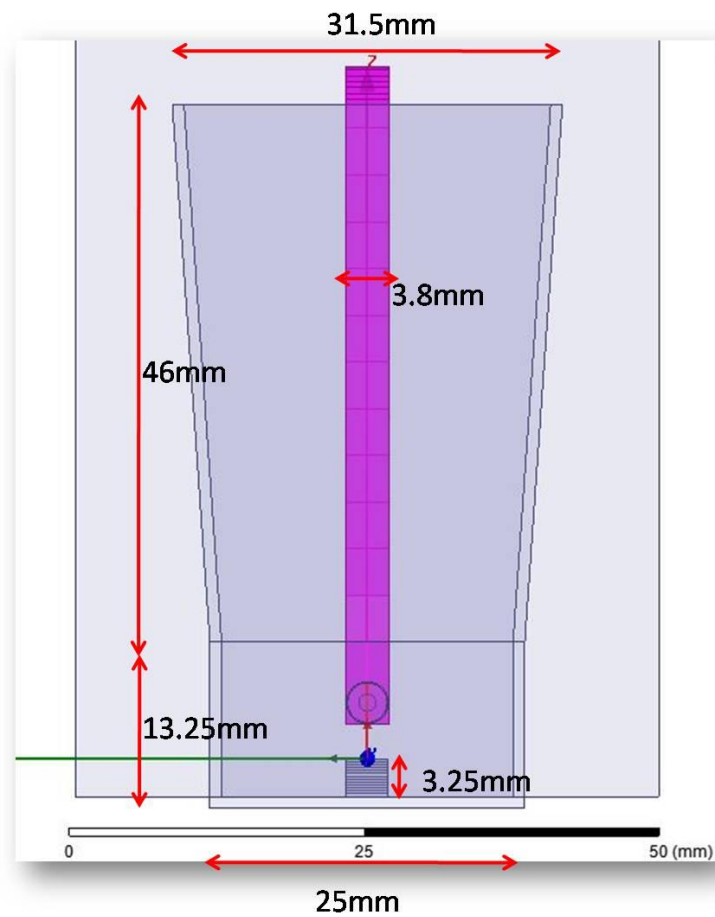


Figure 9.2: Side view of the designed Antenna in XZ plane

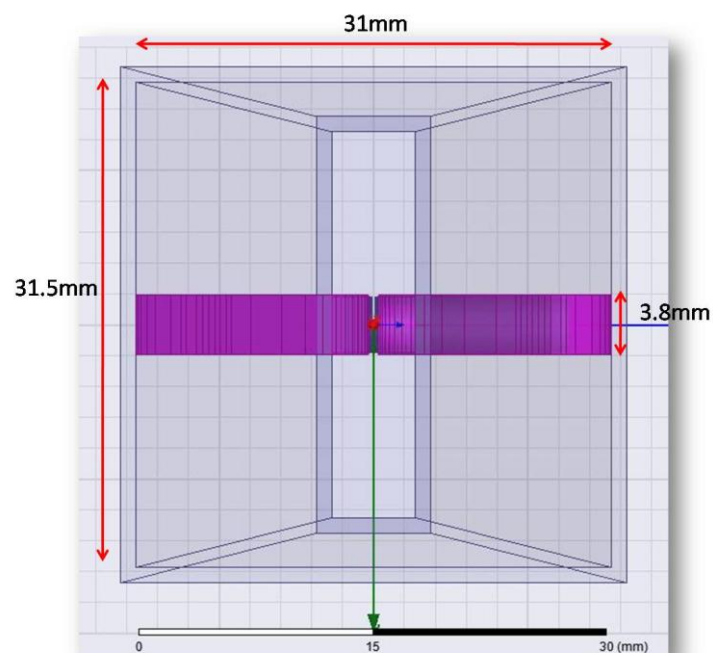


Figure 9.3: Top view of the designed Antenna in XY plane

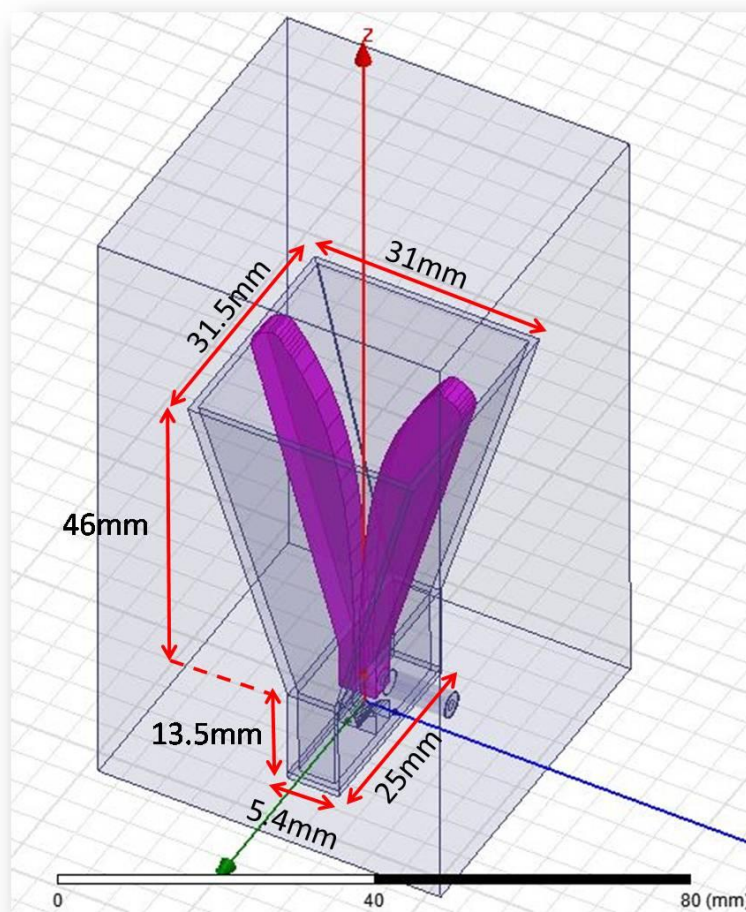


Figure 9.4: Isometric view of the designed Antenna

Future Work:

The Double Ridged Horn Antenna (DRHA) also have certain disadvantages, certain modifications can be done to the present design which could result in the reduction in the beam angle of the radiation pattern. The wider beam angle of the radiation pattern results in the need for the secondary for the radio telescope. However this problem can be overcome by extending the flare section of the designed horn antenna and by choosing the appropriate tapering for the ridges for that extended portion. With the modifications (if required) the feed section is fabricated by RRI (Raman Research Institute) and integrated into the Active Integrated Antenna (AIA).

BIBLIOGRAPHY

- [1] J. L. Kerr, "Short axial length broad-band horns," *IEEE Trans. Antennas Propagate.*, vol. 21, no. 5, pp. 710–714, 1973.
- [2] Requirements for the Control of Electromagnetic Interference Characteristics of Subsystems and Equipment, MIL-STD-461-F, Dec. 2007.
- [3] American National Standard for Instrumentation-Electromagnetic Noise and Field Strength, 10 kHz to 40 GHz, ANSI C63.2, 1987.
- [4] Specification for radio disturbance and immunity measuring apparatus and methods – Part 1-4: Radio disturbance and immunity measuring apparatus – Ancillary equipment – Radiated disturbances, CISPR 16-1-4, 2007.
- [5] C. Bruns, P. Leuchtmann, and R. Vahldieck, "Analysis and Simulation of a 1-18-GHz broadband double-ridged horn antenna," *IEEE Trans. Electromagnet. Compact.* vol. 45, no. 1, pp. 55–60, 2003.
- [6] "Comprehensive analysis and simulation of a 1-18 GHz broadband parabolic reflector horn antenna system," *IEEE Trans. Antennas Propagate.*, vol. 51, no. 6, pp. 1418–1422, 2003.
- [7] "Full wave analysis and experimental verification of a broad band ridged horn antenna system with parabolic reflector," in *IEEE Antennas and Propagation Soc. Int. Symp.*, 2001, vol. 4, 2001.
- [8] M. Abbas-Azimi, F. Arazm, and J. Rashed-Mohassel, "Sensitivity analysis of a 1 to 18 GHz broadband DRGH antenna," in *IEEE Antennas and Propagation Society Int. Symp.* 2006. pp. 3129–3132, 2006.

-
- [9] M. Botello-Perez, H. Jardon-Aguilar, and I. G. Ruiz, "Design and Simulation of a 1 to 14 GHz Broadband Electromagnetic Compatibility DRGH Antenna," in 2nd Int. Conf. Electrical and Electronics Engineering, pp. 118–121, 2005.
- [10] V. Rodriguez, "New broadband EMC double-ridged guide horn antenna," RF Design., pp. 44–47, 2004.
- [11] M. Abbas-Azimi, F. Arazm, J. Rashed-Mohassel, and R. Faraji-Dana, "Design and optimization of a new 1-18 GHz double ridged guide horn antenna," J. of Electromagn. Waves and Appl., vol 21, no. 4, pp. 501- 516, 2007.
- [12] V. Rodriguez, "Dual Ridge Horn Antenna," U. S. Patent 6 995 728 B2, Feb., 7, 2006.
- [13] B. Jacobs, J. W. Odendaal, and J. Joubert, "The Effect of Manufacturing and Assembling Tolerances on the Performance of Double-Ridged Horn Antennas", J. of Electromagn. Waves and Appl., vol 24, no. 10, pp. 1279-1290, 2010.
- [14] K. L. Walton, and V. C. Sundberg, "Broadband ridged horn design," Microwave J., 96–101, 1964.
- [15] D. Baker, and C. Van Der Neut, "A compact, broadband, balanced transmission line antenna derived from double-ridged waveguide." Antennas and Propagat. Soc. Int. Symp., vol. 20, 1982.
- [16] EM Software & Systems, FEKO User's Manual, Suite 5.4, July 2008
- [17] Li, H., B. Z. Wang, and W. Shao, "Novel broadband reflect array antenna with compound-cross-loop elements for millimeter-wave application," Journal of Electromagnetic Wave and Applications, Vol. 21, No. 10, 1333–1340, 2007.
- [18] Ren, W., J. Y. Deng, and K. S. Chen, "Compact PCB monopole antenna for UWB applications," Journal of Electromagnetic Wave and Applications, Vol. 21, No. 10, 1411–1420, 2007.

-
- [19] Coulibaly, Y., T. A. Denidani, and L. Talbi, "Design of a broadband hybrid dielectric resonator antenna for X-band," *Journal of Electromagnetic Wave and Applications*, Vol. 20, No. 12, 1629–1642, 2006.
- [20] Naghshvarian-Jahromi, M., "Compact UWB bandnotch with transmission-line-fed," *Progress In Electromagnetics Research B*, Vol. 3, 283–293, 2008.
- [21] Khan, S. N., J. Hu, J. Xiong, and S. He, "Circular fractal monopole antenna for low VSWR UWB applications," *Progress In Electromagnetics Research Letters*, Vol. 1, 19–25, 2008.
- [22] Saed, M. A., "Broadband CPW-FED planar slot antennas with various tuning stubs," *Progress In Electromagnetics Research*, PIER 66, 199–212, 2006.
- [23] Xia, S., J. Chen, X.-F. Liu, and B. Z. Wang, "Spatial focusing characteristics of time reversal UWB pulse transmission with different antenna arrays," *Progress In Electromagnetics Research B*, Vol. 2, 189–206, 2008.
- [24] Yin, X.-C., C. Ruan, Y.-C. Ding, and J.-H. Chua, "A planar U type monopole antenna for UWB applications," *Progress In Electromagnetics Research Letters*, Vol. 2, 1–10, 2008.
- [25] Jiao, J.-J., G. Zhao, F.-S. Zhang, H.-W. Yuan, and Y.-C. Jiao, "A broadband CPW-FED T shape slot antenna," *Progress In Electromagnetics Research*, PIER 76, 237–242, 2007. *Progress In Electromagnetics Research*, PIER 91, 2009 285
- [26] Walton, K. L. and V. C. Sundberg, "Broadband ridged horn design," *Microwave J.*, 96–101, March 1964.
- [27] Kerr, J. L., "Short axial length broad-band horns," *IEEE Trans. Antennas Propagat.*, Vol. 21, 710–714, September 1973.
- [28] Hopfer, S., "The design of ridged waveguides," *IRE Trans. Microwave Theory Tech.*, Vol. 3, 20–29, October 1955.

-
- [29] Cohn, S. B., "Properties of ridged waveguide," Proc. Vol. 35, 783–788, August 1947.
- [30] Jarvis, D. A. and T. C. Rao, "Design of double-ridged rectangular wave guide of arbitrary aspect ratio and ridge height," IEE Proc. — Microw. Antenna Propagat., Vol. 147, 31–34, 2000.
- [31] Reig, C. and E. Navarro, "FDTD analysis of E-sectoral horn antenna for broadband applications," IEEE Trans. Antennas Propag., Vol. 45, No. 10, 1484–1487, October 1997.
- [32] Bungler, R., R. Beyer, and F. Arndt, "Rigorous combined mode-matching integral equation analysis of horn antennas with arbitrary cross section," IEEE Trans. Antennas Propag., Vol. 47, No. 11, 1641–1648, November 1999.
- [33] Bruns, C., P. Leuchtman, and R. Vahldieck, "Analysis and simulation of a 1–18 GHz broadband double-ridged horn antenna," IEEE Transaction on Electromagnetic Compatibility, Vol. 45, 55–59, February 2003.
- [34] Botello-Perez, M., H. Jardon-Aguilar, and I. Ruiz, "Design and simulation of a 1 to 14GHz broadband electromagnetic compatibility DRGH antenna," ICEEE-ICE 2005, 2nd International Conference on Electrical and Electronics Engineering, 118–121, September 2005.
- [35] Rodriguez, V., "New broadband EMC double-ridged guide horn antenna," R. F. Des., 44–47, May 2004.
- [36] Abbas-Azimi, M., F. Arazm, J. R. Mohassel, and R. Faraji- Dana, "Design and optimization of a new 1–18 GHz double ridged guide horn antenna," Journal of Electromagnetic Wave and Applications, Vol. 21, No. 4, 501–506, 2007.
- [37] A.K Bhattacharjee., S.R Bhadra., D.R. Pooddar and S.K. Chowdhury, "Equivalence of impedance and radiation properties of square and circular microstrip patch antennas," IEE Proc. vol.136, Pt, H, no.4, pp338-342.,1989.

-
- [38] L. I. Basilio, M. A. Khayat, J. T. Williams, and S. A. Long, "The dependence of the input impedance on feed position of probe and microstrip line-fed patch antennas," *IEEE Trans. Antennas Propagat.*, vol. 49, no. 1, pp 45-47, 2001.
- [39] Z.N. Chen and M.Y.W. Chia, "Broadband suspended plate antenna with probe-fed strip," *IEE Proc.- Microw. Ant. Prop.*, vol. 148, no.1, pp3 7-40, 2001.
- [40] I.J. Bahl and P. Bhartia, "Microstrip antennas," Artech Hous, Inc., 1980.
- [41] A. Hussien, " Microstrip backfire antenna", M.Sc. Thesis, College of Science , Al-Nahrain university (Formerly Saddam University), Baghdad, Iraq, 1995.
- [42] E. C., S. A. Long and W. F. Richards, "An experimental investigation of electrically thick rectangular microstrip antennas," *IEEE Trans. Antennas Propagat.*, vol. AP-34, no. 6, pp 767 772, 1986.
- [43] Z. N. Chen, M.Y.W. Chia, and C. L. Lim, "A stacked suspended plate antenna" *Microwave and Optical Technology Letters*, vol.37, no.5, pp 337-339, 2003.
- [44] J. R. James and P. S. Hall, "Handbook of microstrip antennas," *IEE Electromagnetic Waves Series 28*, Peter Peregrinus Ltd, 1989.
- [45] Y.T. Lo, P. Solomon, and W.F. Richards, "Theory and experiment on microstrip antennas," *IEEE Trans. Antennas Propaga.*, vol. Ap-27, no. 2, pp.113 7-145,. 1979.
- [46] W.F. Richards, Y.T. Lo, and D.D. Harrison, "An improved theory for microstrip antennas and applications," *IEEE Trans. Antennas Propagat.*, vol. AP-29, no. 1, pp.38-46, 1981.
- [47] G. V. and A. V.D. Cappelle, "A study of the effect of the top patch in rectangular dual patch microstrip antenna," *Ann. Telecom.*, vol. 47, no. 3-4, pp.135-141, 1992.

- [48] K.R. Carver and J.W. Mink, "Microstrip antenna technology," *IEEE Trans. Antennas Propagat.*, vol. Ap-29, pp.2-24, 1981
- [49] Z.-F. Lui, P.-S. Kooi, M.-S. Leong and T.-S. Yeo, "A method for designing broadband microstrip antennas in multilayered planar structures," *IEEE Trans. Antennas Propagat.*, vol. 47, no. 9, 1999.

APPENDIX:

This example is intended to show you how to create, simulate, and analyze using the Ansoft HFSS Design Environment.

Getting Started: Click the Microsoft Start button, select **All Programs>Ansoft>HFSS 13>HFSS 13** or double click on the **HFSS 13** icon on the Windows Desktop.

Adding a Project and Design:

To insert a design into an open project:

- Click **Project>Insert HFSS Design** or on the Toolbar click the Insert HFSS Design icon. The new HFSS design appears in the Project tree.

Setting Tool Options:

To set the tool options:

Note: In order to follow the steps outlined in this example, verify that the following tool options are set:

1. Click **Tools>Options>HFSS Options**
2. In the **HFSS Options** dialog click the **General** tab .Check “Use Wizards for data input when creating new boundaries”. Check “Duplicate boundaries/mesh operations with geometry.”
3. Click OK to close the **HFSS Options** dialog.
4. Click **Tools>Options>Modeler Options**.
5. The **Modeler Options** dialog opens with the **Operation** tab.
6. Check “Automatically cover closed polyline.”
7. Click the **Drawing** tab .Check “Edit property of new primitives”. This causes the **Properties** window for new primitives to open automatically.
8. Click the **OK** button.

Set Solution Type:

To set the solution type:

1. Click **HFSS>Solution Type** .The **Solution Type** dialog opens.
2. Choose Driven Terminal.
3. Click the OK button.

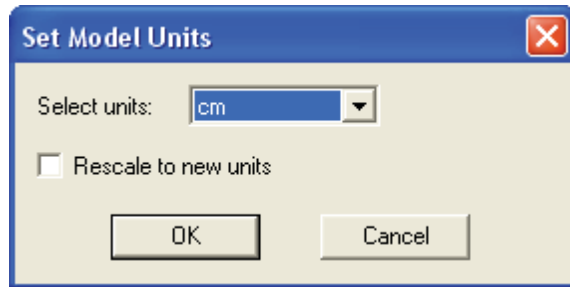
Set Model Units:

To set the units:

Click **Modeler>Units**

Set Model Units:

Select Units: cm

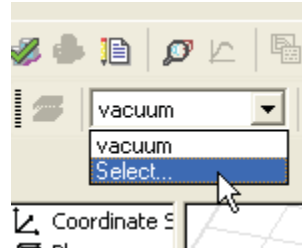


Click the OK button

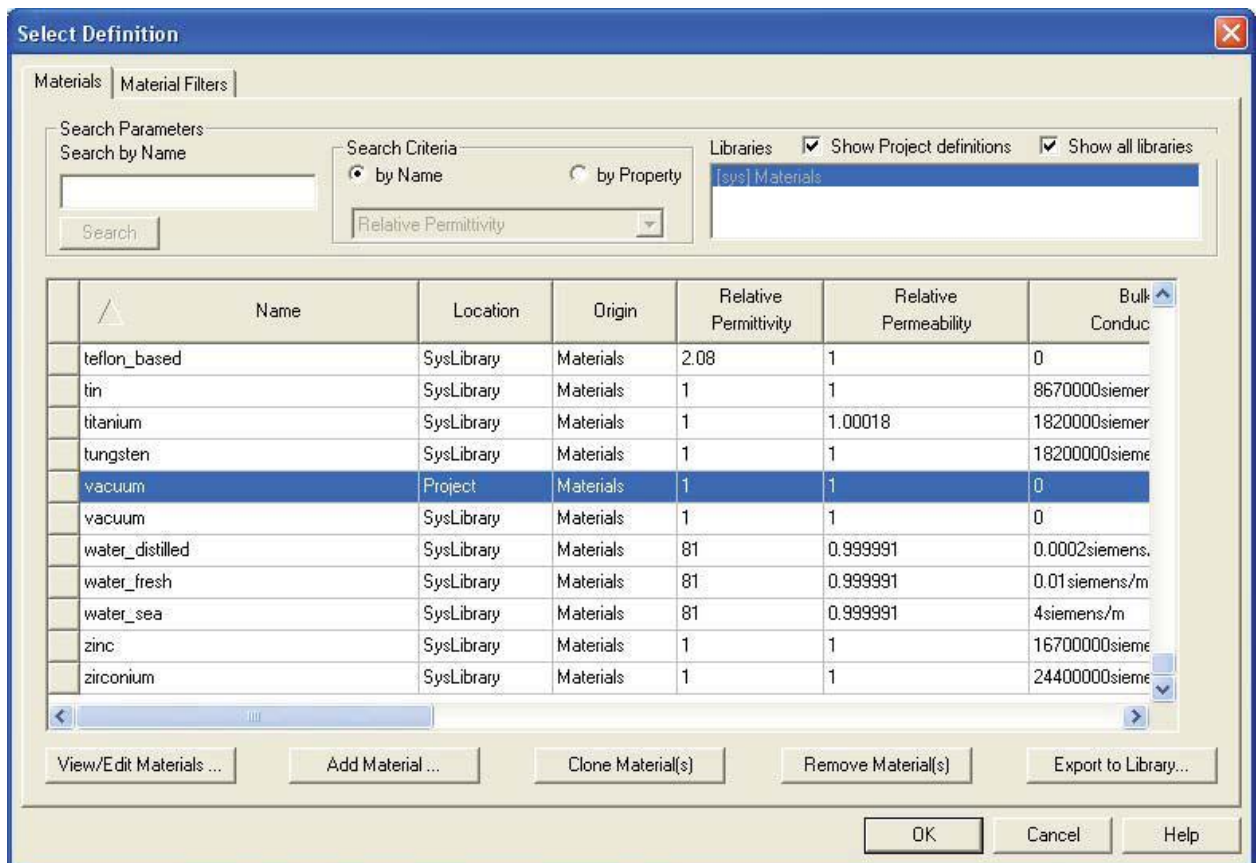
Set Default Material:

To set the default material:

1 .Using the 3D Modeler Materials toolbar, choose **Select...**



2 .This opens the **Select Definition** window with the Material tab.



3. In the Search by Name field, type Rogers RT/ duroid 5880 (tm). Click the OK button

Create Substrate:

To create the substrate:

1. Click **Draw>Box**

2. using the coordinate entry fields, enter the box position

X: -5.0 Y: -4.5, Z: 0.0, Press the Enter key

3. using the coordinate entry fields, enter the opposite corner of the box

dX: 10.0, dY: 9.0, dZ: 0.32,

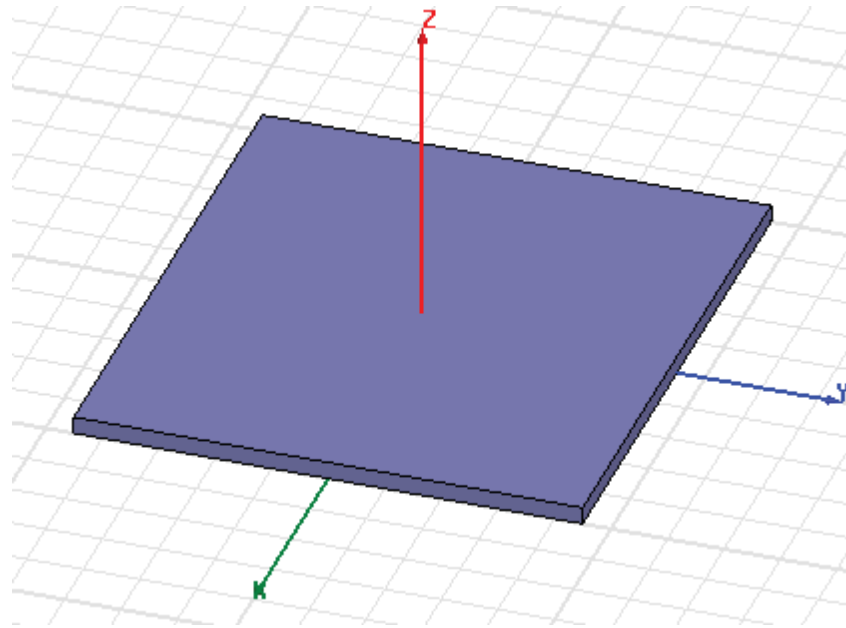
Press the Enter key

To set the name:

1. In the **Properties** window Name field type: Sub1

2. Click the OK button

To fit the view: Click **View>Fit All>Active View**, or press the CTRL+D.



Create Infinite Ground:

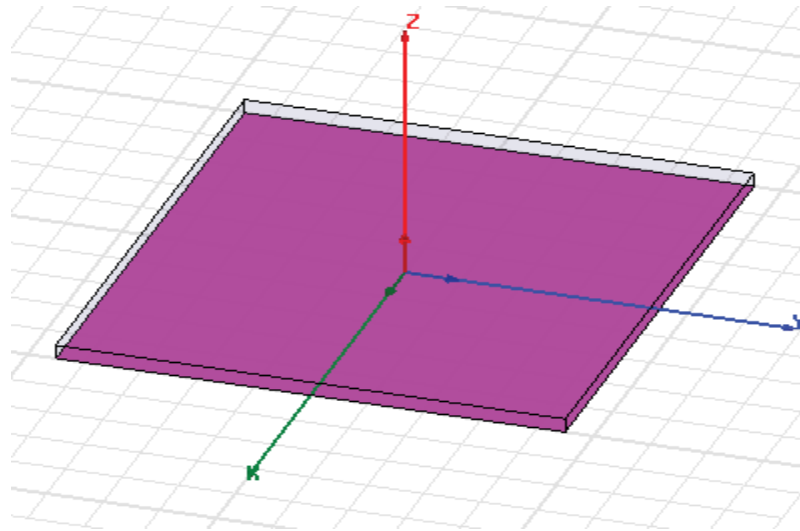
To create the infinite ground:

1. Click **Draw>Rectangle**.
2. Using the coordinate entry fields, enter the rectangle position
X: -5.0, Y: -4.5, Z: 0.0. Press the Enter key
3. Using the coordinate entry fields, enter the opposite corner
of the rectangle:
dX: 10.0, dY: 9.0, dZ: 0.0, Press the Enter key

To set the name:

1. In the **Properties** window Name field type: Inf_GND
2. Click the OK button

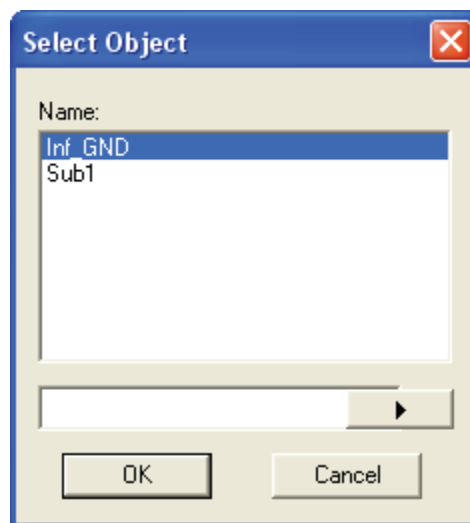
To fit the view:



Assign a Perfect E boundary to the Infinite Ground:

To select the trace:

1. Click **Edit>Select>By Name**. The Select Object dialog opens.
2. Select the objects named: Inf_GND.

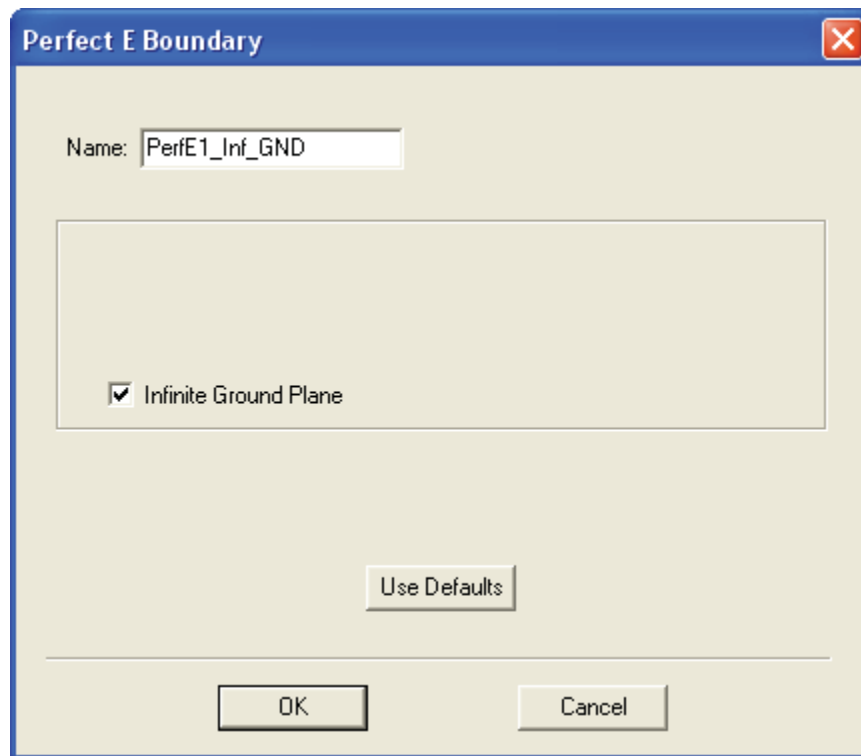


3. Click the OK button

To assign the Perfect E boundary

1. Click **HFSS>Boundaries>Assign>Perfect E**. The **Perfect E Boundary** dialog opens.
2. Specify the Name as: PerfE_Inf_GND

Check “Infinite Ground Plane.”



3. Click the OK button.

Create Infinite Ground Cut Out

To create the cut out:

1. Click **Draw>Circle**
2. Using the coordinate entry fields, enter the center position
X: -0.5, Y: 0.0, Z: 0.0, Press the Enter key
3. Using the coordinate entry fields, enter the radius:
dX: 0.16, dY: 0.0, dZ: 0.0, Press the Enter key

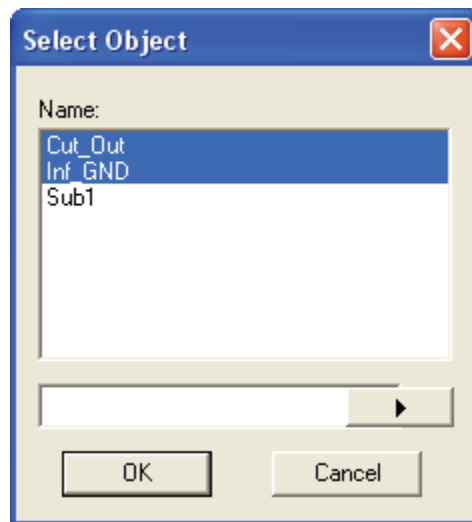
To set the name:

1. In the **Properties** window Name field type: Cut_Out
2. Click the OK button

Complete the Infinite Ground

To select the objects Inf_GND and Cut_Out:

1. Click **Edit>Select>By Name**
The **Select Object** dialog opens.
2. Select the objects named: Inf_GND, Cut_Out



3. Click the OK button

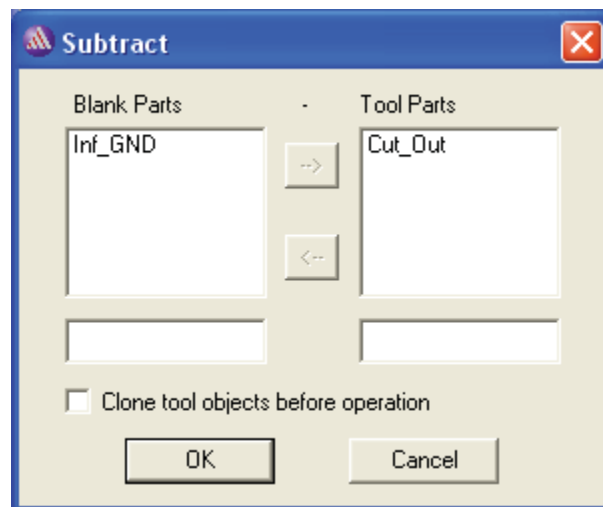
To complete the ring:

1. Click **Modeler>Boolean>Subtract** .The **Subtract** dialog opens:

2. Make the following assignments:

Blank Parts: Inf_GnD, Tool Parts: Cut_Out

Clone tool objects before subtract: Unchecked



3. Click the OK button

Create Patch:

To create the patch:

1. Click **Draw>Rectangle**.

2. Using the coordinate entry fields, enter the rectangle position

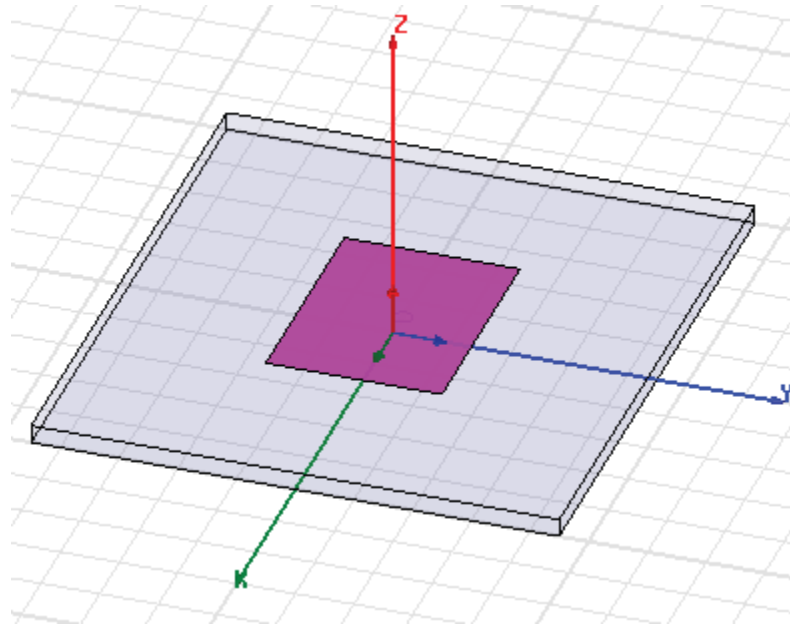
X: -2.0, Y: -1.5, Z: 0.32, Press the Enter key

3. Using the coordinate entry fields, enter the opposite corner of the rectangle:

dX: 4.0, dY: 3.0, dZ: 0.0, Press the Enter key.

To set the name:

1. In the **Properties** window Name field type: Patch
2. Click the OK button.



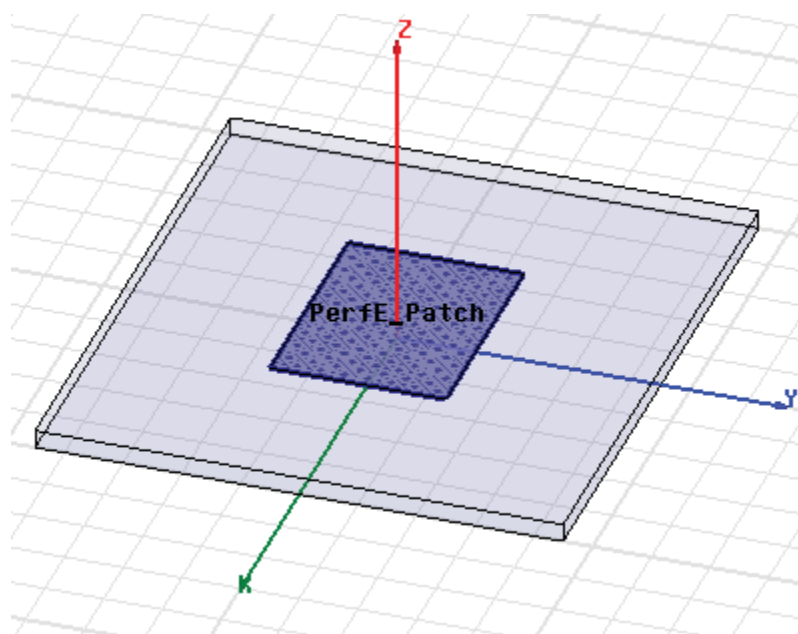
Assign a Perfect E boundary to the Trace

To select the trace:

1. Click **Edit>Select>By Name**. The **Select Object** dialog opens.
2. Select the objects named: Patch
3. Click the OK button

To assign the Perfect E boundary

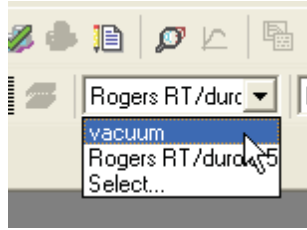
1. Click **HFSS>Boundaries>Assign>Perfect E**. The Perfect E Boundary dialog opens.
2. Specify the Name: PerfE_Patch
3. Click the OK button



Create the Coax:

To set the default material:

1. Using the 3D Modeler Materials toolbar, choose vacuum.

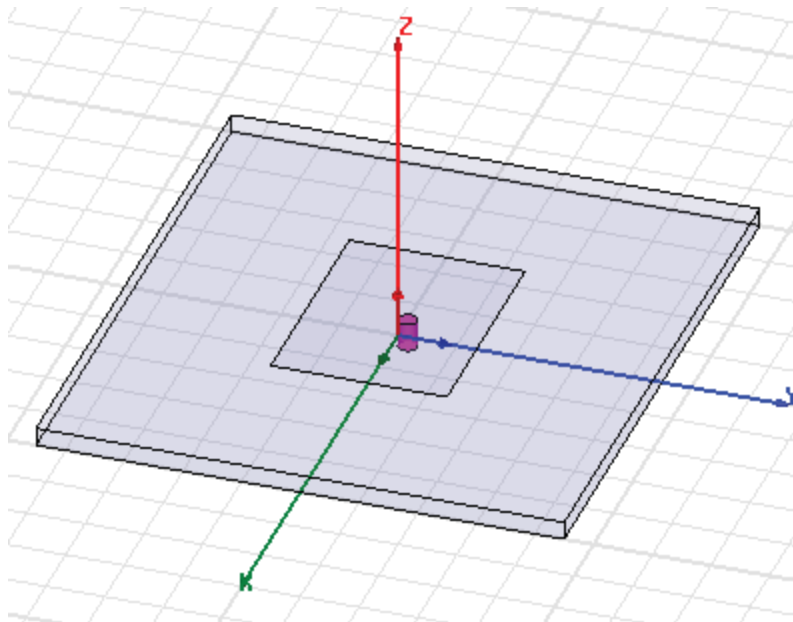


To create the coax:

1. Click **Draw>Cylinder**
2. Using the coordinate entry fields, enter the cylinder position
X: -0.5, Y: 0.0, Z: 0.0 Press the Enter key
3. Using the coordinate entry fields, enter the radius:
dX: 0.16, dY: 0.0, dZ: 0.0 Press the Enter key.
4. Using the coordinate entry fields, enter the height:
dX: 0.0, dY: 0.0, dZ: -0.5 Press the Enter key

To set the name:

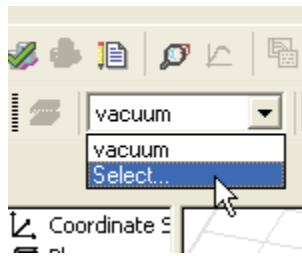
1. In the **Properties** window Name field type: Coax
2. Click the OK button.



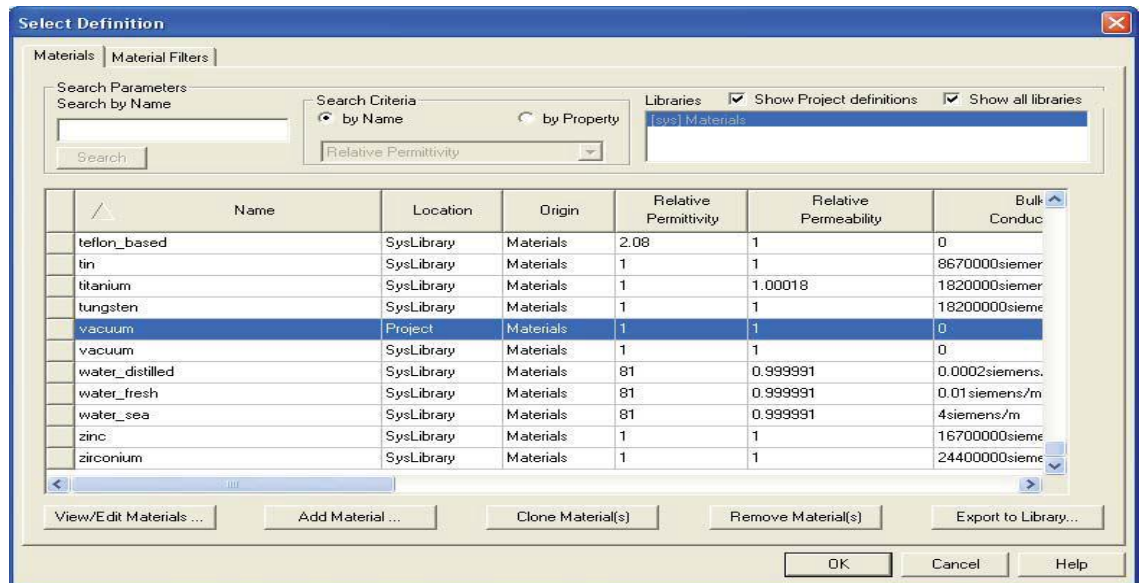
Set Default Material:

To set the default material:

1. Using the 3D Modeler Materials toolbar, choose **Select...**



2. This opens the **Select Definition** window with the Materials tab.



3. Type pec in the Search by Name field. This highlights the pec material.

4. Click the **OK** button.

This sets the default material to pec.

Create the Coax Pin:

To create the coax pin:

1. Click **Draw>Cylinder**.

2. Using the coordinate entry fields, enter the cylinder position

X: -0.5, Y: 0.0, Z: 0.0 Press the Enter key

3. Using the coordinate entry fields, enter the radius:

dX: 0.07, dY: 0.0, dZ: 0.0 Press the Enter key.

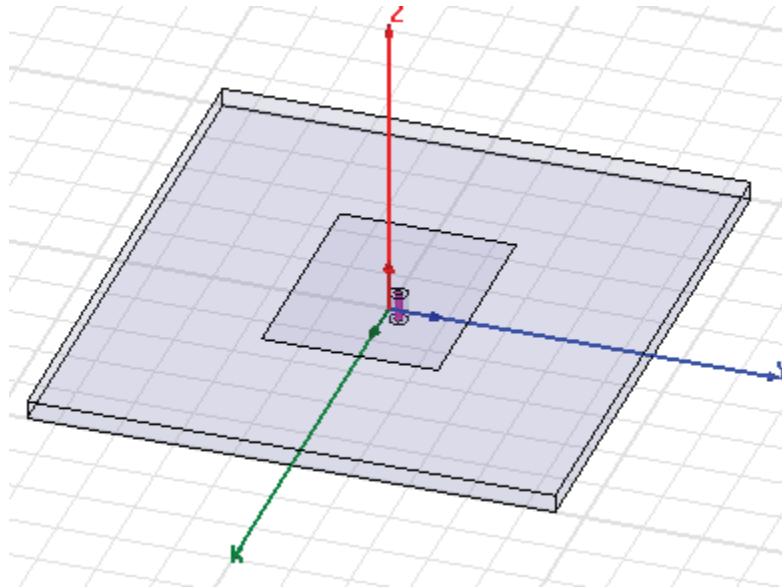
4. Using the coordinate entry fields, enter the height:

dX: 0.0, dY: 0.0, dZ: -0.5 Press the Enter key

To set the name:

1. In the **Properties** window Name field type: Coax_Pin

2. Click the OK button.



Create the Wave port:

To create a circle that represents the port:

1. Click **Draw>Circle**
2. Using the coordinate entry fields, enter the center position
X: -0.5, Y: 0.0, Z: -0.5. Press the Enter key
3. Using the coordinate entry fields, enter the radius of the circle:
dX: 0.16, dY: 0.0, dZ: 0.0 : Press the Enter key

To set the name:

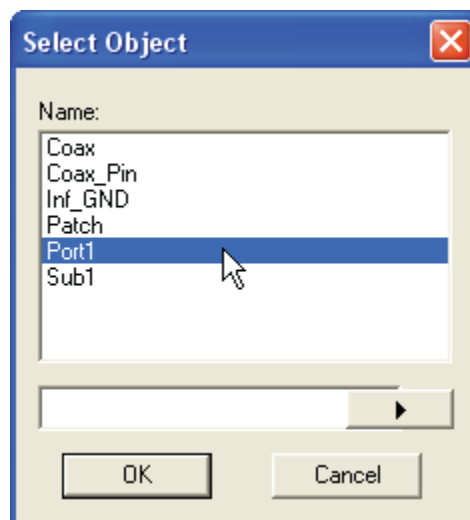
1. In the **Properties** window Name field type: Port1
2. Click the OK button

To select the object Port1:

1. Click **Edit>Select>By Name**

This opens the Select Object dialog,

2. Select the objects named: Port1



3. Click the OK button

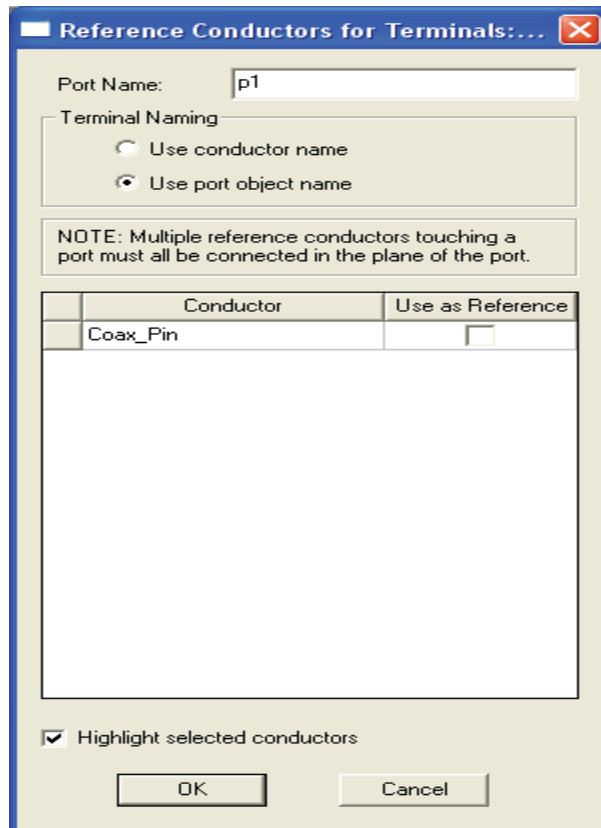
To assign wave port excitation

1. Click **HFSS>Excitations>Assign>Wave Port**

The **Reference Conductors for Terminals** dialog opens.

2. specify the Name: p1

3. Select “Use port object name.”



4. Leave Use as Reference unchecked and Highlight selected conductors checked.

5. Click OK.

The terminal is created under Excitations for the p1 Port in the Project tree.



Create the Probe:

To create the probe:

1. Click **Draw>Cylinder**

2. Using the coordinate entry fields, enter the cylinder position

X: -0.5, Y: 0.0, Z: 0.0 Press the Enter key

3. Using the coordinate entry fields, enter the radius:

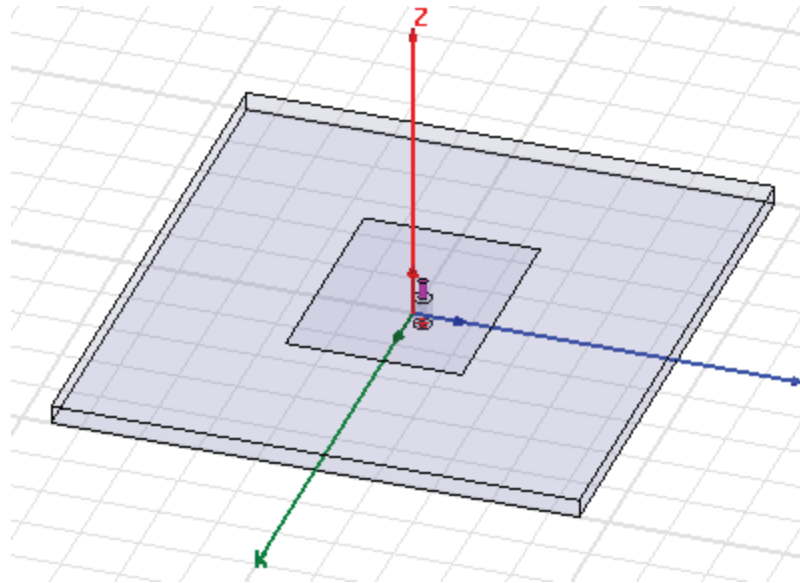
dX: 0.07, dY: 0.0, dZ: 0.0 Press the Enter key

4. Using the coordinate entry fields, enter the height:

dX: 0.0, dY: 0.0, dZ: 0.32 Press the Enter key

To set the name:

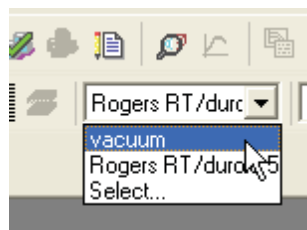
1. In the **Properties** window Name field type: Probe
2. Click the OK button



Set Default Material :

To set the default material:

1. Using the 3D Modeler Materials toolbar, choose vacuum.



Create Air :

To create the air:

1. Click **Draw>Box**
2. Using the coordinate entry fields, enter the box position
X: -5.0, Y: -4.5, Z: 0.0, Press the Enter key
3. Using the coordinate entry fields, enter the opposite corner
of the box dX: 10.0, dY: 9.0, dZ: 3.32, Press the Enter key

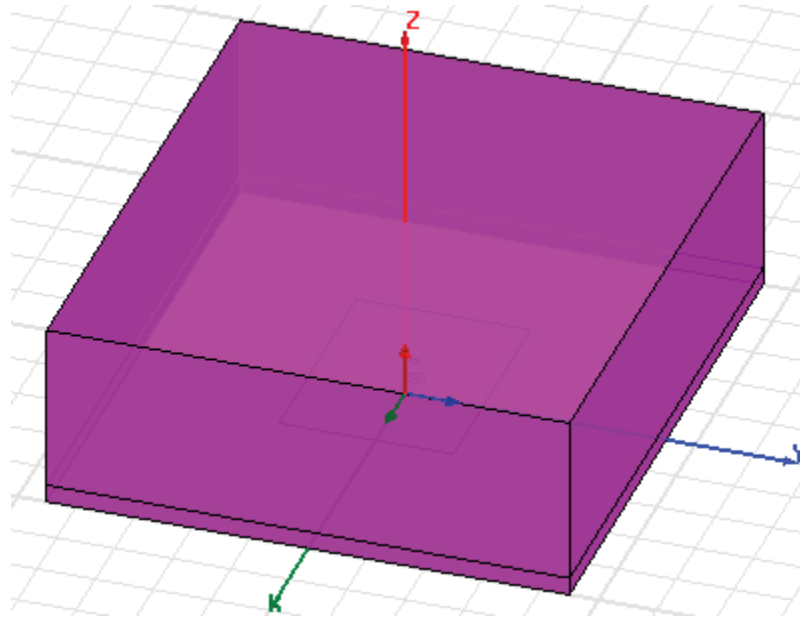
To set the name:

- 1 In the **Properties** window Name field type: Air

Click the OK button

To fit the view:

Click **View>Fit All>Active View**.



Create Radiation Boundary :

Pick the faces:

1. Click **Edit>Select>Faces**
2. Graphically select all of the faces of the Air object except the face at $Z=0.0\text{cm}$. (The bottom)

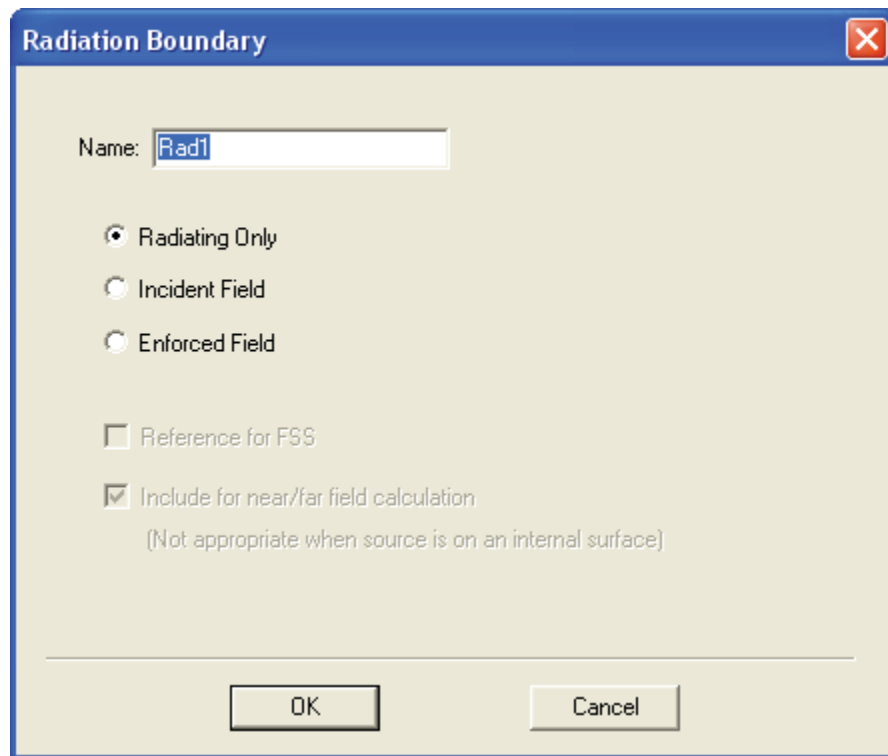
You can hold down the Alt key, and click the top face, and then hit the “b” key to select a “face behind.” After selecting the two faces behind, you can select the remaining three surface faces.

To create a radiation boundary

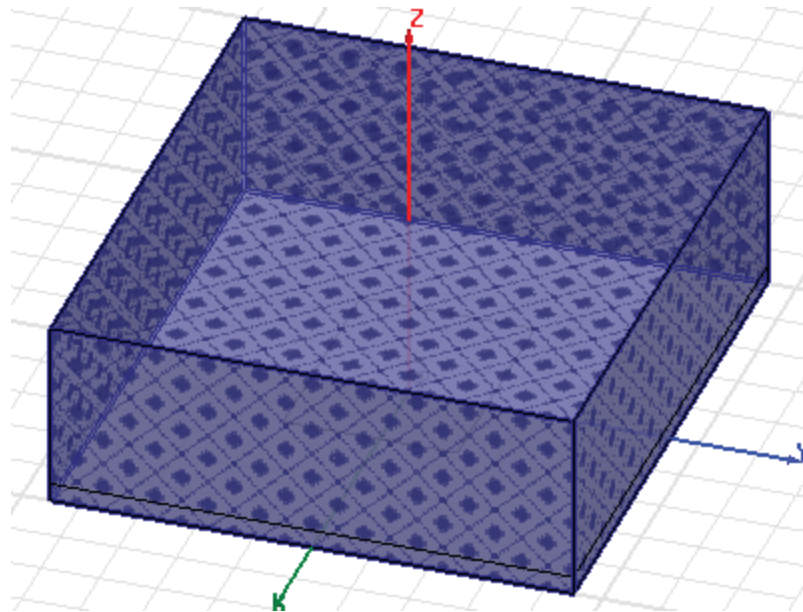
1. Click **HFSS>Boundaries>Assign>Radiation**

The Radiation Boundary dialog opens.

2. Name: Rad1



3. Click the OK button.



Create a Radiation Setup :

To define the radiation setup

1. Click **HFSS>Radiation>Insert Far Field Setup>Infinite Sphere**

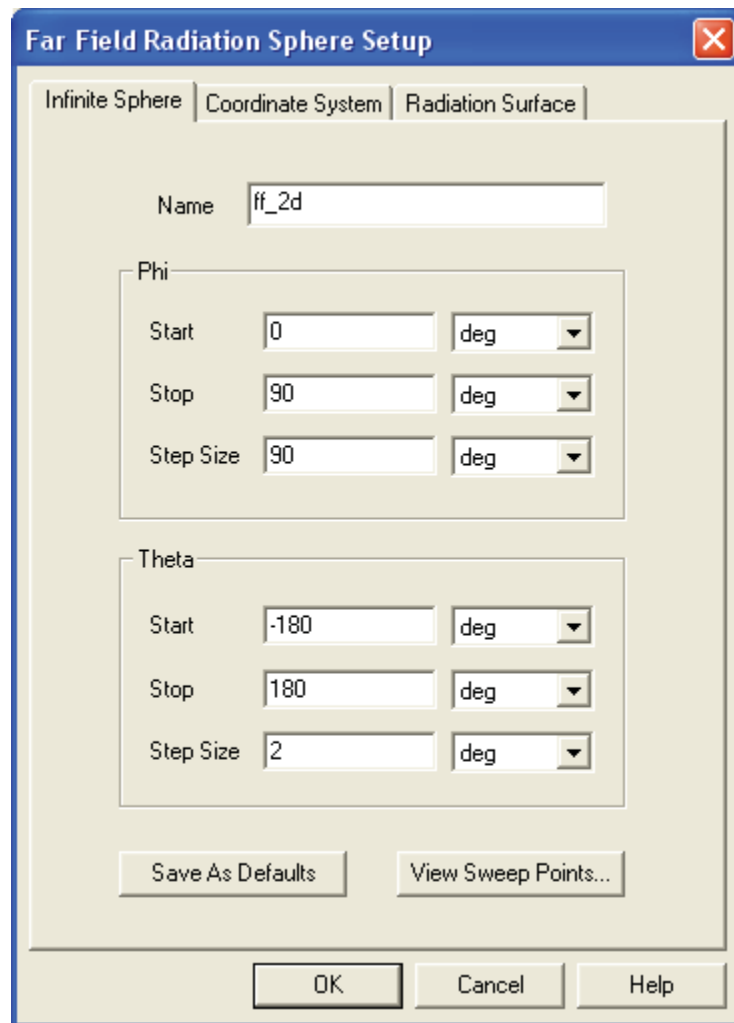
The **Far Field Radiation Sphere Setup** dialog opens.

2. Select the Infinite Sphere Tab

Name: ff_2d

Phi: (Start: 0, Stop: 90, Step Size: 90)

Theta: (Start: -180, Stop: 180, Step Size: 2)



3. Click the OK button

Analysis Setup :

Creating an Analysis Setup

To create an analysis setup:

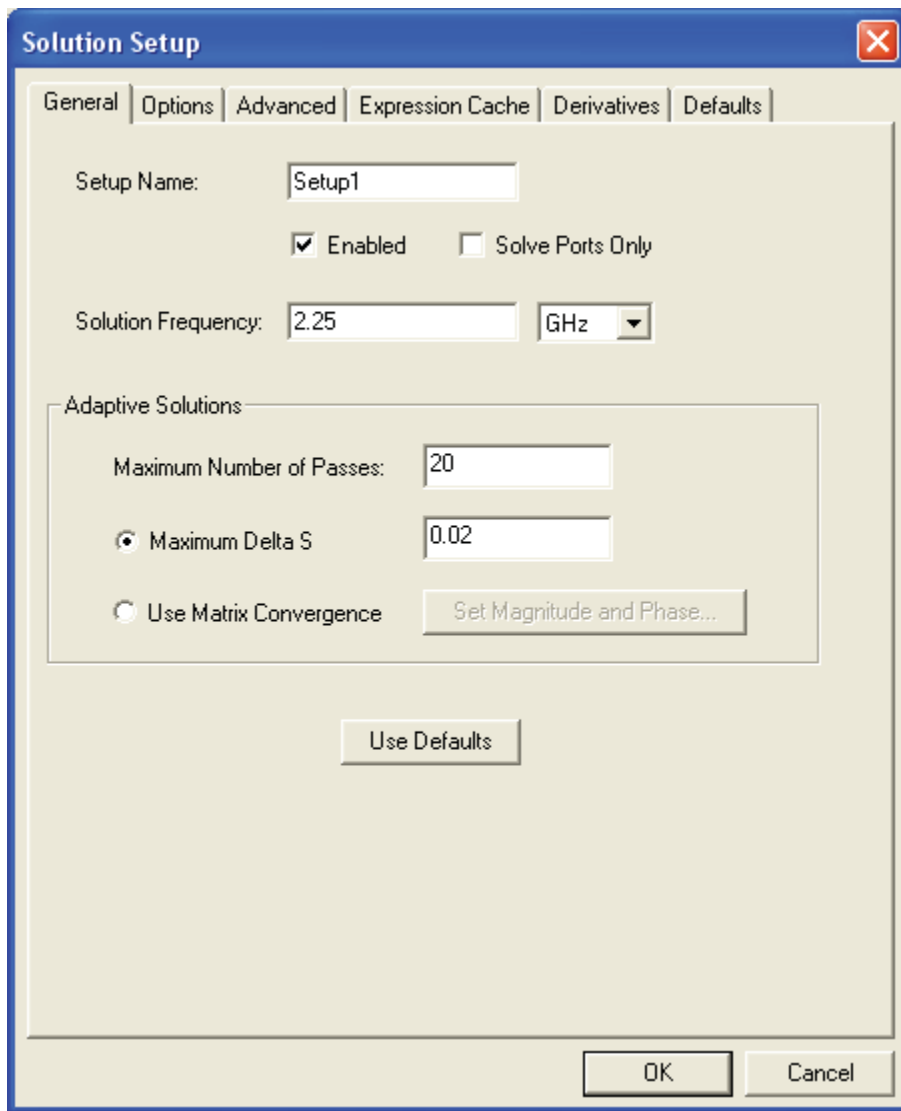
1. Click **HFSS>Analysis Setup>Add Solution Setup** .The **Solution Setup** dialog opens.

2. In the **General** tab:

Solution Frequency: 2.25 GHz

Maximum Number of Passes: 20

Maximum Delta S per Pass: 0.02



3. Click the OK button.

Adding a Frequency Sweep:

To add a frequency sweep:

1. Click **HFSS>Analysis Setup>Add Sweep**

The **Add/Edit Sweep** dialog opens.

2. Specify the following:

Sweep Type: Fast

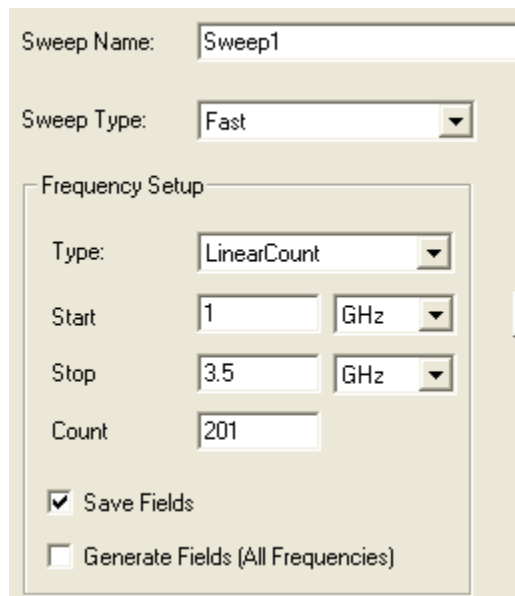
Frequency Setup Type: Linear Count

Start: 1.0GHz

Stop: 3.5GHz

Count: 201

Save Fields: Checked



Sweep Name: Sweep1

Sweep Type: Fast

Frequency Setup

Type: LinearCount

Start: 1 GHz

Stop: 3.5 GHz

Count: 201

Save Fields

Generate Fields (All Frequencies)

3. Click the OK button

Save Project

To save the project:

1. In an Ansoft HFSS window, click **File>Save As**.
2. From the Save As window, type the Filename: hfss_probepatch
3. Click the Save button

Analyze :

Model Validation:

To validate the model:

1. Click **HFSS>Validation Check**
2. Click the Close button

Note: To view any errors or warning messages, use the Message Manager.

To start the solution process:

1. Click **HFSS>Analyze All**

Solution Data

To view the Solution Data:

1. Click **HFSS>Results>Solution Data**

The Solution Data dialog opens.

To view the Profile:

Click the Profile Tab.

To view the Convergence:

Click the Convergence Tab

Note: The default view for convergence is Table. Select the Plot radio button to view a graphical representation of the convergence data.

To view the Matrix Data:

Click the Matrix Data Tab

Note: To view a real-time update of the Matrix Data, set the Simulation to Setup1, Last Adaptive

2. Click the Close button

Create Reports :

Create Terminal S-Parameter Plot - Magnitude

To create a report:

1. Click **HFSS>Results>Create Terminal Solution Data Report**.

The **Reports** window opens.

2. Make the following selections:

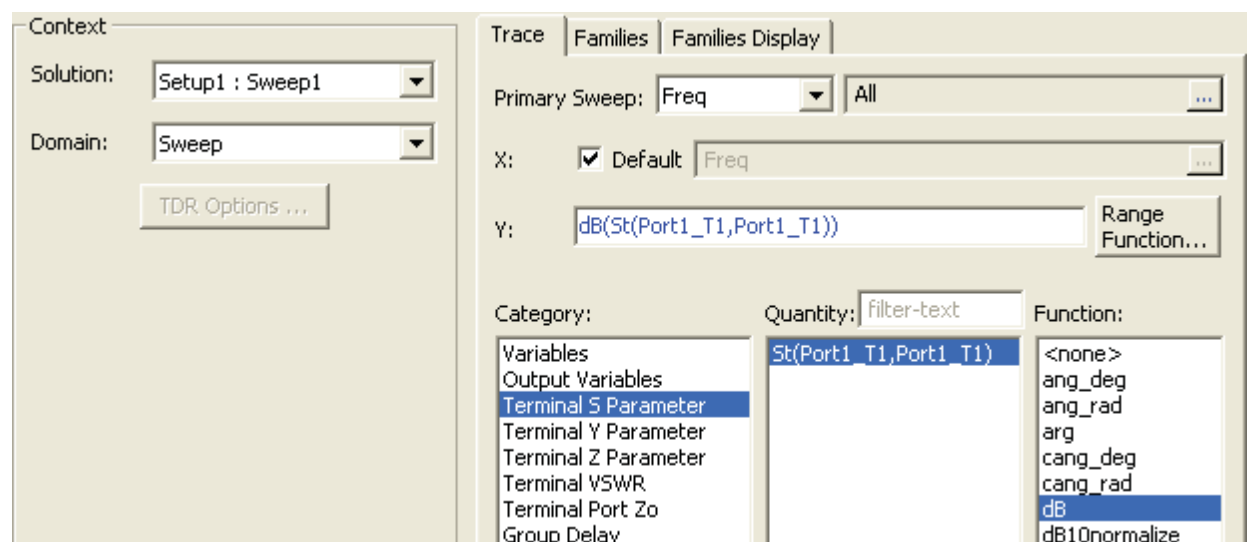
Solution: Setup1: Sweep1

Domain: Sweep

Category: Terminal S Parameter

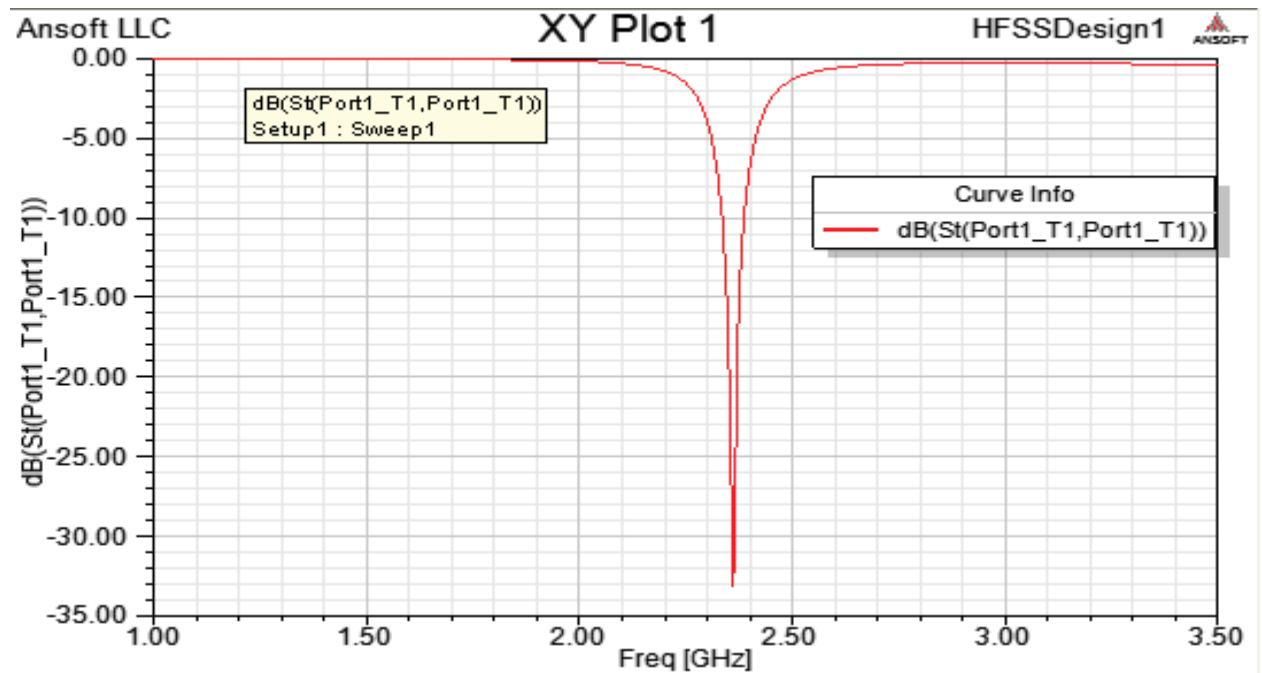
Quantity: St(Port1_T1,Port1_T1),

Function: dB

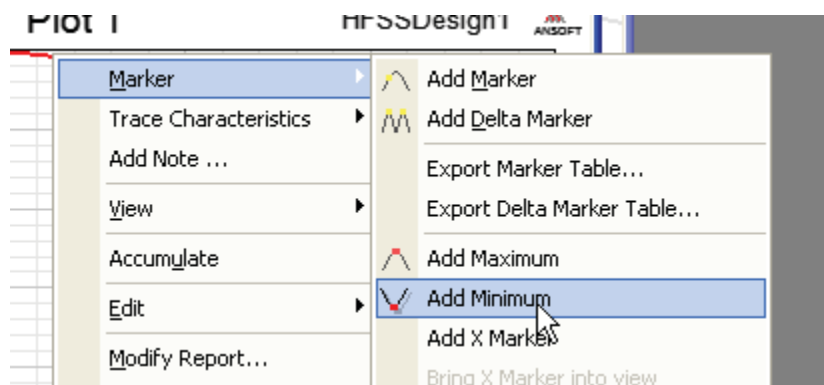


3. Click the **New Report** button.

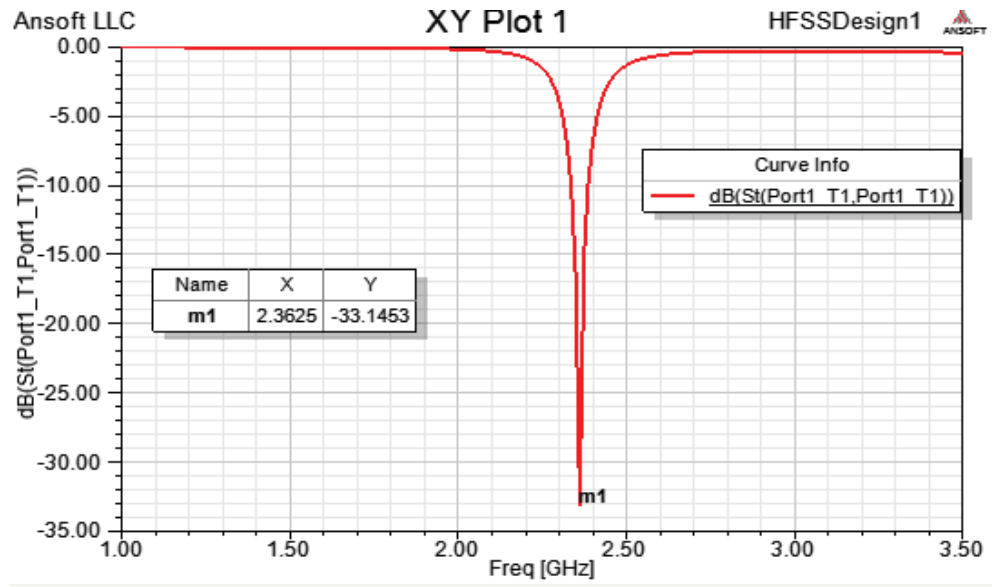
4. Click the **Close** button.



5. Select the trace on the plot.
6. Right click to display the shortcut menu and click **Marker>Add Minimum**.



A minimum marker (m1) appears on the trace, and a marker table lists the x and y coordinates values.



Far Field Overlays

Create Far Field Overlay

To create a 2D polar far field plot :

1. Click **HFSS>Results>Create Far Fields Report>Radiation Pattern.**

The **Reports** dialog appears.

2. Specify the following:

Solution: Setup1: Sweep1

Geometry: ff_2d

In the **Trace** tab:

Select Theta the primary sweep.

Category: Gain

Quantity: GainTotal

Function: dB

3. Click **New Report.**

